



Faculty of Engineering and Technology
Joint Master Program in Electrical Engineering (JMEE)

**Radio Propagation Model and Performance Analysis
Based on LoRa Communication Network in Birzeit**

**Submitted By
Mai Hawwa**

**Supervisor
Dr. Alhareth Zyoud**

July 2023



Faculty of Engineering and Technology
Joint Master Program in Electrical Engineering (JMEE)

**Radio Propagation Model and Performance Analysis Based on LoRa
Communication Network in Birzeit**

نموذج الانتشار الراديوي وتحليل الأداء القائم على شبكة اتصالات لورا في بيرزيت

Submitted By

Mai Hawwa

Supervisor

Dr. Alhareth Zyoud

*This Master Thesis was submitted in partial fulfillment of the Requirements for the
Master's Degree in Electrical Engineering from the Faculty of Engineering and
Technology at Birzeit University, Palestine*

Committee

Dr. Alhareth Zyoud

Dr. Wael Hashlamoun

Dr. Qadri Mayaleh

**Radio Propagation Model and Performance Analysis Based on LoRa
Communication Network in Birzeit**

نموذج الانتشار الراديوي وتحليل الأداء القائم على شبكة اتصالات لورا في بيرزيت

Submitted By

Mai Hawwa

Approved by the Examining Committee

Dr. Alhareth Zyoud

..... الحارث محمد زيويد الحارثي

Dr. Wael Hashlamoun

..... Wael Hashlamoun

Dr. Qadri Mayaleh

.....

July 24, 2023

Declaration

I declare that this thesis entitled “Radio Propagation Model and Performance Analysis Based on LoRa Communication Network in Birzeit” is the result of my own research except as cited in the references. It is being submitted to the master’s degree in Electrical Engineering from the Faculty of Engineering and Technology at Birzeit University, Palestine. The thesis has not been accepted for any degree and is not concurrently submitted in candidature of any other degree.

Signature:

Name:

Date:

Abstract

The growth of the Internet of Things (IoT) enables the deployment of numerous wireless network-based applications, including security, industrial monitoring, smart homes, smart cities, and smart agriculture. Therefore, next-generation wireless network technologies are expected to have massive connections to tens of billions of devices to enable these devices to communicate and collaborate to deliver intelligent services in various environments while maintaining user transparency. For IoT applications, long-range connections, low data rates, low power consumption, and cost effectiveness are some of the key characteristics and requirements. Low Power Wide Area Network (LPWAN) technologies for wireless networking are a potential solution for IoT applications. Various standards and industry associations have investigated several LPWAN technologies. Long Range Wide Area Network (LoRaWAN) is one of the most studied and implemented LPWAN technologies due to its properties and the potential to build private networks on an open standard. This study proposes the use of LoRa network technology to measure received signal strength to understand the channel behavior and to provide realistic, and trustworthy empirical parameters for the path loss propagation model in the city of Birzeit in Palestine. A set of proposed parameters for path loss model for the performance of LoRa technology in 16 different scenarios in indoor and outdoor settings are presented. The lowest RMSE between the proposed parameters for the model and the model based on measurements was 1.253 for the effect of walls scenario at 433MHz in an indoor environment, while it was 2.155 in the same scenario at 868MHz. As for the highest RMSE at 433 MHz, it was 7.946 in the corridor scenario, while it was 7.352 at 868 MHz in the ceiling and floor scenario. For the outdoor environment, the lowest RMSE obtained at 433 MHz equals 1.753 for the effect of trees' trunks, while it was 2.091 in the same scenario at 868 MHz. As for the highest RMSE obtained, it was 3.294 at 433 MHz in the complex outdoor scenario, while it was 7.051 at 868 MHz in the same scenario. These proposed parameters for path loss model validated and compared with the performance of models in the literature. This comparison demonstrated that Lee's model performed most closely to the measurements' fitted curve in the outdoor environment, while the performance of the indoor environment models varied depending on the scenarios and how the models handled the various influences in the indoor environments. ITU-R 2318 was the closest to the proposed parameters of path loss model in the corridor scenario compared to all models in all scenarios in the indoor environment, as it had the lowest RMSE of 5.36 at 868 MHz, while the worst model was IEEE802.11, with an RMSE of 73.94 in the ceiling and floor scenario at a frequency of 433

MHz. In the outdoor environment, the Lee Model effect approached all measurements with the least RMSE compared to other models. In the sub-scenarios of trees, its best performance was in the trees' trunks scenario, where RMSE was 3.89 at 433 MHz and 2.86 at 868 MHz. As for the worst model, it was Free Space, with an RMSE of 61.45 at 433 MHz in the trees' leaves scenario and 55.79 at 868 MHz in the trees' trunks scenario. As for the complex outdoor environment, the best model was the LEE model, with RMSEs of 18.34 at 433 MHz and 1.45 at 868 MHz. As for the worst model, it was Okumura Hata, with RMSEs of 77.31 at 433 MHz and 94.32 at 868 MHz. Finally, the shadow curves demonstrated that the suggested parameters for path loss model have a normal distribution with a mean close to zero and a variable variance that depends on how the data are distributed around the mean.

المستخلص

يتيح نمو إنترنت الأشياء (IoT) نشر العديد من التطبيقات القائمة على الشبكات اللاسلكية، بما في ذلك الأمن، المراقبة الصناعية، المنازل الذكية، المدن الذكية والزراعة الذكية. لذلك من المتوقع أن يكون لتقنيات الشبكات اللاسلكية من الجيل التالي اتصالات ضخمة لعشرات المليارات من الأجهزة لتمكينها من التواصل والتعاون لتقديم خدمات ذكية في بيئات مختلفة مع الحفاظ على توفير الشفافية للمستخدم. بالنسبة لتطبيقات إنترنت الأشياء، تعد الاتصالات طويلة المدى ومعدلات البيانات المنخفضة والاستهلاك المنخفض للطاقة والتكلفة المنخفضة بعضًا من الخصائص والمتطلبات الرئيسية. تعد تقنيات شبكة المنطقة الواسعة منخفضة الطاقة (LPWAN) للشبكات اللاسلكية حلاً محتملاً لتطبيقات إنترنت الأشياء. قامت العديد من المعايير والجمعيات الصناعية بدراسة العديد من تقنيات LPWAN. تعد الشبكات طويلة المدى (LoRaWAN) واحدة من أكثر تقنيات LPWAN التي تمت دراستها وتنفيذها نظرًا لخصائصها وإمكانية استخدامها لبناء شبكات خاصة دون وجود محددات. تقترح هذه الدراسة استخدام تقنية شبكة LoRa لقياس قوة الإشارة المستقبلية والتنبؤ بمعلمات نموذج خسارة المسار لفهم سلوك القناة ولتقديم معايير تجريبية واقعية وموثوقة لنموذج الانتشار في مدينة بيرزيت في فلسطين. يتم تقديم مجموعة من المعلمات المقترحة لنموذج خسارة المسار لأداء تكنولوجيا LoRa في 16 سيناريو مختلفًا في الإعدادات الداخلية والخارجية. كان أقل RMSE بين النموذج المعتمد على المعلمات المقترحة والقياسات 1.253 لتأثير سيناريو الجدران عند 433 ميغا هرتز في بيئة داخلية، بينما كان 2.155 في نفس السيناريو عند 868 ميغا هرتز. أما بالنسبة لأعلى RMSE عند 433 ميغا هرتز، فقد كان 7.946 في سيناريو الممر، بينما كان 7.352 عند 868 ميغا هرتز في سيناريو السقف والأرضية. بالنسبة للبيئة الخارجية، فإن أدنى RMSE تم الحصول عليه عند 433 ميغا هرتز يساوي 1.753 لتأثير جذوع الأشجار، بينما كان 2.091 في نفس السيناريو عند 868 ميغا هرتز. بالنسبة لأعلى RMSE تم الحصول عليه، فقد كان 3.294 عند 433 ميغا هرتز في السيناريو الخارجي المعقد، بينما كان 7.051 عند 868 ميغا هرتز في نفس السيناريو. ثم تم التحقق من صحة هذه الطريقة المقترحة ومقارنتها بأداء النماذج من الأدبيات. أظهرت هذه المقارنة أن أداء نموذج Lee كان أقرب إلى المنحنى المناسب للقياسات في البيئة الخارجية، بينما اختلف أداء نماذج البيئة الداخلية اعتمادًا على السيناريوهات وكيفية تعامل النماذج مع التأثيرات المختلفة في البيئات الداخلية. كان ITU-R 2318 هو الأقرب لنموذج خسارة المسار اعتمادًا على المعلمات المقترحة في سيناريو الممر مقارنة بجميع النماذج في جميع السيناريوهات في البيئة الداخلية، حيث كان أقل RMSE يبلغ 5.36 عند 868 ميغا هرتز، بينما كان أسوأ نموذج IEEE802.11، مع RMSE يبلغ 73.94 في سيناريو السقف والأرضية بتردد 433 ميغا هرتز. في البيئة الخارجية، اقترب تأثير Lee Model من جميع نماذج خسارة المسار التي اعتمدت على المعلمات المقترحة بأقل نسبة RMSE مقارنة بالنماذج الأخرى. في السيناريوهات الفرعية للأشجار، كان أفضل أداء لها في سيناريو جذوع الأشجار، حيث كان RMSE 3.89 عند 433 ميغا هرتز و 2.86 عند 868 ميغا هرتز. بالنسبة لأسوأ نموذج، كان Free Space، مع RMSE يبلغ 61.45 عند 433 ميغا هرتز في سيناريو أوراق الأشجار و 55.79 عند 868 ميغا هرتز في سيناريو جذوع الأشجار. بالنسبة للبيئة الخارجية المعقدة، كان أفضل نموذج هو نموذج LEE، مع RMSE يبلغ 18.34 عند 433 ميغا هرتز و 1.45 عند 868 ميغا هرتز. أما بالنسبة لأسوأ نموذج كان Okumura Hata، حيث بلغ 77.31 RMSE عند 433 ميغا هرتز و 94.32 عند 868 ميغا هرتز، وأخيرًا، أظهرت منحنيات الظل أن نموذج خسارة المسار اعتمادًا على المعلمات المقترحة له توزيع طبيعي بمتوسط قريب من الصفر ومعامل انحراف معياري يعتمد على كيفية توزيع البيانات حول المتوسط.

Acknowledgment

The student is grateful to the Research Committee, Faculty of Graduate Studies and Research, Birzeit University for supporting the study by research grant Ref: 2021/69.

Table of Contents

Chapter 1	Introduction	1
1.1	Overview	1
1.2	Research Problem	1
1.3	Research Goal	2
1.4	Importance and Expected Impact	2
1.5	Research Methodology	2
1.6	Report Outline	3
Chapter 2	Literature Reviews	4
2.1	Indoor Scenarios	4
2.2	Outdoor Scenarios	6
2.2.1	Urban areas	6
2.2.2	Suburban areas	12
2.2.3	Rural areas	13
2.3	Indoor-Outdoor Scenarios	17
Chapter 3	LoRa Communication Technology	22
3.1	Physical Layer of LoRa Technology	22
3.2	Background of Physical Layers Parameters for LoRa Technology	23
3.3	Overview about LoRa Network Layer	28
3.4	Mathematical Modeling	29
3.5	LoRa Technology	35
3.6	LoRa Connection	37
3.7	Measurements Scenarios	38
Chapter 4	Results and Discussion	51
4.1	Measurements and Proposed Fitted Model	51
4.2	Path Loss	65
4.3	Model Validation	77
4.4	Shadow Fading	83
Chapter 5	Conclusion and Future Works	97
5.1	Conclusion	97
5.2	Contributions	97

5.3	Research Limitations	98
5.4	Future Works	98
	References	99

Table of Figures

Figure 3-1: Comparison between different Wireless technologies.....	23
Figure 3-2: A linear chirp waveform is a sinusoidal wave that increases linearly in frequency over time [36].....	27
Figure 3-3: LoRa modulated signal [36].....	27
Figure 3-4: Communication network for LoRa technology	29
Figure 3-5: Curve Fitting tool in MATLAB	32
Figure 3-6: Data imported from CFtool in MATLAB workspace.....	33
Figure 3-7: Curve fitting general models in MATLAB.....	33
Figure 3-8: Fitting options	34
Figure 3-9: A Data fitting example.....	34
Figure 3-10: An Illustration of a fitted coefficient and fit outcomes.....	35
Figure 3-11: SX1276RF1JAS LoRa transceiver [64].....	36
Figure 3-12: 868 MHz and 433 MHz frequency band antennas [64].....	37
Figure 3-13: connecting wires, Arduino Uno chip, and breadboard.....	37
Figure 3-14: LoRa transmitter and receiver circuits.....	38
Figure 3-15: Campus of Birzeit University	39
Figure 3-16: Faculty of Information Technology (Munib Al-Masri) building.....	39
Figure 3-17: Tx and Rx in indoor LoS_ scenario A	40
Figure 3-18: LoS measurement location between Tx and Rx in indoor LoS_ scenario A	41
Figure 3-19: Tx Location in indoor ceiling and floor NLoS_ scenario B	41
Figure 3-20: First location (ceil) of Rx where the measurements were taken in indoor ceiling and floor NLoS_ scenario B	42
Figure 3-21: Second location (floor) of Rx where the measurements were taken in indoor ceiling and floor NLoS_ scenario B.....	42
Figure 3-22: Tx location in indoor multiple walls NLoS_ scenario D	43
Figure 3-23: Rx locations in indoor multiple walls NLoS_ scenario D were the measurements taken after walls	43
Figure 3-24: Shawqi Shaheen building for public lectures.....	44
Figure 3-25: Tx location in indoor lectures theater NLoS_ scenario E	45
Figure 3-26: lecture theater in Shawqi Shaheen building_ scenario E.....	45
Figure 3-27: Tx location in outdoor trees' leaves NLoS and LoS_ scenario A.....	46
Figure 3-28: Trees' Leaves where the Rx moves behind in outdoor NLoS and LoS_ scenario A.....	46
Figure 3-29: Waleed and Helen Kattan Presidency building.....	47
Figure 3-30: Tx location in outdoor trees' trunks NLoS and LoS_ scenario B.....	48
Figure 3-31: Trees' trunks where the Rx moves behind in outdoor NLoS and LoS_ scenario B	48
Figure 3-32: Places where Tx is fixed and Rx moves towards Ramallah city in complex outdoor NLoS and LoS_ scenario C	49

Figure 3-33: Places where Tx is fixed and Rx moves towards Birzeit and Rawabi city in complex outdoor NLoS and LoS_ scenario C	49
Figure 3-34: Places where LoS connection formed between Tx and Rx in complex outdoor NLoS and LoS_ scenario C.....	50
Figure 4-1: Fitted path loss and scatter plot of Actual path loss in an indoor environment at 868MHz	51
Figure 4-2: Averaged actual and fitted path loss at 433 MHz in indoor LoS _scenario A.....	54
Figure 4-3: Averaged actual and fitted path loss at 868 MHz in indoor LoS_ scenario A.....	54
Figure 4-4: Averaged actual and fitted path loss at 433 MHz in indoor NLoS ceilings and floors_ scenario B	55
Figure 4-5: Averaged actual and fitted path loss at 868 MHz in indoor NLoS ceilings and floors_ scenario B	56
Figure 4-6: Averaged actual and fitted path loss at 433 MHz in indoor NLoS emergency stairs_ scenario C	57
Figure 4-7: Averaged actual and fitted path loss at 868 MHz in indoor NLoS emergency stairs_ scenario C	57
Figure 4-8: Averaged actual and fitted path loss at 433 MHz in indoor NLoS multiple walls_ scenario D	58
Figure 4-9: Averaged actual and fitted path loss at 868 MHz in indoor NLoS multiple walls_ scenario D	58
Figure 4-10: Averaged actual and fitted path loss at 433 MHz in indoor NLoS in theater lectures_ scenario E	59
Figure 4-11: Averaged actual and fitted path loss at 868 MHz in indoor NLoS in theater lectures_ scenario E	59
Figure 4-12: Averaged actual and fitted path loss at 433 MHz in outdoor NLoS and LoS for Trees' Leaves_ scenario A.....	60
Figure 4-13: Averaged actual and fitted path loss at 868 MHz in outdoor NLoS and LoS for Trees' Leaves_ scenario A.....	62
Figure 4-14: Averaged actual and fitted path loss at 433 MHz in outdoor NLoS and LoS for Trees' trunks_ scenario B	63
Figure 4-15: Averaged actual and fitted path loss at 868 MHz in outdoor NLoS and LoS for Trees' trunks_ scenario B	63
Figure 4-16: Averaged actual and fitted path loss at 433 MHz in outdoor NLoS and LoS for Complex Environment_ scenario C	64
Figure 4-17: Averaged actual and fitted path loss at 868 MHz in outdoor NLoS and LoS for Complex Environment_ scenario C	65
Figure 4-18: Estimated path loss as a function of distance at 433 MHz.....	66
Figure 4-19: Estimated path loss as a function of distance at 868 MHz.....	66
Figure 4-20: Models and fitted path loss at 433 MHz in indoor LoS _scenario A.....	67
Figure 4-21: Models and fitted path loss at 868 MHz in indoor LoS _scenario A.....	67
Figure 4-22 : Models and fitted path loss at 433 MHz in indoor NLoS ceilings and floors_ scenario B.....	68
Figure 4-23: Models and fitted path loss at 868 MHz in indoor NLoS ceilings and floors_ scenario B.....	69

Figure 4-24: Models and fitted path loss at 433 MHz in indoor NLoS Emergency stairs_ scenario C.....	69
Figure 4-25: Models and fitted path loss at 868 MHz in indoor NLoS Emergency stairs_ scenario C.....	70
Figure 4-26: Models and fitted path loss at 433 MHz in indoor NLoS multiple walls_ scenario D	71
Figure 4-27: Models and fitted path loss at 868 MHz in indoor NLoS multiple walls_ scenario D	71
Figure 4-28: Averaged actual and fitted path loss at 433 MHz in indoor NLoS in Theater Lectures_ scenario E.....	72
Figure 4-29: Averaged actual and fitted path loss at 868 MHz in indoor NLoS in Theater Lectures_ scenario E.....	73
Figure 4-30: Averaged actual and fitted path loss at 433 MHz for outdoor NLoS and LoS for Trees' Leaves_ scenario A.....	74
Figure 4-31: Averaged actual and fitted path loss at 868 MHz for outdoor NLoS and LoS for Trees' Leaves_ scenario A.....	74
Figure 4-32: Averaged actual and fitted path loss at 433 MHz in outdoor NLoS and LoS for Trees' Trunks_ scenario B	75
Figure 4-33: Averaged actual and fitted path loss at 868 MHz in outdoor NLoS and LoS for Trees' Trunks_ scenario B	75
Figure 4-34: Averaged actual and fitted path loss at 433 MHz in NLoS and LoS complex outdoor_ scenario C	76
Figure 4-35: Averaged actual and fitted path loss at 868 MHz in NLoS and LoS complex outdoor_ scenario C	77
Figure 4-36: Path loss at emergency stairs at 433MHz and new path loss based on new measurements.....	78
Figure 4-37: Path loss at emergency stairs at 433MHz and new path loss based on new measurements.....	78
Figure 4-38: Path loss with trees trunks at 433MHz and new path loss based on new measurements.....	79
Figure 4-39: Path loss without trees trunks at 433MHz and new path loss based on new measurements.....	79
Figure 4-40: Path loss with trees trunks at 868MHz and new path loss based on new measurements.....	80
Figure 4-41: Path loss without trees trunks at 868MHz and new path loss based on new measurements.....	80
Figure 4-42: Histogram for path loss based on measured data at 433 MHz in indoor LoS _scenario A	84
Figure 4-43: Fitted PDF generates for the plotted histogram at 433 MHz in indoor LoS _scenario A	84
Figure 4-44: Fitted PDF when histogram hides at 433 MHz in indoor LoS _scenario A	85
Figure 4-45: CDF vs shadowing at 433 MHz in indoor LoS _scenario A	85
Figure 4-46: Fitted CDF vs shadowing at 433 MHz in indoor LoS _scenario A	86
Figure 4-47: PDF and CDF for indoor LoS at 868 MHz _scenario A.....	86

Figure 4-48: PDF and CDF for indoor NLoS ceilings and floors at 433 MHz _ scenario B ..	87
Figure 4-49: PDF and CDF for indoor NLoS ceilings and floors at 868 MHz _ scenario B ..	87
Figure 4-50: PDF and CDF for indoor NLoS emergency stairs at 433 MHz _ scenario C	88
Figure 4-51: PDF and CDF for indoor NLoS emergency stairs at 868 MHz _ scenario C	88
Figure 4-52: PDF and CDF for indoor NLoS multiple walls at 433 MHz _ scenario D	89
Figure 4-53: PDF and CDF for indoor NLoS multiple walls at 868 MHz _ scenario D	89
Figure 4-54: PDF and CDF for indoor NLoS theater lecture at 433 MHz _ scenario E	90
Figure 4-55: PDF and CDF for indoor NLoS theater lecture at 868 MHz _ scenario E	90
Figure 4-56: PDF and CDF for outdoor NLoS with trees' leaves at 433MHz_ scenario A....	91
Figure 4-57: PDF and CDF for outdoor NLoS without trees' leaves at 433MHz_ scenario A	92
Figure 4-58: PDF and CDF for outdoor NLoS with trees' leaves at 868 MHz _ scenario A..	92
Figure 4-59: PDF and CDF for outdoor NLoS without trees' leaves at 868MHz_ scenario A	93
Figure 4-60: PDF and CDF for outdoor NLoS with trees' trunks at 433MHz_ scenario B	93
Figure 4-61: PDF and CDF for outdoor NLoS without trees' trunks at 433MHz_ scenario B	94
Figure 4-62: PDF and CDF for outdoor NLoS with trees' trunks at 868MHz_ scenario B	94
Figure 4-63: PDF and CDF for outdoor NLoS without trees' trunks at 868MHz_ scenario B	95
Figure 4-64: PDF and CDF for outdoor NLoS and LoS complex outdoor environment at 433 MHz_ scenario C	95
Figure 4-65: PDF and CDF for outdoor NLoS and LoS complex outdoor environment at 868 MHz_ scenario C	96

List of Tables

Table 2.1: The proposed model variables for indoor environments	7
Table 2.2: The proposed model variables for urban outdoor environments	12
Table 2.3: The proposed model variables for sub urban outdoor environments	13
Table 2.4: The proposed model variables for rural outdoor environments.....	17
Table 2.5: The proposed model variables for indoor-outdoor environments	19
Table 2.6: Parameters of Previous Empirical Models in Indoor environment	20
Table 2.7: Parameters of previous empirical models in outdoor environment.....	21
Table 3.1: Characteristics of LoRa Technology Protocol [33].....	25
Table 3.2: The effect of physical layer parameters configuration on communication performance [38],[40]	28
Table 3.3: LoRa and Arduino Uno Pins connection	37
Table 4.1: Proposed Parameters of the path loss model in the indoor environment based on two approaches, scenario, environment, distance, frequency and their RMSE.....	53
Table 4.2: Proposed Parameters of the path loss model in the outdoor environment based on two approaches, scenario, environment, distance, frequency and their RMSE.....	61
Table 4.3: RMSE between previous and new path loss calculated based on measurements for two scenarios indoor and outdoor for validation	81
Table 4.4: RMSE for path loss model based on the proposed parameters and different models in the literature in indoor scenarios.....	82
Table 4.5: RMSE for path loss model based on the proposed parameters and different models in the literature in vegetation outdoor scenarios	82
Table 4.6: RMSE for path loss model based on the proposed parameters and different models in the literature in complex outdoor scenarios	83
Table 4.7: Mean and standard deviation for the shadow fading in indoor scenarios.....	91
Table 4.8: Mean and standard deviation for the shadow fading in outdoor scenarios.....	96

List of Abbreviations

3GPP	Third Generation Partnership Project
ANN	Artificial Neural Networks
BR	Bit Rate
BW	Bandwidth
CF	Carrier Frequency
CR	Coding Rate
CSS	Chirp Spread Spectrum
DR	Data Rate
ED	End Node
ESIB-USJ	Joseph University campus in Beirut
ETSI	European Telecommunications Standards Institute
FCC	Federal Communications Commission
FEC	Forward Error Correction
FSK	Frequency-Shift keying
GCU	Glasgow Caledonian University
GW	Gateway
HF	High-Frequency
IDE	Integrated Development Environment
IDPM	Indoor Dominant Path Model
IUM	International Islamic University in Malaysia
IoT	Internet of Things
ISM	Industrial Scientific Medical
ITU-R	International Telecommunication Union Radio communication
LAN	Local Area Network
LBT	Listen Before Talk
LF	Low-Frequency
LoRaWAN	Long Range Wide Area Network
LoS	Line of Sight
LPWAN	Low Power Wide Area Network
MSE	Mean Squared Error
MWF	Multi-Wall-and-Floor
NB	Narrowband
NLoS	Non-Line of Sight
OOK	On–Off Keying
PDR	Packet Delivery Rate
PL	Payload Length
Ptx	Transmission Power
R _c	Chips Rate
RF	Radio Frequency
R _M	Modulation Rate
RMSE	Root Mean Squared Error
R _s	Symbol Rate
RSSI	Received Signal Strength Indicator
Rx	Receiver
SF	Spreading Factor

SINR	Signal to Interference and Noise Ratio
SMA	SubMiniature version A
SNR	Signal to Noise Ratio
SUI	Stanford University Interim
UMa	Unlicensed Mobile access
WI	Walfish-Ikegami
WSN	Wireless Sensor Networks

Chapter 1 Introduction

1.1 Overview

The Internet of Things (IoT) will serve as the basis for a wide variety of smart applications, making it a potential paradigm for integrating any device into the Internet environment [1]. There are many applications seek to offer users comfort, security, and efficiency while keeping prices down [2]. Low-Power Wide Area Network (LPWAN) was created to suit the needs of these applications since they are characterized by long range, low Data Rate (DR), low power consumption, and low cost. These networks include a variety of technologies, like Long Range Communication Technology (LoRa), Sigfox, Narrowband (NB-IoT), and others, and they operate in both licensed and unlicensed bands. LoRa is one of them and is highly popular and sought-after by numerous research and industry communities [1]. LoRa technology represents an all-encompassing wireless solution because of its unique characteristics, such as low power consumption while in use, long distance transmission, and strong penetration [2], as well as security against interference and different network attacks [3]. The sensor node that serves as the end node in the LoRa technology system is typically connected to the IoT system via a gateway to transfer data to the network server and subsequently to the application server [3]. Between the end node and the gateway, radio waves are transferred; as a result, the transmitted signal is impacted by the environment and a loss occurs. The various channel measurements attempt to show trustworthy, realistic models. Propagation models can be further divided into deterministic models [4],[5] and empirical models [6],[7]. The first type is characterized by the requirement for detailed knowledge of the location, dimensions, and various physical parameters, while the second type derives the values of different parameters by matching the measurement data to a suitable function for a specific environment [1]. Accordingly, the empirical model will be used in this research to examine the performance of LoRa technology in Palestine.

1.2 Research Problem

Because of the rapid technological advancement and the resulting IoT applications, an efficient wireless network is needed to provide communication and information exchange between these devices, but this wireless network must match the requirements of these

applications in terms of low cost, low data transfer rate, and long coverage, in addition to low energy consumption. In this study, LoRa network technology will be investigated to verify the efficiency and the possibility of using such technology to transfer information in the future between these types of applications in a specific region by calculating the received power strength at the receiver side and predicting the parameters for the path loss model in the studied region.

1.3 Research Goal

- Collect real measurements using LoRa modules.
- Propose new parameters for path loss model in different scenarios in indoor and outdoor environments for LoRa technology.
- Validate the proposed parameters for path loss model.

1.4 Importance and Expected Impact

- This study will help to understand the channel behavior based on the received signal strength.
- This study will also provide accurate empirical propagation parameters for path loss model for Birzeit city using real-world data measurements using LoRa devices (transmitter (Tx) and receiver (Rx)).
- The proposed empirical propagation model parameters' for Birzeit city will help in future to optimize the network parameters when deploying IoT applications and achieve the best connection and provide a high quality of experience in this region.

1.5 Research Methodology

This thesis will present an in-depth study of the radio propagation characteristics, considering different distances between Tx and Rx in Birzeit. In particular, indoor and outdoor tests will be performed. Based on empirical results, new parameters for path loss models for LoRa communications under various scenarios will be proposed. This will be applied by the following working scenarios:

1. The measurement setup parameters will be set on the Tx device, such as Carrier Frequency (CF), Bandwidth (BW), Transmission Power (Ptx), Spreading Factor (SF), and Coding Rate (CR).
2. Measure the power received at the Rx nodes (Gateways) at different distances between Tx node and Rx.
3. Understand and use the measured data to propose new parameters for path loss models for the studied city.

1.6 Report Outline

The report is divided into five chapters, which are arranged as follows:

- Chapter 2 summarizes a group of prior studies about LoRa communication in various environments, including indoor, outdoor, and indoor-outdoor environments.
- Chapter 3 presents the physical layer of LoRa technology, followed by a mathematical model of this research, information about the Semtech LoRa module SX1276RF1JAS, instructions on how to connect the module and use it properly, and finally measurement scenarios.
- Chapter 4 presents the path loss model based on measurements and the fitted model based on proposed parameters, then moves on to discuss path loss and compare the fitted models based on proposed parameters with other models in the literature, then a validation of the fitted model based on the new parameters is provided and finally shadow fading for measurements is presented.
- Chapter 5 concludes the research, summarizes the contribution, and discusses the limitations before finally addressing future works.

Chapter 2 Literature Reviews

This chapter presents prior studies that utilized propagation models to investigate LoRa technology. These studies were carried out in indoor, outdoor, as well as indoor-outdoor environments. The research problem, its findings, and the parameters of the proposed models will all be illustrated in this chapter.

2.1 Indoor Scenarios

Most smart IoT application technologies will rely on LoRaWAN wireless technology to communicate in the future. To achieve the best network performance, the deployment of these applications requires a careful study of path loss and frequency budget allocation. The authors in [1] presented an extensive study of an indoor environment at the Saint Joseph University campus in Beirut (ESIB-USJ). Based on actual experiments, an accurate model of path loss for LoRaWAN at 868 MHz was developed and compared to other known models in the region. The practical experiment was conducted in a multi-story building on the university campus. All obstacles were considered (walls, floors, offices and classes), and the end devices were moved in 70 locations across four floors, covering a distance of 5 m –110 m. The effect of the walls and the floor was investigated, and the cumulative distribution function of the shadowing was calculated for the difference between the measured and estimated values using well-known models; Cost 231- Multi-Wall-and-Floor (MWF) model, International Telecommunication Union Radiocommunication (ITU-R) model, free space and Third Generation Partnership Project (3GPP) model for Cellular-IoT. The results were demonstrated that the proposed model more accurately represents the practical measured readings followed by ITU-R with mean of 0.48 and standard deviation of error of 8.3 dB, free space underestimate the measured value, Cost 231-MWF and 3GPP models also with standard deviation of error of 8.7 and 10.2, respectively.

The authors in [8] investigated the performance of LoRa technology in indoor buildings. The test was carried out in four different buildings: An office building, a residential building, a parking lot, and a warehouse. The first building has six floors and a basement; the second has five floors and three basements; the third only has five floors; and the final building only has one floor. Distance-dependent path loss measurements are used to determine the large-scale fading characteristics. The automatic correlation for shadowing is calculated and has decreased exponentially with distance. The Tx and Rx were placed in one of two scenarios: Either on the same floor and at the same height or on

different levels, so in the case of warehouse, Tx and Rx was separated by a number of shelves. The findings demonstrated the potential of the slope path as a first-order predictor of path loss in the indoor environment. The attenuation factor model is required if we want to increase the accuracy of the path loss in a multi-story building, and the decorrelation distance in a multi-story building is short, indicating that the large-scale fading is independent of area to area.

A study of the performance and range of the LoRa link at 2.4 GHz was presented in [9]. The investigation of the maximum communication range in free space, indoor, and urban outdoor environments, along with a mathematical description of the physical layer, was done along with simulations of signal propagation at various Spreading Factors (SFs) and BandWidths (BWs). The Indoor Dominant Path Model (IDPM) model in an office setting was used to represent the indoor path, and the free space path loss model was used to represent the free space environment. The results showed that as the distance between the Tx and Rx increased, the DR decreased logarithmically. Additionally, the maximum range in free space and indoor area was 133 km and 74 m respectively.

Kulkarni et al. conducted a study at a university campus in the United Arab Emirates (UAE) to support claims in the literature about the coverage of LoRa technology, which refers to distances of several kilometers in difficult conditions and challenging environments [10]. The peripherals are placed in both indoor and outdoor environments on campus. First, for an indoor environment, the authors set up three end nodes in the same building as the Gateway (GW), one inside the cafeteria, two on the same floor but on the opposite end with no Line of Sight (LoS), and one on a different floor but with None Line of Sight (NLoS) as well. According to the results of the tests conducted for this study, a range of 500 m or less was the maximum that could be achieved in an obstructed NLoS environment when Ptx was set to a high level. Performance can be affected by selecting conservative parameter settings, such as using worse SF and Coding Rate (CR) values depending on the deployment scenario.

The effectiveness of LoRa was evaluated during the construction of the so-called smart campus on the National Chiao Tung University campus at a frequency of 915 MHz [11]. Three different scenarios were examined in this research; indoor, outdoor and outdoor air quality measurements. When the end devices were initially placed on the second floor in indoor environment, the effect of distance on packet loss was first investigated. The findings indicated that at a distance of 1200 m, the percentage of loss increased to reach

60% or 90% due to the placement of end node in the second floor, and the greater the distance, the greater the loss which means IoT applications for indoor environments cannot be reliably supported with LoRa technology. Given that the Payload (PL) was set to 8, 16, and 22 bytes for two devices and that data was gathered from two LoRa GWs, the results for the packet loss with PL demonstrated that increasing PL does not always result in an increase in the loss percentage. According to the findings, the first device suffered the greatest loss at 16 bytes, while the second device suffered less loss at the same size. The same settings were used to examine how the weather affected the packets, and the results revealed that a light afternoon rain increased loss by 20%.

The performance and characteristics of Semtech's LoRa technology have been validated in terms of coverage in various scenarios, battery life, capacity, and the relationship between different LoRa parameters in [12]. The study was done in Singapore's Nanyang Technological University in Indoor environment to investigate the extent of coverage of this type of technology in the indoor and semi-indoor environments, where the internal environment refers to terminal nodes placed inside the building and the semi-internal environment refers to nodes placed under a shelter [12]. For ten minutes, each node sent a packet with a PL of ten bytes. The experiment was conducted in an area of 2 x 2 km for the indoor and semi-indoor environments, and SF12 was able to cover the area with little degradation. The placement of gateways and end nodes must be carefully considered in order to ensure LoS for the best coverage.

2.2 Outdoor Scenarios

The outdoor environment is divided based on the studied environment into three types: urban, suburban, and rural. Studies of each type will be reviewed separately in the following sections.

2.2.1 Urban areas

The LoRaWAN network has been adopted as a promising technology for smart IoT applications due to its properties. Because of the large number of sensors that send and exchange data, IoT applications rely on a large and dense network. The network's scalability in urban environments was investigated using the confirmed and unconfirmed modes [13]. The findings indicated that the use of SF12 in urban environments is higher than

Table 2.1: The proposed model variables for indoor environments

Reference	Publication Year	Parameter	Scenario	Proposed Model
[1]	2019	f	NLoS	-
		f_0		-
		d_0		1m
		d		m
		A		2.85
		B		-
		G		120.4
		$X(\sigma)$		8 dB
		PL_w		$n_w L_w + n_f \binom{n_f+2}{n_f+1} L_f$, where $b=0.47$, $L_f = 10$ and $L_w = 1.41$
[8]	2020	f	NLoS	-
		f_0		-
		d_0		1m
		d		m
		A		Non fixed intercept→First building: 3.54, second building:3.33, third building: 3.93, fourth building: 2.41 Fixed intercept→First building: 4.36, second building:4.29, third building: 4.13, fourth building: 3.11
		B		-
		G		-
		$X(\sigma)$		Non fixed intercept→First building: 5.34, second building:4.83, third building: 4.86, fourth building:5.27 Fixed intercept→First building: 5.38, second building:5.04, third building: 5.07, fourth building: 5.74
		PL_w		Non fixed intercept→ First building: 40.7, second building:39, third building: 41.3, fourth building:42.7 Fixed intercept→First building: 37, second building:37, third building: 36, fourth building: 36
[9]	2020	f	NLoS	-
		f_0		-
		d_0		1m
		d		m
		A		5
		B		-
		G		40 dB
		$X(\sigma)$		-
		PL_w		$\sum_i L_{W_i} + \sum_j L_{B_j}$ where $\sum_i L_{W_i} = 6$ and $\sum_j L_{B_j} = 3$

other values, and compared to free space also. The ratio of transmission success decreases as the number of end nodes increases for both confirmed and unconfirmed modes, that the unconfirmed mode achieves the best transmission success ratio compared to the confirmed mode for both free space and urban area, and that the free space path loss model outperforms the urban model in both modes.

Three empirical propagation models in [14] were used to predict the strength of the received signal at the LoRaWAN GW using NS3 simulation tool: Okumura-Hata, COST-231 Hata, and COST-Walfish-Ikegami (WI). The actual study was carried out in an urban environment in Glasgow, Scotland, and the actual measurements were compared to the predicted ones resulting from NS3 to calculate the accuracy of these models in prediction. The gateways were spread out over three locations at varying heights; one was located atop the George More building at Glasgow Caledonian University, another was a top of Skypark, and the last one was a top of the James Weir building at Strathclyde University at heights of 30 m, 27 m, and 27 m, respectively. These three GWs receive packets from End Nodes (EDs) that change their location within the city. According to the findings, the COST-WI model overestimated the power of the received signal, while the other two models underestimated it. The Okumura-Hata model was the most accurate, while the COST-WI model was the least accurate.

In [15], the coverage area and signal strength of a LoRaWAN network in DKI Jakarta, Indonesia, were investigated, which faces many challenges in deploying such technology due to its urban nature. The DKI Jakarta is divided into six regions, five of which are serviced by the LoRaWAN Network, as reported in the results. It categorizes based on RSSI into three categories: $RSSI \leq -110$ dBm, -109 dBm \leq $RSSI \leq -62$ dBm, and $RSSI \geq -61$ dBm. However, eight blank spots were not covered as a result of high-rise buildings. The percentages of covered area and blank spots were 79.392% and 20.608%, respectively. According to the authors, careful planning of the link budget and radio frequency allocation is required.

The study of LoRa technology in tropical environments at a frequency of 433 MHz is the basis for the research in [16]. The results of LoS communication in an urban environment show that LoRa suffers from attenuation due to the climate in those environments. The study also demonstrated that the ability to adjust SF and BW has an effect on improving coverage, but paying attention to the DR must be considered. For LoS scenario, the distance between the Tx and Rx changed from 20 m to 1500 m, and the

Received Signal Strength Indicator (RSSI) was then measured. The minimum RSSI was equal to -98 dBm at 1170 m.

The efficiency of LoRaWAN technology was studied in an urban environment with a high population density, factories, buildings, gardens, and streets in Beirut, Lebanon [1]. The experiment was carried out over 60 Km² area, with the GW placed at a height of 200 m and the EDs moving around it with a height of 20 cm, 1.5 m, and 3 m at a maximum distance of 9 km. The results confirmed the effect of antenna height on path loss reduction. It also revealed that medium obstacles caused a partial block in NLoS communication such as trees, whereas large obstacles, such as buildings, cause a complete block in NLoS communication and prevent some areas from being covered, such as the Ras Beirut area, which is 9 km from the gateway, while the El Manara area, which is 8.5 m away, is partially blocked, but reaching Packet Data Rate (PDR) of 90%. It was discovered that the proposed model represents the measured data with greater accuracy than other models which are free-space path loss, Okumura–Hata model, Cost 231-Hata and 3GPP-Unlicensed Mobile access (UMa) model. Okumura–Hata model and Cost 231-Hata predict higher value of path loss with a mean of 2 and 3.9 dB, respectively, and 7.6 dB of a standard deviation of error, while 3GPP-UMa model gives low predicted values with a mean error of -1dB and standard deviation of 7.4 dB. The proposed model fits the measured data in an accurate way compared to other models.

Actual measurements were taken at the Oulu campus in Finland to study LoRa coverage at 868 MHz and model channel attenuation [17]. Two scenarios were discussed: the first involved placing the ED on a car moving at a certain speed at a height of 2 meters above the ground, and the second involved placing the ED in a boat on the water. The base station for Kerlink's LoRa was installed on a tower at the University of Oulu at an altitude of 24 meters above sea level. According to measurements, the communication range on the ground was greater than 15 km and was 30 km in the water and the number of received packet decreased as the distance increased. The measured data, expected loss, and free space loss model of the data sent from the end nodes to the base station were plotted. The expected model in both scenarios was more in line with the measured data than the free space path loss model.

Dobrilovic et al carried out a study to examine the effectiveness of the Lee model in managing and planning networks based on LoRa technology in urban areas, where the measured results were compared with the calculations of the propagation model [18]. Using

a frequency of 868 MHz, the study was carried out in Zrenjanin, Vojvodina. Measurements are taken at seventeen different locations differ in terms of latitude and longitude of the measurement position, as well as the distance from the central location, then the RSSI is calculated. The expected signal strength was calculated for urban areas of Philadelphia, Newark, Tokyo and sub-urban, rural and free space for the seventeen locations. Mean Squared Error (MSE) and Root Mean Squared Error (RMSE) calculations were used to determine the accuracy of the models to represent the measured data. The findings demonstrated the usefulness of Lee's model for designing and planning LoRa networks in urban settings. Tokyo had the lowest RMSE, with Philadelphia and Newark coming in second and third, respectively, with average differences of 6.71731 dB, 15.0949 dB, and 19.5495 dB.

Using two mobile nodes operating at frequencies of 433 MHz and 868 MHz in Dortmund, Germany, the researchers in [19] examined the availability of LoRa technology while considering scenarios for smart cities. The measurement results were then compared with those of other well-known models, including the Free Space, Okumura-Hata, ITU Advanced, Winner+, and 3GPP Spatial (Urban) path loss models. In the first scenario, the GW was positioned at a height of 30 m on a building on the campus of the University of Dortmund, and the EDs were mounted at a height of 1.7 meters on a moving vehicle. A number of nodes were installed in the city at specific locations to conduct the reliability test. According to the availability analysis's findings, blind spots caused by shadows started to appear at a distance of 2 km, and the signal could be received up to a distance of 5.8 km. Finally, due to other models' inaccurate representations of the measured data, two new path loss models at 433 MHz and 868 MHz are proposed and the path loss in Dortmund increased steeper with distance due to high building compared to Oulu.

LoRa is presented by the authors in [20] as an adhoc network option for integration in an urban environment. Where the viability of using public transportation that carries these sensors that form Wireless Sensor Networks (WSN) to transmit data for environmental monitoring, such as environmental pollution and meteorological parameters, is evaluated, and data is then transferred to a central node for processing. Path loss, shadowing, and multipath were taken into account as the researchers worked to provide a theoretical analysis of propagation performance in terms of range and receiving power. These results indicate that the LoRa nodes mounted on vehicles may be able to communicate with the 500-meter GW at 0 dBi.

The performance of LoRaWAN was examined by the authors in [21] in a variety of urban, rural, and suburban scenarios. Various physical layer configurations were assessed based on the propagation circumstances. Using the Okumura-Hata model and topographical maps, a precise mapping tool evaluated the signal level. The base station was placed in the Faculty of Computer Science on the top of a five-story building in the University of Murcia, Spain, and the antenna was pointed towards the test area. Since the antenna was constant throughout the experiment, the goal of this process was to improve gain. The route went through a downtown area with three streets and tall buildings up to 15 stories. The radio planning tool was used to estimate the signal strength of the areas the base station covered in order to present the results for theoretical coverage first. By providing maps based on antenna gain and height, receiver sensitivity, and capacity, the impact of terrain heights on signal propagation was studied. The estimates were obtained using the Okumura-Hata model, and the findings indicated that the coverage range was 7km in urban area.

The authors in [12] extends their work to study the performance of LoRa technology in various scenarios in outdoor area. A new algorithm has been proposed to determine the optimal values of coverage and power consumption, as well as to investigate the feasibility of implementing medium access in such technology. This study was carried out at Singapore's Nanyang Technological University. LoRa has demonstrated a greater ability to communicate in direct LoS environments as claimed, while its performance degrades in the presence of obstacles. In terms of the direct LoS path, the experiment was carried out on a beach near a few buildings, and the packets were sent with a PL of 10 bytes for a distance of 9.08 km from each node using the same settings. The NLoS experiment was carried out on the university campus, where the density of buildings with heights of 100 m, with high vegetation density. and packets with a PL of 10 bytes were sent for ten minutes. The results showed that for direct LoS, SF7 can cover up to 4 km with a packet rate of 90% and SF12 can cover distances greater than 9 km with a packet rate of 70%. In terms of NLoS, buildings obstructed the communication path, resulting in coverage of up to 0.1 km with a packet rate of 90% at SF7 and less than 2 km with a packet rate of 70% at SF12.

2.2.2 Suburban areas

In [1], a performance of LoRaWAN in a suburban area on the ESIB-USJ campus was studied, where the campus dimensions were 200 m from north to south and 280 m from east to west. The campus area has a medium user density, buildings with up to four floors,

Table 2.2: The proposed model variables for urban outdoor environments

Reference	Publication Year	Parameter	Scenario	Proposed Model
[1]	2019	f	NLoS	-
		f_0		-
		d_0		1m
		d		m
		A		4.179
		B		-
		PL_0		102.86
		X_{TX}		-6.3 dB
		X_{RX}		
		$X(\sigma)$		7.2 dB
[17]	2015	f	NLoS	-
		f_0		-
		d_0		1m
		d		m
		A		For car: 2.32, Boat:1.76, freespace:2
		B		-
		PL_0		For car: 128.95, Boat:126.43, freespace:91.22
		X_{TX}		-
		X_{RX}		-
		$X(\sigma)$		For car: 7.8dB, Boat:8dB, freespace:-
[19]	2017	f	NLoS	-
		f_0		-
		d_0		1m
		d		m
		A		For Oulu 868 MHz: 2.32, Dortmund 868 MHz:2.65, Dortmund 433 MHz:2.65
		B		-
		PL_0		For Oulu 868 MHz: 128.95, Dortmund 868 MHz:132.25, Dortmund 433 MHz:126.50
		X_{TX}		-
		X_{RX}		-
		$X(\sigma)$		-

trees, and mountains. The results demonstrated the effect of antenna height on path loss reduction and RSSI improvement. Linear polynomial compatibility was used as a function of logarithmic distance and ED antenna height. The proposed model demonstrated its ability to accurately represent the measured data. Despite the high shadowing rate in the region, LoRa's PDR, Signal to Noise Ratio (SNR), and RSSI were 80%, 8.5, and -86 dB, respectively.

Authors in [16] investigated NLoS paths in a suburban area in order to investigate the effect of attenuation on LoRa in the tropics environment. The RSSI was calculated after the signal passed through eight buildings on Jalan Medan Bakri in Muar, Johor. The signal Ptx was set to 20 dBm, and the results showed that the more buildings that passed through, the lower the RSSI, but LoRa has promising future in NLoS communication. RSSI was -110 dBm when passing through the eighth building and -96 dBm when passing through the first building.

The performance of Narrow Band (NB)-IoT technology was evaluated in the Brazilian city of Santa Rita do Sapuca-MG [22]. The measurements were taken along four distinct routes. The performances of three well-known diffusion models, Cost-231 Hata, ITU-R 1225, and Erceg-Greenstein, were compared. The measurement environment was carried out on four roads: the first, a straight-line path with some small elevation differences; the second, a path that crosses the city with residential buildings; the third, similar to the second but with vegetation; and the final, on the highway, where RSSI was measured. The results demonstrated that the Cost-231 Hata model is the most accurate in measurements representation, with the lowest mean absolute error of 3,588488 followed by ITU-1225 with mean absolute error 8,568521 and then the third one Erceg-Greenstein with mean absolute error of 14,74494.

Table 2.3: The proposed model variables for sub urban outdoor environments

Reference	Publication Year	Parameter	Scenario	Proposed Model
[1]	2019	f	NLoS	-
		f_0		-
		d_0		1m
		d		m
		A		3.119
		B		-
		PL_0		140.7
		X_{TX}		-4.7 dB
		X_{RX}		-
		$X(\sigma)$		9.7 dB

2.2.3 Rural areas

A study of the rural area was conducted by Chall et al [1], which is characterized by low user density, vegetation, and hills. The GW was installed at a height of 70 m on the top of the Kefraya tower, and the EDs were installed at heights of 20 cm, 1.5 m, and 3 m, with a maximum distance of 20 km. The relationship between the antenna height of end devices and path loss was confirmed, which plays an important role compared to urban areas,

whether in LoS or NLoS paths. The proposed model was compared to Okumura–Hata model and 3GPP-UMa model and found to be the most accurate. In more details, the effect of antenna height versus path loss was studied, the results show that at height of 1.5 m and 3 m, n was 1.95 which close to free space loss model, and at 20 cm the effect of Frensel zone cause NLoS, and the high density of vegetation is the main reason for path loss in this type of region. Compared to the urban area loss factor in rural area is higher, and increasing the antenna higher in this region improve the strength of the received signal. Okumura–Hata model underestimates the path loss with mean and standard deviation of -17 and 6.9 dB, 3GPP-UMa model is closer compared to Okumura–Hata with error mean and standard deviation of 1 and 6.9 dB, and the proposed model was the accurate one with mean 0 and standard deviation of 6.45 dB. The results also show that the EDs can communicate up to 9 km in urban area and up to 47 Km in rural area.

Masadan et al [23] studied the effect of vegetation on the propagation model on the campus of the International Islamic University in Malaysia (IIUM), focusing on five types of trees which are *Licuala Grandis*, *Mimusops Elengi*, *Mangifera Indica*, *Cyrtostachys Renda* and *Livistona chinensis*. To calculate the RSSI, the researchers ran several horizontal and slant scenarios with different antennas' heights for Tx and Rx. Because of the tropical environment in this region, the RSSI in LoS paths was lower than expected, and NLoS paths were influenced by obstacles between the Tx and Rx, in addition to the tropical environment effect. Okumura-Hata, Log-Normal Shadowing, and Vegetation and Foliage Models are three models used to develop this type of propagation. The researchers concluded that the Okumura-Hata model failed to measure the effect of foliage and vegetation when compared to the measured value of path loss with separation distance from 71 m to 1.4 km due to the nature of Malaysia weather, they also demonstrate that the tree trunk provides the greatest signal attenuation among the three types of path crossings, and discover that the *Mimusops Elengi* tree provided the greatest signal attenuation up to 20 dB among the five studied types of trees due to the density of its crown and its large size in slant NLoS path. The results at the horizontal path showed that as the number of obstructing trees increases, the RSSI value decreases for both LoS and NLoS paths. The results also showed that the highest attenuation happened at the first tree and lowest at the last two trees due to a gradual change in attenuation due to scattering.

According to [24], the authors provided a detailed illustration of the scenarios and measurements used to investigate the impact of vegetation in [23]. The research dealt with

the beginning of the LoS scenario between the Rx and the Tx at Saidina Hamzah Stadium in the IIUM university in a horizontal and slant path, where the height of the transmitting and receiving antennas in the horizontal path was 0.65 m and the height of the transmitting antenna in the slant path was 4.5 m. The results showed that when the distance between Tx and Rx gradually increased from 1 m to 15 m, the values of RSSI and path loss in the horizontal path ranged from -53 dBm to -74 dBm and 83 dB to 104 dB, respectively. As for the slant path, the distance ranged from 6 m to 25 m and the angle of inclination ranged from 9 to 30, the values of RSSI and path loss were -62 dBm to -80 dBm and 92 dB to 110 dB, respectively, with a fluctuation. The results showed that in both cases there is a big difference between the measurements and the actual values. In the case of NLoS in transmission due to tree foliage, it was divided into a slant passing from the trunk, branches, and top of one of five existing types of trees and a horizontal passing through one tree and a line of trees. The results showed that the angle of inclination for the tilted model ranged from 9 to 33, RSSI from -60 dBm to -94 dBm, and the attenuation from 1dB to 25dB. The results also showed the big difference between the measured and the predicted path loss by Okumura-Hata model. The model needs to be modified by adding the foliage and construction effects as in [23].

Another study was conducted on the Cocoa Research Institute of Eastern Ghana's farm in Taful in [25] to investigate the effect of vegetation in a tropical environment on LoRaWAN communications. A dense semi-deciduous rainforest surrounded the research site. The researchers set out to evaluate the performance of the LoRaWAN network and compare it to traditional propagation models such as COST-235, ITU-R, fitted ITU-R, and free space model. The results showed that fitted ITU-R underestimate the path loss, ITU-R underestimate the path loss at distance below 1Km but gives better estimation at a large distance, and the free-space model was the best at representing the measurements, despite the fact that it reduced the estimation in the tree canopy region by 56 dB, and COST325 fits the data at distance beyond 1Km.

Another study was carried out on a palm oil plantation in Kuala Kubu Bharu, Selangor, Malaysia, to assess the performance of LoRaWAN technology at 433 MHz [26]. The LoS measurements were taken in order to calculate the path loss exponent at various BWs and SFs. The NLoS measurements were used to investigate the effect of the trunk and canopy on path loss, and the expected path loss model was then compared to the Weissberger and ITU-R models, respectively. Multiwall path loss predicted model performed better than

Weissberger and ITU-R, with a MSE of 2.74 dB, followed by Weissberger with a MSE of 5.32, and finally ITU-R with a MSE of 23.24 dB. The proposed propagation model is based on an empirical study and is not appropriate for severe weather and heavy rain and more research and experiments should be taken in order to increase the accuracy.

To predict path loss in LoRaWAN communications, a new model called propagation loss based on Artificial Neural Networks (ANN) was proposed by Habaebi et al in [27]. The research was carried out at the IUM Gombak campus. This proposed model can predict the path loss based on a data set that is supplied to learn the channel behavior and then accurately find the path loss. The Tx was installed at a height of 30 m in the Mahallah Ruqayyah dormitory building on campus, while the receiving antenna was at 1.5 m. The separation distance increased by one step from 10 m to 1 km. Three ANN models were created: the first uses two inputs: distance and LoRa module Sn value; the second uses distance, BW, and RF factor; and the third model uses six inputs: Stanford University Interim (SUI), LEE, Hata (suburban) and Hata (urban), distance, and Sn value. The first model achieved 20-25 RMSE with most frequent errors less than 1 dBm, the second model achieved 23-26 RMSE with most frequent errors less than 4 dBm, and the third model, the hybrid model, achieved 15-16 RMSE with most frequent errors less than 3 dBm. These three models have demonstrated their efficiency in comparison to other well-known ones such as SUI, LEE, Hata (suburban), and HATA (urban), where they represented actual value with high accuracy. These findings were confirmed by RMSE, which showed that the proposed models had the lowest RMSE value, less than 14, indicating the best performance when compared to other models and the performance is better with lower values of RMSE. This demonstrates that this proposal will play a significant role in tropical climatic environments.

The performance of LoRa technology in the rural area was also examined by the authors in [21]. The average speed of the vehicles was set at 32.5 km/h with a 0.05 level of confidence. The test area was flat, almost free of structures of any size, and barely had high vegetation. In this instance, a base station was installed on the roof of the four-story Technology Transfer Center in the Fuente Lamo Technology Park. The chosen route used low traffic roads to travel up to 20 km east from the base station. According to an estimation made using a radio planning tool, the coverage area in rural areas was 19 km as a maximum distance. The distances in the rural areas was 18.5 at DR0/SF12 for the practical tests.

2.3 Indoor-Outdoor Scenarios

Hosseinzadeh et al [28] investigated the propagation of LoRa technology in an indoor-outdoor scenario and compared it to other well-known models such as log-distance and

Table 2.4: The proposed model variables for rural outdoor environments

Reference	Publication Year	Parameter	Scenario	Proposed Model
[1]	2019	f	NLoS	-
		f_0		-
		d_0		1m
		d		m
		A		3.033
		B		-
		PL_0		111.75
		X_{TX}		-6.65dB
		X_{RX}		-
		$X(\sigma)$		6.4 dB
[23]	2018	f	LoS	-
		f_0		-
		d_0		1m
		d		m
		A		3.03
		B		-
		PL_0		-
		X_{TX}		-
		X_{RX}		-
		$X(\sigma)$		16.71 dB
[23],[24]	2018,2019	f	NLoS	-
		f_0		-
		d_0		1m
		d		m
		A		4.81
		B		-
		PL_0		-
		X_{TX}		-
		X_{RX}		-
		$X(\sigma)$		17.51 dB
[26]	2022	f	NLoS	433 MHz
		f_0		1 MHz
		d_0		1m
		d		m
		A		2.34 for BW of 125 to 250 kHz, 2.9 for BW of 500 kHz
		B		2
		PL_0		$-27.55 + \sum_{C=1}^N C_N + \sum_{T=1}^N T_N$ where for $T \rightarrow y = -1.658 \ln(x) + 7.6515$ and for $C \rightarrow y = -2.256 \ln(x) + 9.242$
		X_{TX}		-
		X_{RX}		-
		$X(\sigma)$		-

COST231. The researchers also modified the second model, called the new one Adjusted COST231, to make it valid for outdoor scenarios as well. A hybrid model of a ANN and Adjusted COST231 was proposed, which improved propagation accuracy while decreasing the amount of data needed to train the ANN model. An optimization for the first three models' parameters was proposed. These experiments were done on the campus of Glasgow Caledonian University (GCU). Data was collected on the seventh and eighth floors of the Hamish Wood Building and the mobile moves inside the building. The first model yielded a path loss exponent of 3.9, constant loss of 3.4 dB, and a shadow fading mean and standard deviation of 0.25 and 6.8 dB, respectively. For the second model, constant loss was determined to be 17.32 dB, with wall attenuation ranging from 12.79 dB to 1 dB, with the first wall causing the greatest attenuation value, and this type of model does not provide accurate results for this type of scenario. The path loss exponent for the adjusted type to include the outdoor scenario was 2.4, constant loss of 4.1 dB, and the attenuation range varied from 1 dB to 8 dB. After optimization, MSE calculated log-distance, COST231, adjusted COST231, and the readings as follows: 45, 20.47, and 21.83, respectively, the first model did not provide good accuracy, while the difference between the following two models was small in estimating prevalence. The change in COST231 reduced the first wall attenuation from 12.79 to 5.10 dB while also determining the propagation characteristics. Attenuation-based distance and loss exponents, the number of walls blocking LoS, location coordinates, and optimized wall attenuation were passed to the network in the hybrid model. It is used to correct errors and inaccuracies and improve the performance and optimize COST231. ANN was used to generate estimation error of the optimized COST231. For the COST231 model, the hybrid model reduced the MSE from 21 to 11.23.

The study in [29] sought to investigate the feasibility of developing a smart campus based on LoRa technology at the University of A Coruña Campus of Elviña in Spain. In order to assess operating circumstances and performance, the received power level obtained by the in-house developed 3D Ray Launching simulator—which can simulate the urban environment, people, buildings, and vegetation—was compared with actual experimental measurements on campus. The findings indicated that the environment and characteristics of the university campus have an impact on LoRa performance, but they can be used to inform planning before deploying the LoRaWAN network to support medium-sized smart city applications in the future. The findings revealed that the simulation results and

experimental values had mean errors and standard deviations of 0.18 dB and 8.07 dB, respectively.

The authors in [10] extend their works to include outdoor-indoor environment, the study examines the effectiveness of communication between the studied location in another building, a blocked indoor location inside a student cafeteria with NLoS to the GW, and the GW in a mixed outdoor-indoor environment. The study demonstrates that communication in indoor obstructed environments at a significantly reduced range is feasible with the hardware and antenna used in the study, despite the sub-GHz band having better signal propagation characteristics.

Table 2.5: The proposed model variables for indoor-outdoor environments

Reference	Publication Year	Parameter	Scenario	Proposed Model
[28]	2017	f	NLoS	-
		f_0		-
		d_0		1m
		d		m
		A		2.4
		B		-
		PL_0		4.1
		X_{TX}		-
		X_{RX}		-
		$X(\sigma)$		1 dB – 8 dB

Based on the prior studies in literature that have been reviewed, general equations from previous empirical models can be extracted for indoor and outdoor environments, represented in 2.1 and Equation 2.2, respectively.

$$PL = 10A \log_{10} \left(\frac{d}{d_0} \right) + 10B \log_{10} \left(\frac{f}{f_0} \right) + G + PL_w + x(\sigma) \quad 2.1$$

$$PL = PL_0 + 10A \log_{10} \left(\frac{d}{d_0} \right) + 10B \log_{10} \left(\frac{f}{f_0} \right) + X_{Tx} + X_{Rx} + x(\sigma) \quad 2.2$$

Where PL represents the path loss, A is the variation of path loss with accordance to distance in meters, and the reference distance is d_0 , B represents the frequency dependent factor in GHz , and f_0 is the center frequency, and X_σ is the zero-mean Gaussian random variable in dB for both 2.1 and Equation 2.2. G represents the path loss intercept, and PL_w is the loss raised from walls in indoor environments in Equation 2.1. X_{Tx} and X_{Rx} in

Equation 2.2 are the parameters related the loss due to antenna height of Tx and Rx in outdoor environments. Table 2.6 summarizes parameters of previous empirical indoor models, while Table 2.7 summarizes parameters of previous empirical outdoor models.

Table 2.6: Parameters of Previous Empirical Models in Indoor environment

Parameter		Cost231 (1999)	ITUR (2017)	WINNER II (2008)	3GPP (2016)	IEEE802.11 (2004)
f		Hz	Hz	Hz	Hz	Hz
f_0		1 GHZ	1 MHZ	5 GHZ	1 GHZ	1 GHZ
d_0		1 m	1 m	1 m	1 m	5 m
d		meter	meter	meter	meter	meter
A	LoS	2	2.8	1.87	1.69	2
	NLoS	2	2.8	3.68	4.33	3.5
B	LoS	2	2	2	2	2
	NLoS	2	2	2	2	2
G	LoS	32.44	-28	46.8	32.8	32.44
	NLoS	32.44	-28	43.8	11.5	32.44
PL_w	LoS	-	-	-	-	-
	NLoS	$3.4 \times n_w$	-	$5 \times (n_w - 1)$	$5 \times (n_w - 1)$	-
σ	LoS	4	8	3	3	2
	NLoS	4	8	4	4	3

Table 2.7: Parameters of previous empirical models in outdoor environment

Parameter	Free Space	SUI	3GPP/ ITU-R (ITU-R 1225)	Cost 231 Hata	Lee
f	Hz	HZ	HZ	HZ	HZ
f_0	1 MHZ	2000HZ	1 MHZ	1 MHZ	0.9 MHZ
d_0	1 Km	1 Km	1 Km	1 Km	1 Km
d	meter	meter	meter	meter	meter
A	2	$a - bh_b + c/h_b$ $a=3.6, b=0.005, c=20$	4	$4.49 - 0.655 \times \log_{10}(h_{Tx})$	1.2
B	2	0.6	3	3.39	2
PL_0	32.44	$20 \log_{10} \left(\frac{4\pi d_0}{\lambda} \right)$	49	46.3	100.7
X_{Tx}	0	0	0	$-13.82 \times \log_{10}(h_{Tx})$	$-20 \log_{10} \left(\frac{h_{Tx}}{30.48} \right)$ $-10 \log_{10} \left(\frac{G_{Tx}}{4} \right)$
X_{Rx}	0	$-20 \log_{10} \left(\frac{h_{Rx}}{2} \right)$	0	$-((1.1 \log_{10}(f) - 0.7)h_{Rx} - (1.5 \log_{10}(f) - 0.8))$	$-10 \log_{10} \left(\frac{h_{Rx}}{3} \right)$ $-10 \log_{10} \left(\frac{1}{G_{Rx}} \right)$

Chapter 3 LoRa Communication Technology

This chapter discusses the physical layer of LoRa technology, a mathematical model of this study, some details about the LoRa module, its connection, and measurement scenarios.

3.1 Physical Layer of LoRa Technology

There are many wireless technologies available today, but the majority of them are unsuitable for the IoT as well as smart city communications and applications. Figure 3-1 illustrates how the coverage, DR, and power consumption of wireless networks vary [30]. In terms of the requirements of IoT applications, such as a lower DR, low power requirements, and wide coverage, the graph demonstrates that Wireless Local Area Network (LAN) Technology, Cellular Technology, and Personal Area Network Technology do not meet the needs of IoT applications. Therefore, what is known as LPWANs, whose performance is compatible with the requirements of these applications, was designed to form a wireless network that transmits information with high efficiency. For IoT and smart city applications, LPWANs offer an alternative to traditional wireless technologies [31]. It consists of various technologies, including SigFox, Weightless, Thread, NB-IoT, and LoRa [31]. The majority of these technologies operate in the sub-GHz in Industrial Scientific Medical (ISM) band [31],[32], where LoRa and SigFox, for instance, operate in an unlicensed band while NB-IoT, EC-GSM-IoT, and LTE-M-IoT operate in licensed bands [33],[30] and some of these can operate in licensed and un-licensed bands as Weightless [31]. In addition to that, most LPWAN technologies support physical layer communication using two alternative techniques: Spread spectrum and ultra-narrowband like LoRa and Sigfox, respectively [30]. This technology is characterized by high power efficiency, coverage, scalability, low cost, and simplicity of the network topology, but it has throughput and latency limitations [34]. According to the necessary requirements for coverage, BW, power budget, network cost, and expansion, the suitable technology is chosen for a given application [34].

One of the most important LPWAN technologies is LoRa communication technology. In 2014, LoRa's physical layer, which is primarily based on Chirp Spread Spectrum (CSS) modification, was patented [35]. CSS technology spreads a narrowband signal over a large channel BW, in addition to enabling bi-directional communication [31]. The resulting signal

exhibits noise-like characteristics, making it difficult to detect and more resilient to interference [31].

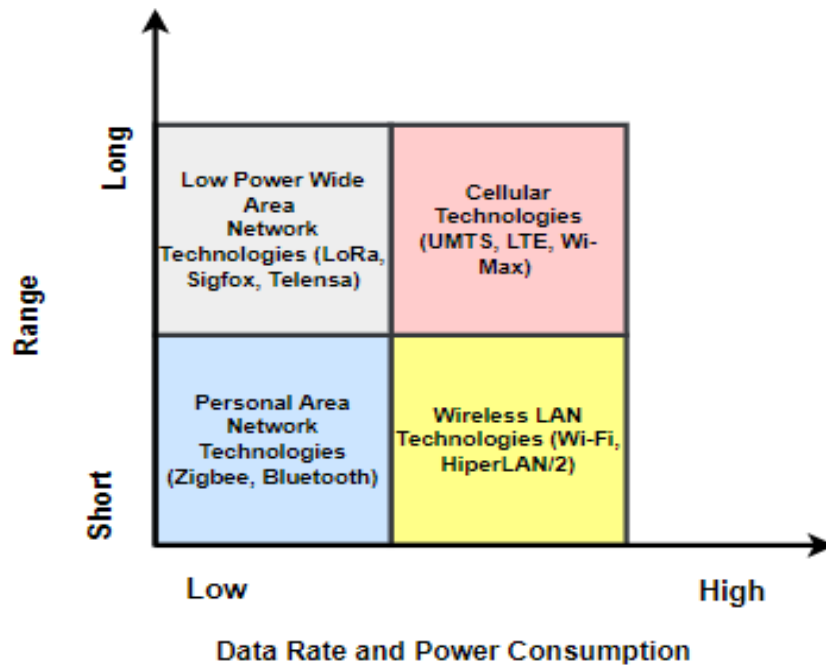


Figure 3-1: Comparison between different Wireless technologies

LoRa technology provides very long range communications and high flexibility against a variety of impacts. Its main method of operation is shaping the CSS with Forward Error Correction (FEC) to enhance the receiver sensitivity [31], [36], [37]. The signals were first processed by the FEC mechanism before being modulated and transmitted as a series of chirp pulses, which stand for linear signals centered in the channel BW of the center frequency [36] and fluctuating in frequency over time [37]. Table 3.1 summarizes a number of the most important characteristics of LoRa technology [33].

3.2 Background of Physical Layers Parameters for LoRa Technology

In the physical layer, BW, SF, center frequency, CR, and Ptx have an impact on the communication performance of this technology as following [38]:

- **Bandwidth (BW)**

BW is the frequency range that LoRa chirps spread over [38],[39],[40]. Three bandwidths are used by LoRa: 125 kHz, 250 kHz, and 500 kHz [38],[39],[40]. The relationship between radio sensitivity and air time with bandwidth is an inverse

relationship [38],[40]. The chip rate used for data transmission is the same as the bandwidth [38],[40]. As a result, a chip rate of 250 kchips/second is equivalent to a bandwidth of 250 kHz [39]. Equation 3.1 describes the Chips Rate (R_C), which is measured in chips/s [38],[40].

$$R_C = \text{Bandwidth} \quad 3.1$$

- Carrier Frequency (CF)

CF serves as the central frequency for the transmission range [39], as both Tx and Rx in LoRa use sub-gigahertz frequencies for communications [38],[40]. LoRa technology operates on the 433 MHz, 868 MHz, and 915 MHz radio frequencies in the ISM band [40].

- Spreading Factor (SF)

SF is the ratio between the chip rate and symbol rate [39]. Each symbol is spread across multiple chips to increase the receiver's sensitivity during the data transmission process [38],[40]. Higher SF leads to the longer the covered distances and the better the signal-to-noise ratio (SNR), but the longer the transmission times [39]. The number of chips per symbol is calculated as 2^{SF} [39]. For instance, 64 chips/symbols are produced when SF is equal to 6. Each increase in SF results in a halving of the transmission rate, ultimately doubling the transmission time and consuming twice as much power [39]. There are 6 to 12 options for the spreading factor [38],[39],[40] and it is used to create a trade-off between DR and coverage area [31]. It is important to note that in LoRa, packets transmitted with various spread factors are sent perpendicular to one another and do not collide if they are sent at the same time [36],[39],[40]. The most important point that the signals of the SFs are quasi-orthogonal, and will successfully separate with a minimum certain value of Signal to Interference and Noise Ratio (SINR) at the GWs [36]. The GWs are capable of decoding up to eight uplink transmissions simultaneously [36],[41]. A spreading rate of 2^2 to 2^{12} chips/symbol is produced based on the value of SF [40]. SF is necessary for calculating the Symbol Rate (R_S) measured in symbols/s defined in Equation 3.2 [38],[40].

$$R_S = \frac{R_C}{2^{SF}} = \frac{\text{Bandwidth}}{2^{SF}} \quad 3.2$$

The Modulation Bit Rate(R_M) that is produced based on R_S can be defined in Equation 3.3 [38],[40].

$$R_M = R_S \times SF = SF \times \frac{\text{Bandwidth}}{2^{SF}} \quad 3.3$$

Table 3.1: Characteristics of LoRa Technology Protocol [33]

Characteristics	LoRa Technology
Standard	LoRa Alliance
Frequency band	Unlicensed ISM band 433MHz, 868MHz, 915MHz
Channel Width	125 KHz, 250KHz, 500KHz
Modulation	Chirp spread spectrum (CSS)
Access Method	ALOHA, Slotted ALOHA
Range	Urban: 2 – 5 Km Rural: 15 Km
Data Rate	EU: 0.3 - 50 kbps US: 0.9 - 100 kbps
Duplex	Half
Topology	Star

- Coding Rate (CR)

CR represents the percentage of bits that carry actual information [41]. LoRa implemented FEC rate by LoRa modems to provide protect against interference bursts [38],[39]. Every data transmission using LoRa employs FEC to increase flexibility in handling corrupted bits [38], but this increases the time required for air transmission. Equation 3.4 represents the Bit Rate (BR) which is measured in bits/s [38],[40]. CR also has variable number of redundant bits' ranges from 1 to 4 [40]. The resulting bit rate (BR) of LoRa measured in bits/s, is written as:

$$BR = R_M \times \frac{4}{4 + CR} = SF \times \frac{\text{Bandwidth}}{2^{SF}} \times \frac{4}{4 + CR} \quad 3.4$$

When more interference bursts are anticipated, a higher CR is necessary to increase the chance of successful packet reception [40]. A higher CR will increase the time on the air even though more protection can be provided [39]. Additionally, radios with the same CF, SF, and BW but a different CR can still communicate [39].

- **Transmission Power (Ptx)**

Like most wireless radios, LoRa transceivers also allow the transmission power to be tuned, dramatically changing the power required to transmit the packet [40]. In most devices, the Ptx needed for transmission ranges from -4 dBm to 20 dBm, directly proportional to the power consumption. For values greater than 17 dBm, the duty cycle, which is computed hourly and corresponds to 36 seconds, is restricted to 1% [40]. The duty cycle represents the amount of time that the Tx is permitted to send data. If Lesson Before Talk (LBT) method is used, the duty cycle value changes [36]. The duty cycle values vary depending on the region because Europe places duty cycle restrictions on frequency bands while the United States of America places them on channels [36]. Table 3.2 summarizes the physical layer parameters' effects on communication performance [38],[40].

- **Chirp Spread Spectrum (CSS)**

Chirp Spread Spectrum (CSS) modulation disperses an input signal in a narrow band over a larger channel bandwidth [40], [42] using carrier signal consists of chirps [40]. CSS which converts each data symbol into a chirp signals with frequency rises or falls over time, is the basis of LoRa technology [43]. It enables signals to be reconfigured even when the received signal's power is 20 dB [40]. Because of the noise-like characteristics of the resulting signal, it is challenging to spot or drown out [42]. This type of modulation is one of LoRa's most important keys. The chirp pulse is a linearly increasing and decreasing frequency signal that fluctuates within the channel BW of the CF and increases linearly, as shown in Figure 3-2 [36]. SFs can be applied to the LoRa CSS signals of particular BWs to produce various gains and spectral efficiencies [36].

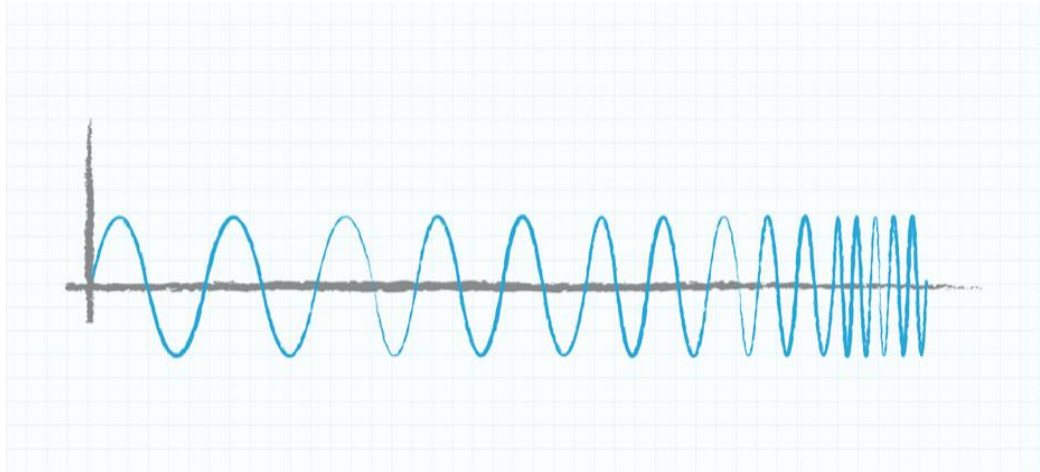


Figure 3-2: A linear chirp waveform is a sinusoidal wave that increases linearly in frequency over time [36].

Figure 3-3 illustrates how each chirp can be distinguished from another chirp of the same SF at the same channel frequency of a particular BW. The CSS signal will stop and restart at the lowest frequency once its instantaneous frequency reaches its maximum value [43]. The rate of increase is determined by the SF that is used, with value of SF ranges from 6 to 12 [44], and sometimes, from 7 to 12 [45]. Anyway, SF6 is not used in practice [36]. With lower SFs than with higher ones, a channel's BW traverses its SFs more quickly, resulting in higher data rates but also increased sensitivity to noise and interference as well as smaller coverage provided [36]. Therefore, data can be modulated over the central frequency of the chosen channel while being encoded using the chosen channel's bandwidth and spreading factor [36]. The chirp signal allows LoRa to operate at various data rates by encoding a number of SF bits with a maximum number of 2^{SF} chirp states possible through the chirp duration to achieve various data rate [36]. Chirp duration (T_s) is represented as in Equation 3.2 [36].

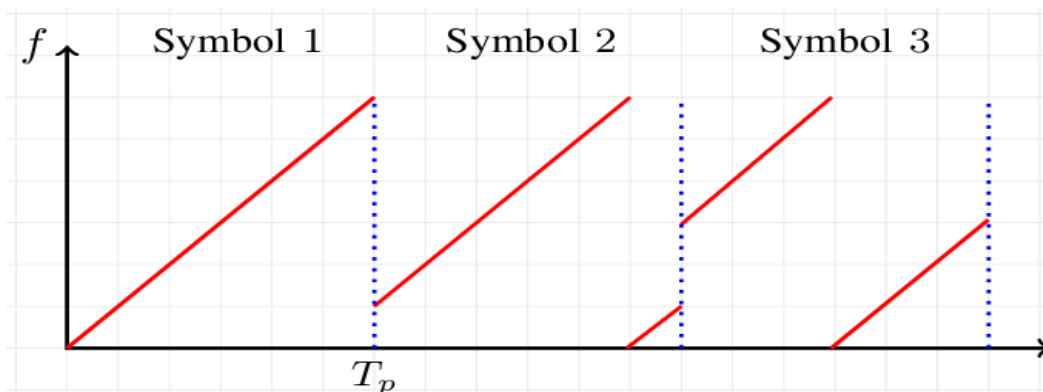


Figure 3-3: LoRa modulated signal [36].

$$T_s = \frac{BW}{2^{SF}} \quad 3.5$$

Table 3.2: The effect of physical layer parameters configuration on communication performance [38],[40]

Adjusted Parameter	Symbol	Value	Impact on Performance
Bandwidth	BW	125KHz, 250 KHz or 500 KHz	Higher bandwidth offers higher transmission and DRs over short distances, and also reduces the receiver's sensitivity and communication range.
Spreading Factor	SF	6 - 12	In addition to a strong signal with higher SNR, higher SF results in longer communication distance due to an improvement in the receiver's sensitivity. However, it offers a lower transmission rate due to longer packets, more time on air, and more energy consumption.
Coding Rate	CR	4/5 - 4/8	Smaller CRs offer better reliability against corruption, but overall they have a significant overhead causing longer packets and consume more energy.
Transmission Power	Ptx	-4 dBm - 20 dBm	Higher transmission power results in better range but in lower SNR and consumes more energy on the transmitter side.

3.3 Overview about LoRa Network Layer

A typical LoRa network is made up of EDs, LoRa GWs, a network server, and an application server [34],[38]. These components are connected with each other to form a star topology [34], where EDs represent sensor nodes that have sensors attached in order to gather the necessary readings for a particular application.

LoRa GW, which serves as a connection for exchanging the messages between EDs and the network server, must send these readings or data from the EDs to the server. The network server then plays a role in controlling the network's security, DR, aggregating data and removal of redundant packets while communicating with the application server, the application server then performs additional analyses on the sensor data before sending it to the specific application. Figure 3-4 illustrates the architecture of LoRa communication network [34], [38].

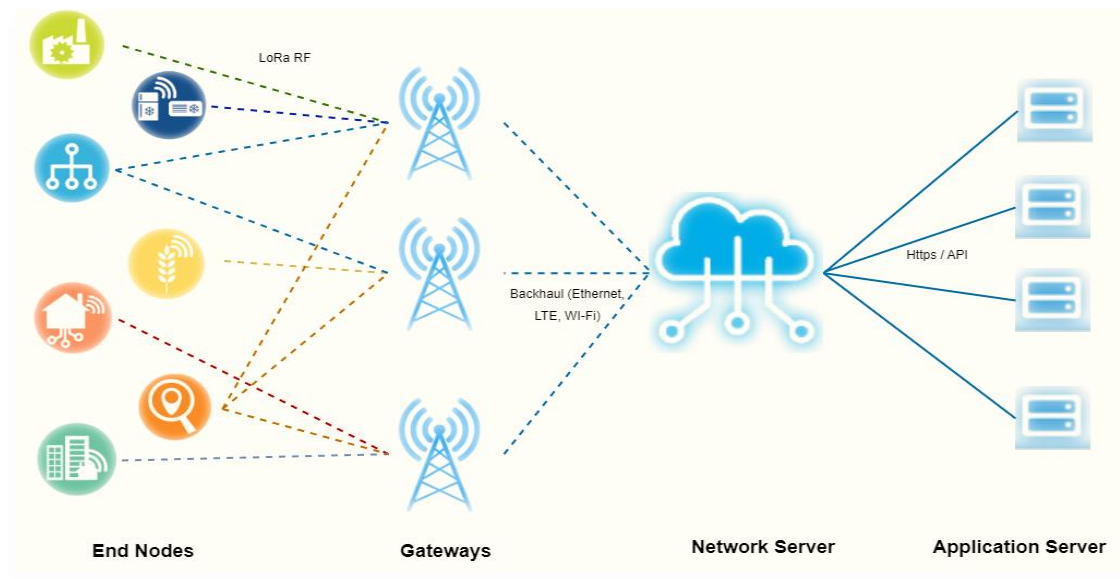


Figure 3-4: Communication network for LoRa technology

3.4 Mathematical Modeling

One of the most popular statistical analysis techniques is regression analysis [46]. These statistical techniques are used in many sciences, including the biological, physical, and social sciences, business, and engineering, for research planning and data analysis [47]. Whether it is a linear or non-linear regression, the concept of regression is based on the fitting of a function to a set of data in the sense of a least squares fit to create a regression line that fits this set of data so that the sum of the squares of the vertical distances from points to the line is the minimum [48],[49]. The regression method is also used to compare measurements with earlier models and determine the path loss model's parameters [50],[51],[52].

Linear regression is one of the basic statistical models used to determine the relationship between dependent and independent variables [49],[53]. The factors used to predict the value of the dependent variable are referred to as explanatory or independent variables, and the variable being predicted is known as the dependent variable, as shown in Equation 3.6, where the path loss represents the dependent variable and logarithmic distance and logarithmic frequency are the independent variables [53]. The result is a vector for various results rather than a single one, and this model is appropriate for simulating a set of inputs with multiple results [53]. The least squares regression technique can be used to model the path loss for both linear and nonlinear relations. Normal matrix techniques cannot estimate the coefficients A,

B, and G of non-linear relations as in Equation 3.6, so appropriate fitting algorithms must be used in order to do so. The two most widely used algorithms are Levenberg-Marquardt [54] and Trust-region [55]. The path loss equation given in accordance to [50],[51],[52],[56],[57],[58],[59],[60] is as follows:

$$PL = 10A \log_{10}\left(\frac{d(m)}{d_0}\right) + 10B \log_{10}\left(\frac{f(GHz)}{f_0}\right) + G + X_\sigma \quad 3.6$$

Where A is the variation of path loss with accordance to distance, d is the separation distance in meters, and the reference distance is d_0 , which is equal to 1m in indoor environments. B represents the frequency dependent factor, f is the frequency in GHz, and f_0 is the center frequency equal to 1GHz in most models except WINNER II. G represents the path loss intercept, X_σ is the zero-mean Gaussian random variable in dB, that represents the change in average received power with standard deviation σ . The regression method's aim is to minimize the value of σ to reach zero by minimizing the squares of the vertical distances between the measured data and the studied model [50]. The following provides an explanation of the regression techniques used to estimate the parameters of the various approaches. As will be demonstrated later, various modeling approaches were taken into consideration in this work. The first approach is to set the parameters B to 2 and to $20 \log_{10}(4\pi/c)$, where c is the speed of light and calculate the path loss exponent (A). The second approach is to extract the A and B parameters from the measurements while holding the G constant to $20 \log_{10}(4\pi/c)$.

The variation of the received signal is represented as follows [50]:

$$X_\sigma = PL - 10A \log_{10}\left(\frac{d(m)}{d_0}\right) - 10B \log_{10}\left(\frac{f(GHz)}{f_0}\right) - G \quad 3.7$$

For the first approach, D is equal to free space loss at a distance of 1m as represented in Equation 3.8

$$D = 10B \log_{10}\left(\frac{f(GHz)}{f_0}\right) + G \quad 3.8$$

Then:

$$X_\sigma = PL - 10A \log_{10}\left(\frac{d(m)}{d_0}\right) - D \quad 3.9$$

Giving that in [61]:

$$\sigma = \sqrt{\frac{\sum X_\sigma^2}{n}} \quad 3.10$$

Where n is the number of measured data, $E = PL - D$, and $F = 10A \log_{10} \left(\frac{d(m)}{d_0} \right)$

then:

$$\sigma = \sqrt{\frac{\sum (E - AF)^2}{n}} \quad 3.5$$

Reduce the value of the numerator to minimize the value of σ . Therefore, the numerator's partial derivative with respect to A should be equal to zero:

$$\frac{\partial \sum (E - AF)^2}{\partial A} = 0 \quad 3.6$$

Giving that:

$$\frac{\partial \sum_{i=1}^n (x_i + Ay_i)^2}{\partial A} = \sum \frac{\partial (x_i + Ay_i)^2}{\partial A} \quad 3.7$$

$$\frac{\partial \sum (E - AF)^2}{\partial A} = \sum 2F(AF - E) \quad 3.8$$

In [62], giving that:

$$\sum_{i=1}^n A = nA \quad 3.9$$

$$\sum_{i=1}^n Ax_i = A \sum_{i=1}^n x_i \quad 3.10$$

Based on Equation 3.8:

$$A = \frac{\sum FE}{\sum F^2} \quad 3.11$$

For the second approach, if $D = PL - G$, then Equation 3.7 can be written as:

$$X_\sigma = D - 10A \log_{10} \left(\frac{d(m)}{d_0} \right) - 10B \log_{10} \left(\frac{f(\text{GHz})}{f_0} \right) \quad 3.12$$

If $F = 10 \log_{10} \left(\frac{f(\text{GHz})}{f_0} \right)$ and $E = 10 \log_{10} \left(\frac{d(m)}{d_0} \right)$, then

$$X_\sigma = D - BF - AE \quad 3.13$$

Based on Equation 3.10:

$$\sigma = \sqrt{\frac{\sum (D - BF - AE)^2}{n}} \quad 3.14$$

Because A and B are both variables and using Equation 3.7, minimizing is equivalent to minimizing the numerator in Equation 3.14. In light of A and B, the numerator is thus partially derived as follows:

$$\frac{\partial \sum (D - BF - AE)^2}{\partial A} = \sum 2E(AE + BF - D) \quad 3.15$$

$$\frac{\partial \sum (D - BF - AE)^2}{\partial B} = \sum 2F(AE + BF - D) \quad 3.14$$

By solving Equations 3. and 3.14:

$$A = \frac{\sum FE \sum FD - \sum F^2 \sum ED}{(\sum EF)^2 - \sum E^2 \sum F^2} \quad 3.15$$

$$B = \frac{\sum FD - A \sum FE}{\sum F^2} \quad 3.16$$

To identify the path loss model's unidentified variables, all the aforementioned equations have been modeled in MATLAB. Additionally, the same parameters were estimated with MATLAB's nonlinear regression technique. The estimation process is more difficult when there are non-linear relations involved. By entering "cftool" in the command window as shown in Figure 3-5, the coefficients of Equation 3.6 can be estimated using the curve fitting tool in MATLAB.

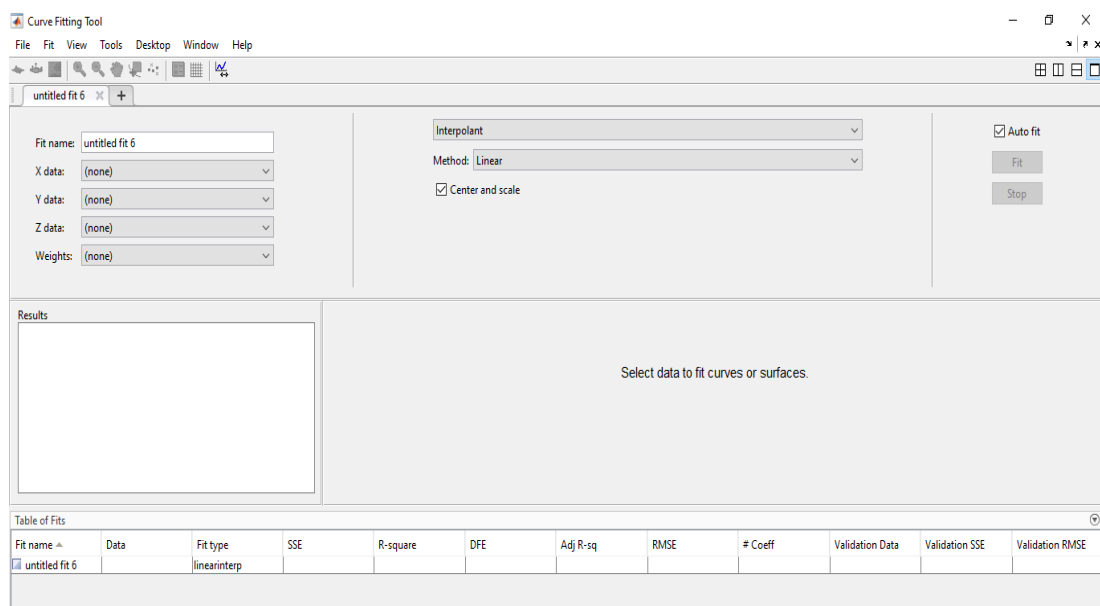


Figure 3-5: Curve Fitting tool in MATLAB

The process of importing the data to be modeled from the work space is first carried out as in Figure 3-6, and then the best model is selected for the measured data as in Figure 3-7. The user can also select a custom equation and create their own formula using the tool. The user can select between two different algorithms, as shown in Figure 3-8. A data fit example is shown in Figure 3-9, and the estimated coefficient of numerical fit results can then be calculated as RMSE as shown in Figure 3-10.

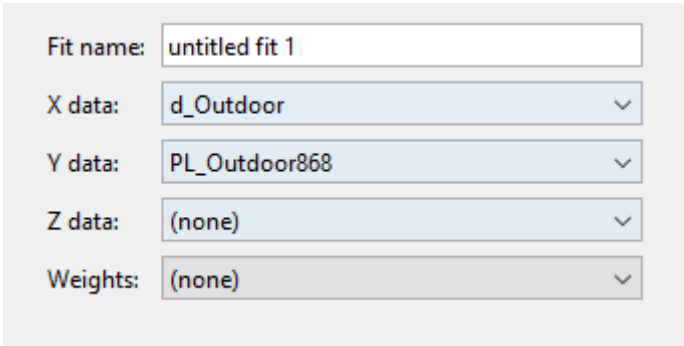


Figure 3-6: Data imported from CFtool in MATLAB workspace

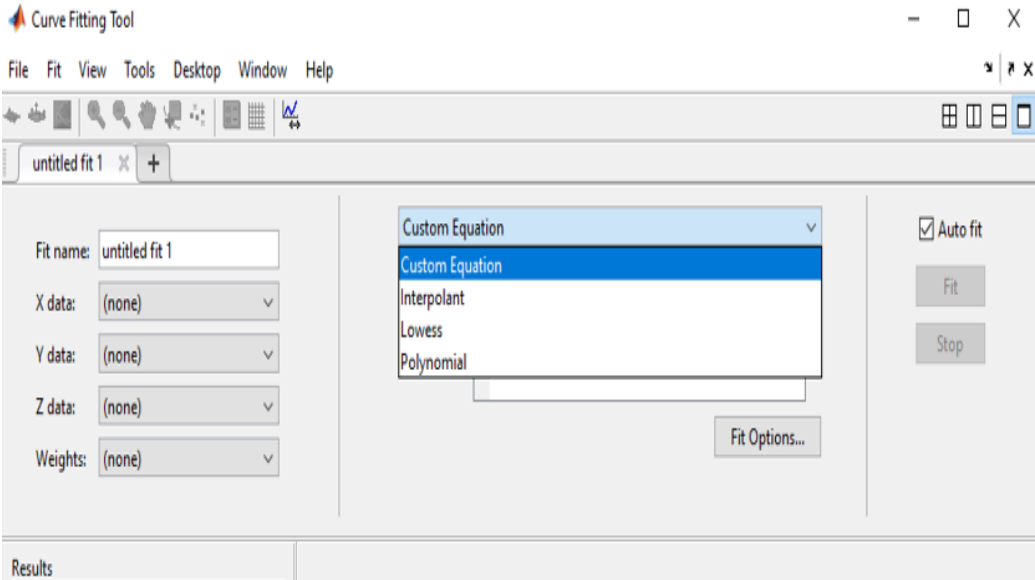


Figure 3-7: Curve fitting general models in MATLAB

Fit Options ✕

Method: NonlinearLeastSquares

Robust: ▾

Algorithm: ▾

DiffMinChange:

DiffMaxChange:

MaxFunEvals:

MaxIter:

TolFun:

TolX:

Coefficie...	StartPoint	Lower	Upper
a	0.4447	-Inf	Inf
b	0.4291	-Inf	Inf
c	0.1670	-Inf	Inf

Figure 3-8: Fitting options

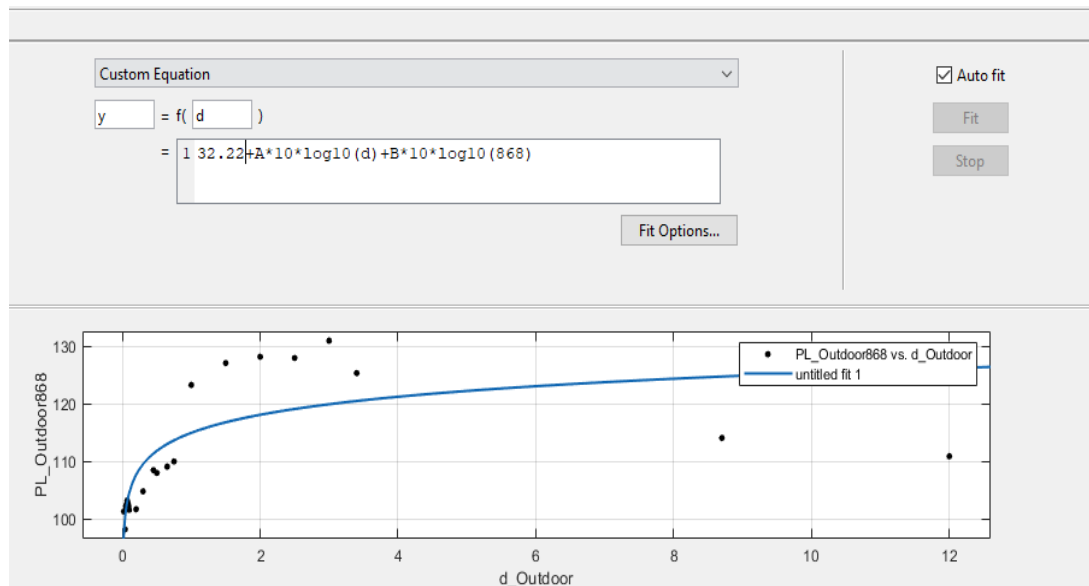


Figure 3-9: A Data fitting example

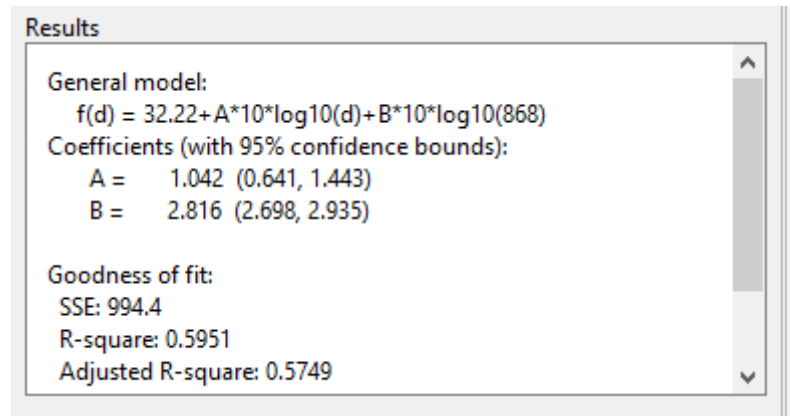


Figure 3-10: An Illustration of a fitted coefficient and fit outcomes

Where SSE in Figure 3-10 is the sum of squared errors, R-square is the coefficient of determination and it measures the goodness of fit between the data and the regression model while a version of R-squared that has been modified to account for the number of predictors in the model is known as adjusted R-squared [63].

3.5 LoRa Technology

For today's high-performance ISM-band RF applications, SX1276 single-chip integrated circuit is the perfect fit [64]. In addition to the well-known, high-performing, and reasonably priced Frequency-Shift keying (FSK) / On-Off Keying (OOK) RF transceiver modem, the SX1276 has a LoRa-specific transceiver modem [64]. While the high level of integration reduces the external bill of materials to a small number of passive decoupling and matching components, this advanced feature set, which includes a cutting-edge packet engine, greatly simplifies system design [64]. It is designed to be used in high-performance, long-distance, half-duplex bi-directional RF links where stable and constant RF performances are required over the device's entire operating range down to 1.8 V [64]. The SX1276 covers all sub-1 GHz frequency bands that are currently available and is designed for applications over a broad frequency range (168 MHz, 434 MHz, 470 MHz, 868 MHz, and 902 MHz) [64]. With a link budget of over 135 dB in FSK and over 155 dB in LoRa, the SX1276 effectively provides the option of two modems in a single unit. The SX1276 is offered in a 5x5 mm QFN 28 lead-free package and complies with Federal Communications Commission (FCC) and European Telecommunications Standards Institute (ETSI) regulatory requirements [64].

This module is divided into 3 types, each of which targets a specific range of RF bands, as follows [64]:

1. SX1276RF1IAS which is designed for 169 MHz and 868 MHz frequency band.
2. SX1276RF1JAS which is designed for 433 MHz and 868 MHz frequency band.
3. SX1276RF1KAS which is designed for 490 MHz and 915 MHz frequency band.

Each module of these three types is equipped with two RF antennas SubMiniature Version A (SMA) connectors. Each of these two antennas is responsible for providing a specific frequency band, one of them is Low-Frequency (LF) antenna connection, and the other is High-Frequency (HF) [64].

In our experiment, SX1276RF1JAS shown in Figure 3-11 with features of LF of 433 MHz and HF of 868 MHz antenna SMA connectors, 32 MHz XTAL reference clock, four PCB Layers, and LF and HF transmission powers of 14dBm or 20dBm [65] was used.

The two different types of antennas which is connected to this module and operates at 433MHz and 868 MHz, shown in Figure 3-12 .

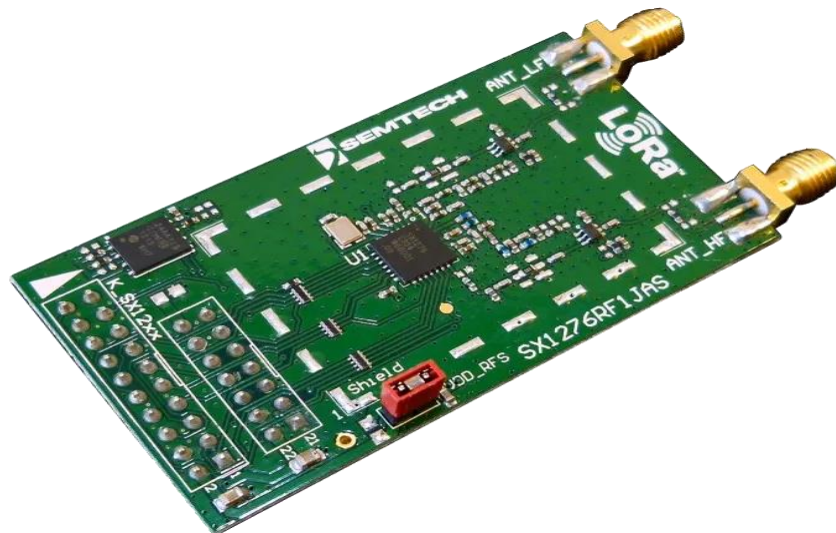


Figure 3-11: SX1276RF1JAS LoRa transceiver [64]



Figure 3-12: 868 MHz and 433 MHz frequency band antennas [64]

3.6 LoRa Connection

Arduino Uno chip, breadboard, and connecting wires shown in Figure 3-13 were used to connect and operate LoRa module. Table 1 summarizes the pins connection between the LoRa chip and Arduino Uno.



Figure 3-13: connecting wires, Arduino Uno chip, and breadboard

Table 3.3: LoRa and Arduino Uno Pins connection

SX1276RFJAS Pins	Arduino UNO Pins
RST-10	9
MOSI-3	11
MISO-8	12
SCK-1	13
DIO0-12	2
NSS-7	10
VDD-22	VDD (3.3V)
GND-24	GND (0V)
High Frequency (868MHz)→FEM_CTX-20	Tx circuit→VDD (3.3V) Rx circuit→GND (0V)
Low Frequency (433MHz)→FEM_CPS-18	Tx circuit→GND (0V) Rx circuit→VDD (3.3V)

As the manufacturer SEMTECH did not clearly explain the method of pins connection, several days spent to figuring out last two lines in the table, which

represent the two most crucial lines for operating the antenna that is connected to the LoRa chip.

Finally, the Tx and Rx circuits were connected to the computers to connect the chips with Arduino IDE 2.1.0 software, as shown in Figure 3-14 below.

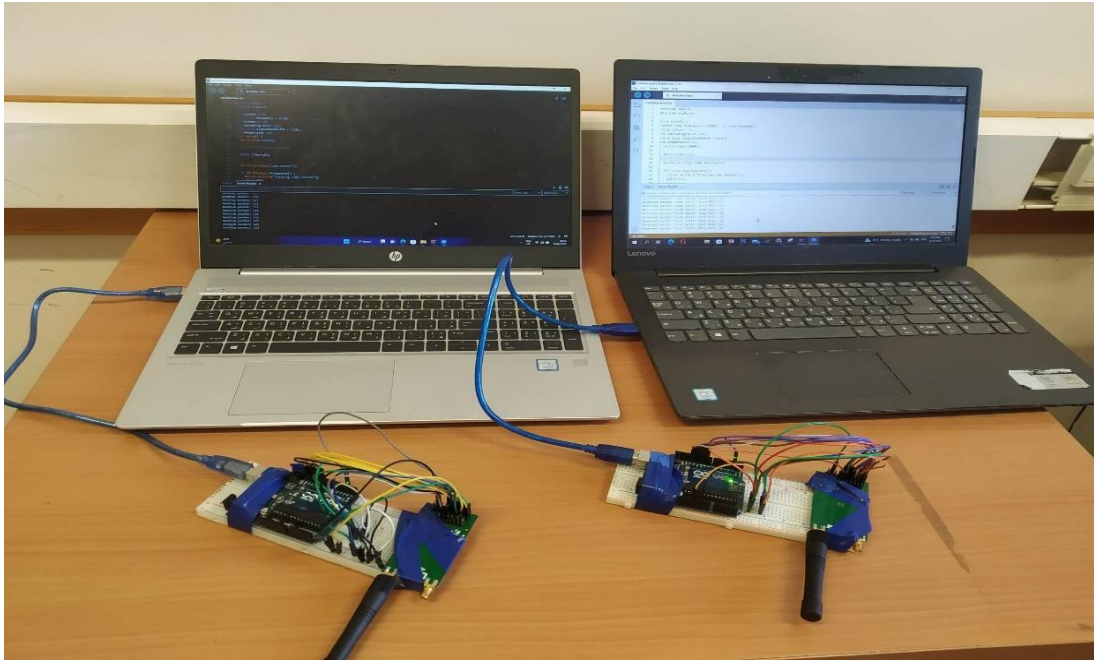


Figure 3-14: LoRa transmitter and receiver circuits.

3.7 Measurements Scenarios

This section outlines the measurement campaigns that carried out in practice in order to examine the effects of different parameters and conditions on the performance of LoRa technology. Our experiment deals with many aspects in indoor, and outdoor environments. Indoor and outdoor tests will be conducted primarily on the campus of Birzeit University shown in Figure 3-15.



Figure 3-15: Campus of Birzeit University

3.5.1 Indoor Scenario

On the campus of Birzeit University, one of the buildings will serve as the location for our indoor measurements. This scenario will be divided into sub scenarios inside Birzeit University's Faculty of Information Technology (Munib Al-Masri) building, shown in Figure 3-16 which has five floors, with structure described as a multiple-story concrete and steel structure for the most part, with interior corridors.

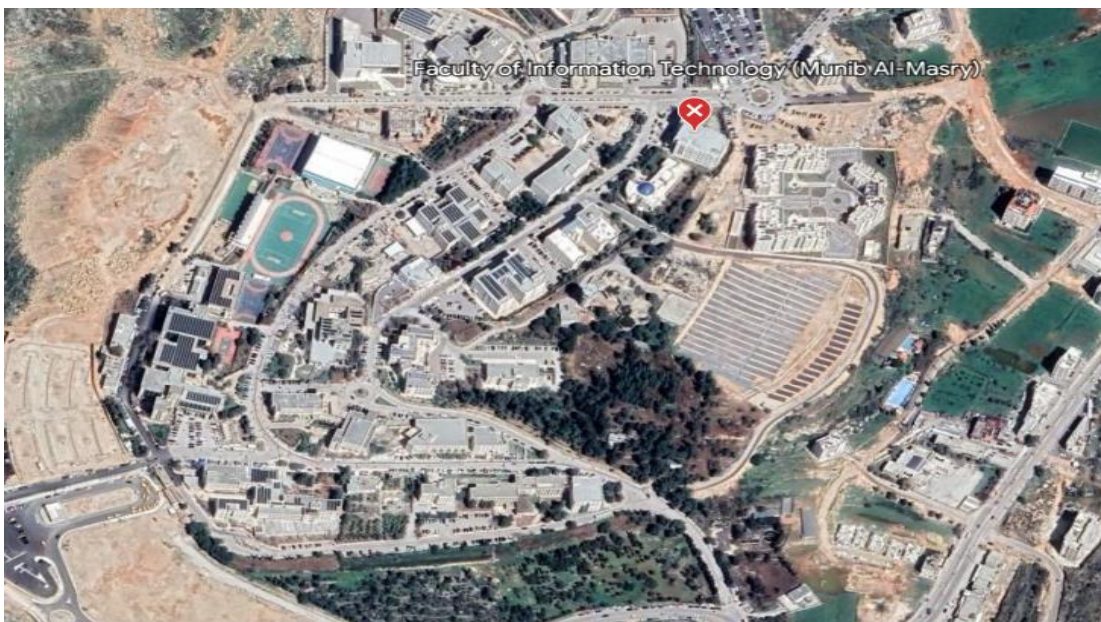


Figure 3-16: Faculty of Information Technology (Munib Al-Masri) building

The studied sub scenarios will investigate how walls, floors, classrooms, and corridors at different distances between the Tx and Rx affect signal reception, as follows:

- A. Tx was installed at a height of 1 m with a 20 dBm P_{tx}, SF to 12, a CR of 5, and a BW of 125 kHz on the fifth floor of the College of Information Technology. To establish a LoS connection, the Rx will move along the corridor on the same floor at a height of 1 m with a LoS connection with the Tx, and at various distances in steps of 1 m until 30 m as shown in Figure 3-17 and Figure 3-18 regarding this scenario, it is important to note that the opening and closing of staff offices, as well as the presence of a group of students on the floor's edges, all definitely played a part in the measurement process.

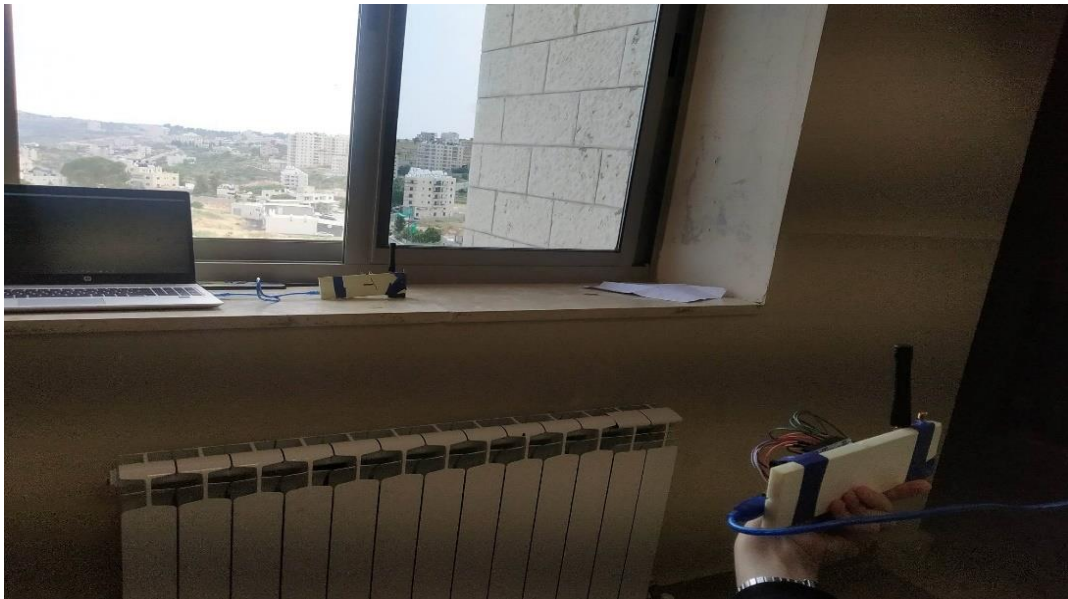


Figure 3-17: Tx and Rx in indoor LoS_ scenario A



Figure 3-18: LoS measurement location between Tx and Rx in indoor LoS_ scenario A

- B. Tx was placed on the ground in the floor on the top of the college of Information Technology with a 20 dBm P_{tx}, SF to 12, a CR of 5, and a BW of 125 KHz, and the strength of the received signal was measured on the ground and ceiling of the fifth lower floors as shown in Figure 3-19 to Figure 3-21. It is worth noting that this scenario was conducted on a normal day with the presence of classrooms full of students on different floors, corridors, laboratories, and teachers' offices.



Figure 3-19: Tx Location in indoor ceiling and floor NLoS_ scenario B



Figure 3-20: First location (ceiling) of Rx where the measurements were taken in indoor ceiling and floor NLoS_ scenario B



Figure 3-21: Second location (floor) of Rx where the measurements were taken in indoor ceiling and floor NLoS_ scenario B

- C. This scenario was also conducted on a typical day with students in the classrooms, corridors, laboratories, and on the stairs. Tx was installed on the top of the emergency stairs with a P_{tx} of 20 dBm, SF to 12, a CR of 5, and a BW of 125 kHz and the Rx was moved along the stairs for a distance of 30 meters, and the received signal strength was tracked.

D. In this building, the last scenario that was conducted to assess how the walls' impact on signal strength. On the ground floor of the building, the Tx was fixed at a Ptx of 20 dBm, SF to 12, a CR of 5, and a BW of 125 kHz as shown in Figure 3-22 and the receiving signal strength was measured after five consecutive walls shown in Figure 3-23 along a distance of 28.46 m at the same height of Tx. Like the previous scenarios, this scenario was conducted on a normal teaching day.

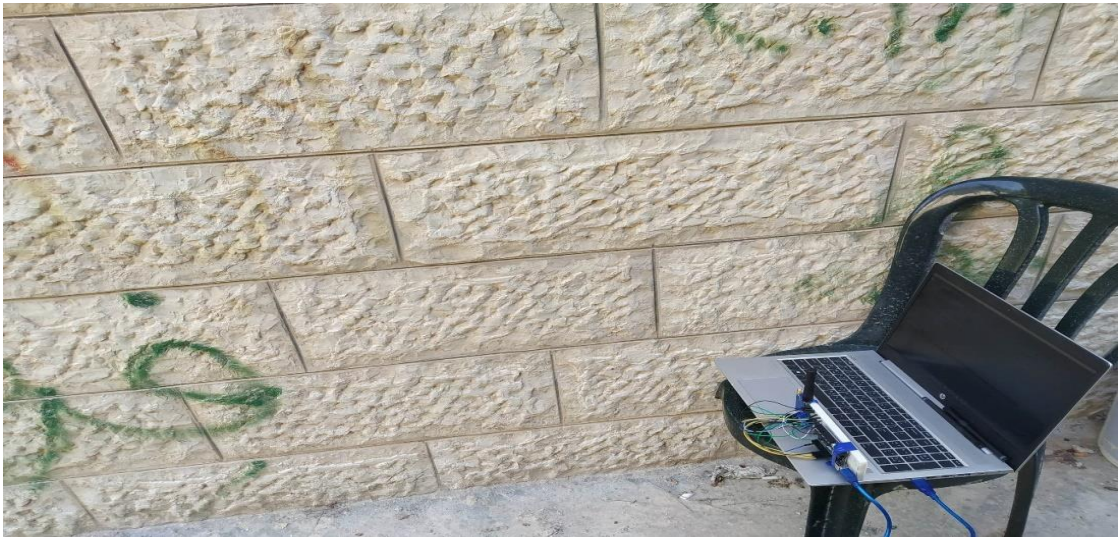


Figure 3-22: Tx location in indoor multiple walls NLoS_scenario D



Figure 3-23: Rx locations in indoor multiple walls NLoS_scenario D were the measurements taken after walls

Another measurement indoor scenario was taken in Shawqi Shaheen building shown in Figure 3-24 for public lectures, since it contains a large theater to give lectures to large numbers of students.

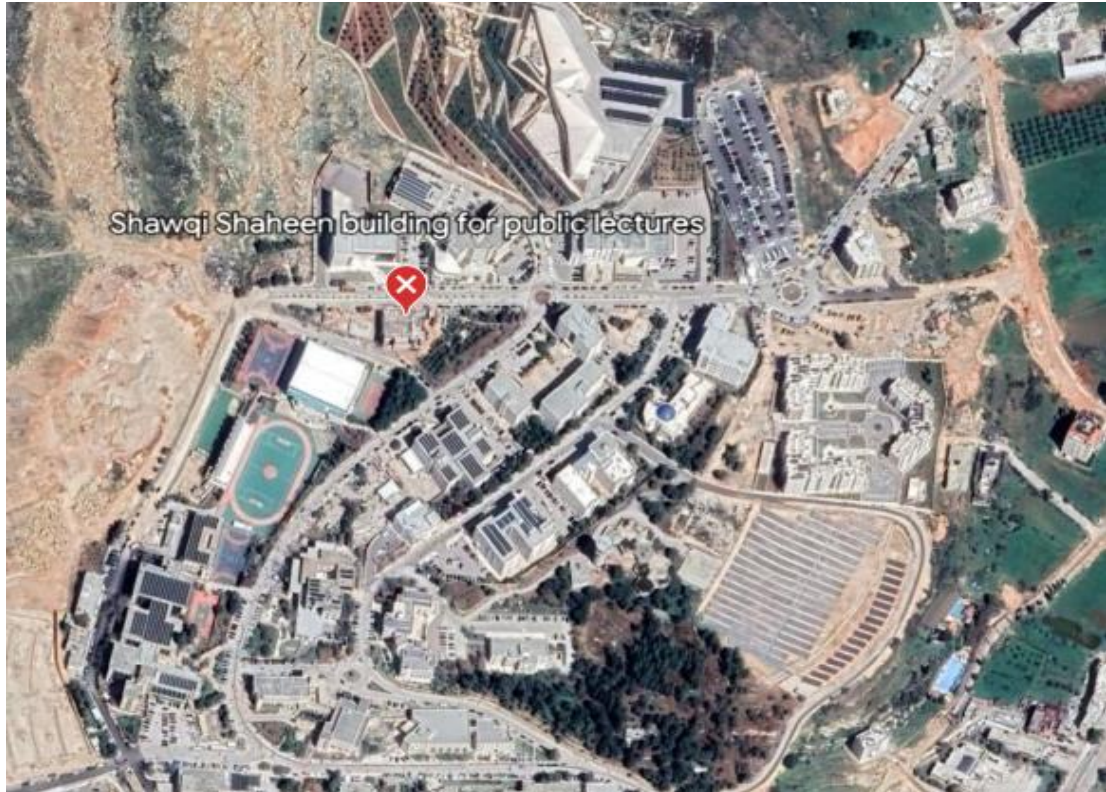


Figure 3-24: Shawqi Shaheen building for public lectures

E. The Tx was installed on the table at the front of the lectures theater, and it was set at a P_{tx} of 20 dBm, SF to 12, a CR of 5, and a BW of 125 KHz as shown in Figure 3-25 . The Rx was moved along and outside the theater for a distance of 20 m. The value of the signal strength reached every 1 m was tracked, which was affected by the student seats and the presence of the wall and the half-open door when exiting outside the lecture theater shown in Figure 3-26.



Figure 3-25: Tx location in indoor lectures theater NLoS_ scenario E



Figure 3-26: lecture theater in Shawqi Shaheen building_ scenario E.

In order to increase accuracy in all scenarios, the received signal strength will be measured at each location, with an average of 10 readings taken at the same distance, and all these scenarios were done in both frequencies 868MHz and 433MHz.

3.5.2 Outdoor Scenario

The outdoor test was divided mainly into two parts: the first part was for testing the effects of trees' leaves and their trunks on the received signal strength on the campus of Birzeit University. The campus area is 810 dunums, and it represents a mixed environment consisting of medium-height buildings, green spaces and trees,

and a medium residential density. The second part was to test the performance of LoRa in a complex outdoor environment. These scenarios summarized as follow:

- A. The Tx was fixed at a specific location near Shawqi Shahin Building shown in Figure 3-24 with a Ptx of 20 dBm, SF to 12, a CR of 5, and a BW of 125 kHz, and Rx was moved to different locations behind seven trees' leaves to check the effect of each tree on the signal strength along a distance of 52.5 m, as shown in Figure 3-27 and Figure 3-28 in a normal teaching day. The same measurements where repeated at the same location without the effect of trees' leaves to form LoS connection between Tx and Rx.



Figure 3-27: Tx location in outdoor trees' leaves NLoS and LoS_ scenario A



Figure 3-28: Trees' Leaves where the Rx moves behind in outdoor NLoS and LoS_ scenario A

B. In accordance with the Trunks effect, the experiment was conducted close to the Waleed and Helen Kattan Presidency building, where there are large pine trees as shown in Figure 3-29. To study the impact of trees' trunks on the received signal strength. Rx was moved behind a series of trunks along a 25m path while the Tx remained fixed with a P_{tx} of 20 dBm, SF to 12, a CR of 5, and a BW of 125 kHz as in Figure 4-30 and Figure 3-31 . The same measurements were repeated at the same location without the effect of trees' trunks to form LoS connection between Tx and Rx.

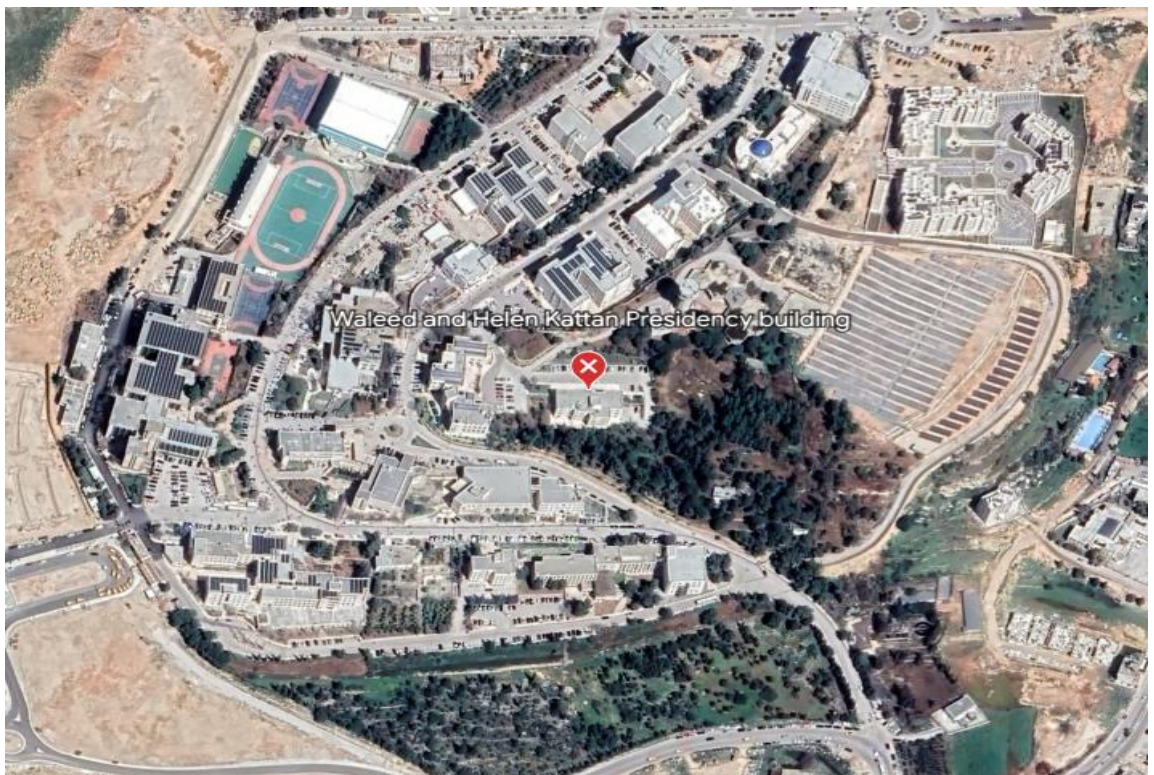


Figure 3-29: Waleed and Helen Kattan Presidency building



Figure 3-30: Tx location in outdoor trees' trunks NLoS and LoS_ scenario B



Figure 3-31: Trees' trunks where the Rx moves behind in outdoor NLoS and LoS_ scenario B

- C. The last measurements testing the impact of the outdoor environment as a whole, which includes buildings of various heights, weather conditions, vegetation, and the movement of people and cars on LoRa signal. A NLoS path formed between the Tx and the Rx after the Tx was installed on top of the Masri building with a P_{tx} of 20 dBm, SF to 7 and 12, a CR of 5, and a BW of 125 KHz at 868MHz and 433MHz, and the measurements were recorded while the Rx was moved toward Birzeit, Rawabi and Ramallah cities with NLoS connection between Tx and Rx. Finally, measurements were recorded at A-Carmel Hotel, Palestine Trade Tower, and at Mazaya

Mall that formed direct LoS communication between the Tx and the Rx shown in the Figure 3-32 to Figure 3-34.



Figure 3-32: Places where Tx is fixed and Rx moves towards Ramallah city in complex outdoor NLoS and LoS_ scenario C



Figure 3-33: Places where Tx is fixed and Rx moves towards Birzeit and Rawabi city in complex outdoor NLoS and LoS_ scenario C



Figure 3-34: Places where LoS connection formed between Tx and Rx in complex outdoor NLoS and LoS_ scenario C

In order to increase accuracy in all scenarios, the received signal strength will be measured at each location, with an average of 10 readings taken at the same distance, and all these scenarios were done in both frequencies 868MHz and 433MHz.

Chapter 4 Results and Discussion

This chapter presents the outcomes of the various scenarios, discusses the results, recommends the best parameters for the path loss model based on the measurements of various scenarios in the different environments, compares the path loss models based on the proposed parameters with the available models in the literature, validate the path loss models based on the proposed parameters and finally presents the shadow fading of the path loss based on measurements.

4.1 Measurements and Proposed Fitted Model

Based on the two approaches discussed in Mathematical Modeling section, the CF tool in MATLAB is used to find the best fit model based on Equation 3. for the measured data in the various scenarios. Finally, the real practical measurements and the best suitable curve are plotted using MATLAB.

4.1.1 Indoor Scenario

First of all, Figure 4-1 represents a scatter plot of data collected in an indoor environment at a frequency of 868MHz.

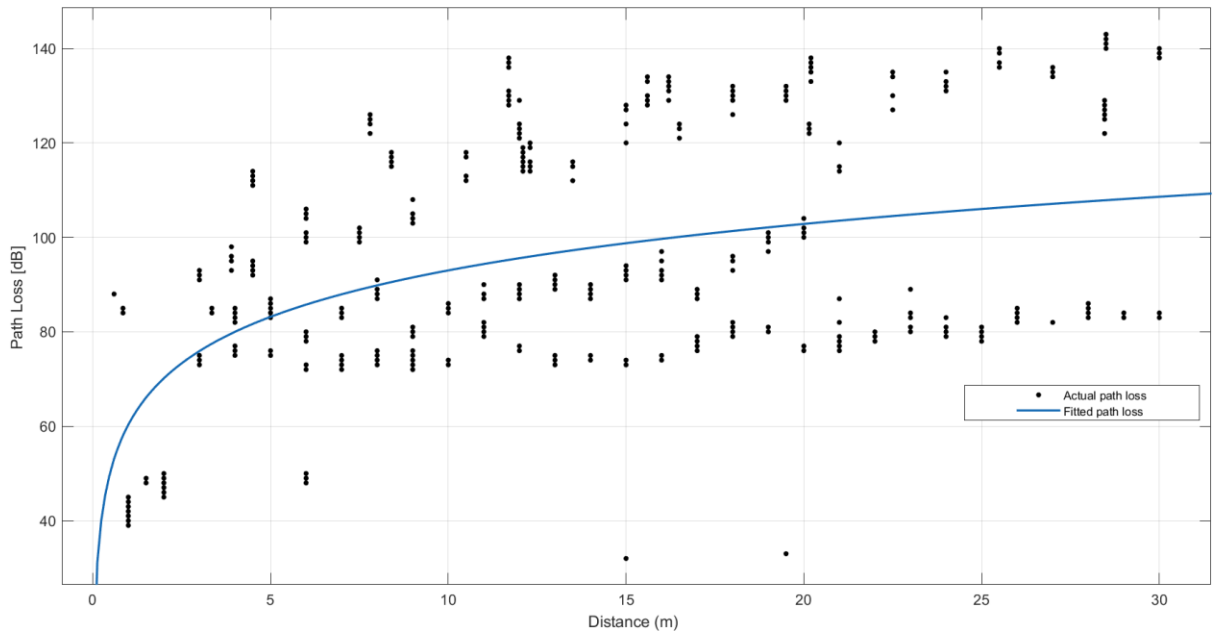


Figure 4-1: Fitted path loss and scatter plot of Actual path loss in an indoor environment at 868MHz

Based on the two strategies that were previously discussed in Section 3.4, Table 4.1 presents the parameters of the proposed path loss model for the indoor environment, where

A is the variation of path loss with accordance to distance, B represents the frequency dependent factor, and G represents the path loss intercept. This table shows the proposed parameters for each approach, their RMSE, and the scenario, environment, distance, and frequency.

In brief, the first method relied on maintaining both the free space and the frequency coefficients and extracted the distance coefficient, whereas the second method fixed the free space coefficient while extracting the other parameters. The best parameters for path loss model is then selected based on the lower RMSE value, and the measurement curve is plotted with the best-fit curve.

For the first scenario, at a frequency of 433MHz, the confidence level was calculated based on the following Equations from 4.1 to 4.4, where x is the measurements, SE is Standard Error, SD is the Standard Deviation, n is the sample size, μ is the mean, Z is the value from the standard normal distribution for the confidence level [63].

$$SD = \sqrt{\left(\frac{\sum(x - \mu)^2}{n}\right)} \quad 4.1$$

$$\mu = \frac{\sum x}{n} \quad 4.2$$

$$SE = \frac{SD}{\sqrt{n}} \quad 4.3$$

$$Confidence\ Interval = mean \pm Z \times SE \quad 4.4$$

Based on the above equations [63] for the indoor LoS scenario in the corridor at 433 MHz, n is 25 for the distance of 25 m, since every one meter ten measurements were taken and then averaged, μ , SD , and SE are calculated based on our measurements and equal to 82.3772, 13.1797, and 2.6359 respectively and the confidence interval was [77.2108, 87.5436], then based on these values, a value of Z was calculated and equal to 1.96, and a confidence level was then found in the Z-Score Table and its 95%. This is applied for all scenarios in indoor and outdoor environments where the confidence level equal 95%.

Table 4.1: Proposed Parameters of the path loss model in the indoor environment based on two approaches, scenario, environment, distance, frequency and their RMSE

Scenario	Environment	Distance Range (m)	Frequency Range (MHz)	A	B	G	RMSE
Corridor	LoS	1-30	433	0.06818	2	32.44	13.46
				2.863	0.7485	32.44	7.946
			868	-1.199	2	32.44	14.99
				2.263	0.5829	32.44	6.655
Ceilings and Floors	NLoS	0.6-20.2	433	4.029	2	32.44	10.4
				2.377	2.676	32.44	6.689
			868	3.129	2	32.44	7.352
				3.251	1.955	32.44	7.771
Emergency Stairs	NLoS	1-30	433	3.14	2	32.44	12.18
				5.618	0.8688	32.44	5.032
			868	2.519	2	32.44	18.31
				6.308	0.4481	32.44	6.849
Walls	NLoS	0.85-28.46	433	2.623	2	32.44	2.939
				2.259	2.169	32.44	1.253
			868	2.407	2	32.44	2.781
				2.682	1.885	32.44	2.155
Lectures Theater	NLoS	1-20	433	0.706	2	32.44	9.519
				2.807	1.165	32.44	5.426
			868	-0.2559	2	32.44	16.14
				3.751	0.571	32.44	5.85

Figure 4-2 and Figure 4-3 depict the performance of the LoRa signal in an indoor setting with a LoS between the Tx and Rx for 30m in the Munib Al Masri building's fifth-floor corridor. In general, as the distance increases, the path loss increases. We take note of the changes in the value of the path loss caused by opening and closing the doors of the employees' offices during the measurements. These offices have windows that allow the

entry of the multipath factor, which significantly affects the path loss, in addition to the movement of students during the measurements that were carried out on a normal learning day.

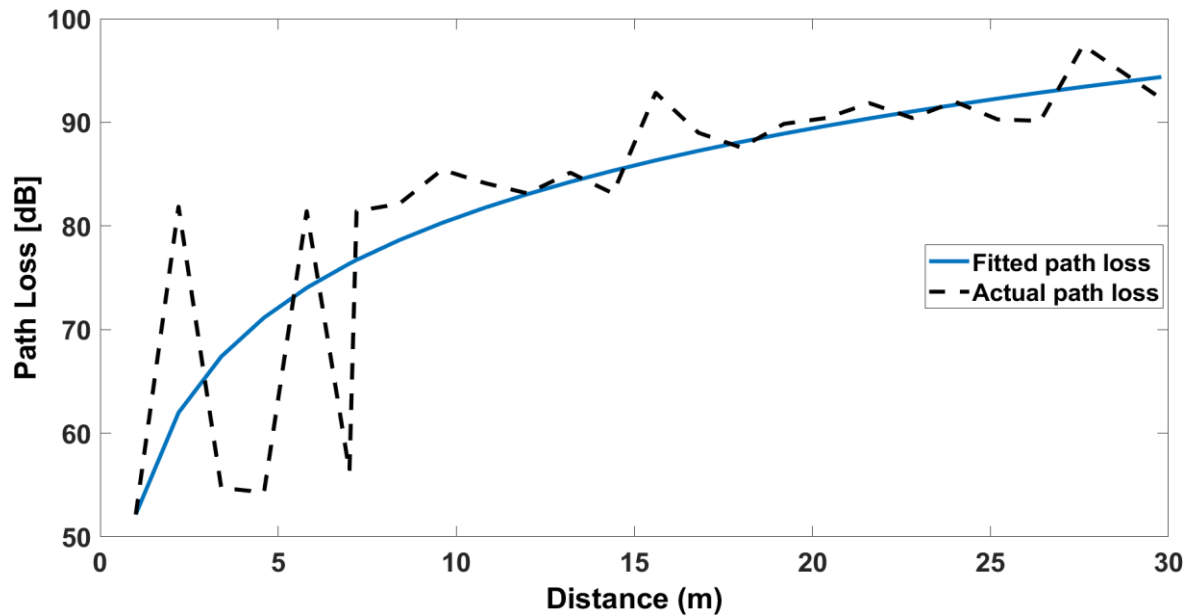


Figure 4-2: Averaged actual and fitted path loss at 433 MHz in indoor LoS_scenario A

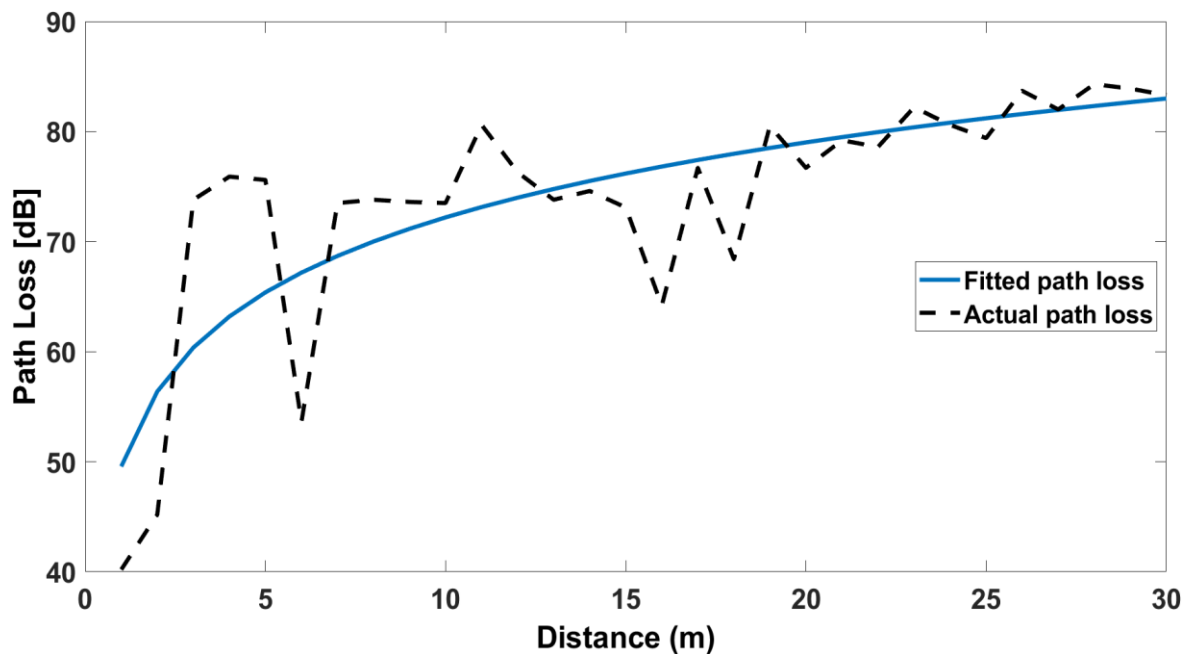


Figure 4-3: Averaged actual and fitted path loss at 868 MHz in indoor LoS_scenario A

The results shown in Figure 4-4 and Figure 4-5, which were obtained by mounting the Tx on the Masri building's top, moving the Rx to the building's other lower five floors to

form a NLoS communication, and taking measurements at the ceilings and floors, that can be easily and clearly detected from the Figures. In general, it is anticipated that the path loss will increase as the distance between the Tx and the Rx increases and that additional path loss will result from the presence of obstacles like floors between them. However, moving down to the third and fourth floors causes the path loss value at the ceiling to drop. This is because the large windows on those floors are larger than those on the upper floors and extend along the floor's corridors in the measurement area, allowing the multipath effect to enter and potentially reduce the path loss value. The ground floor, which is the fifth floor, was the furthest from the Tx and stood out due to its unique shape, the presence of doors—two of which were closed—and the presence of many students, which contributed to the continuing increase in path loss at the ceiling and floor. This experiment was also carried out during a typical learning day, with staff and students present on the floors.

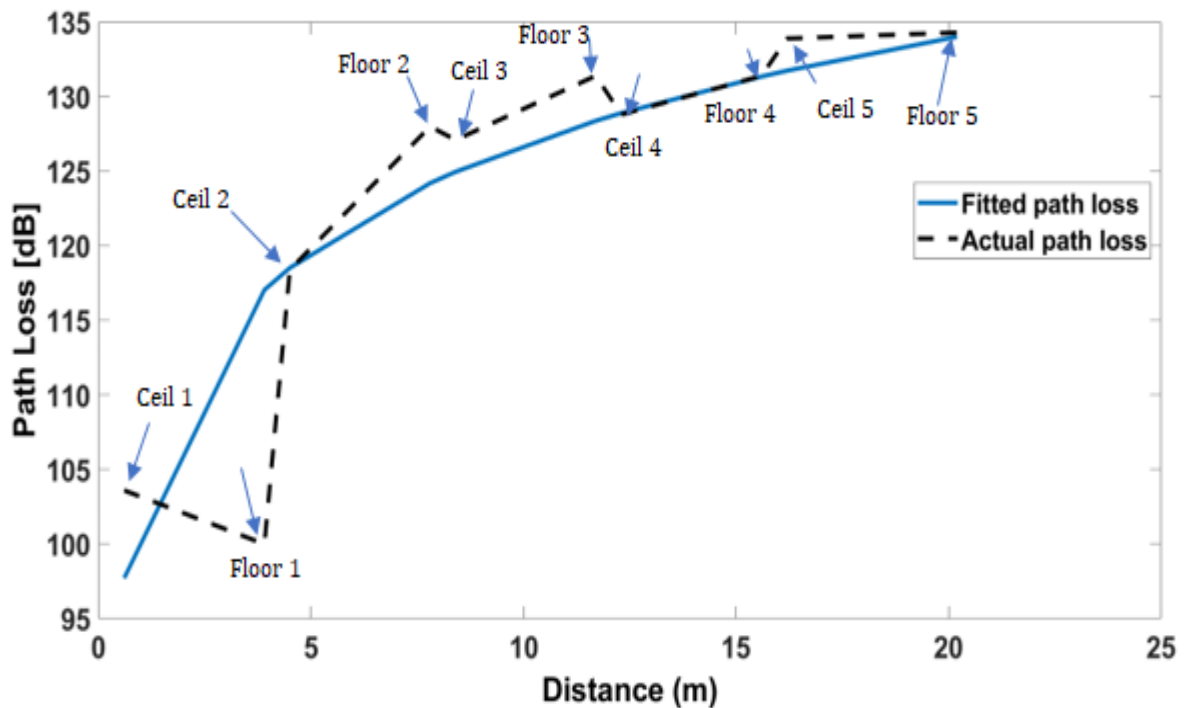


Figure 4-4: Averaged actual and fitted path loss at 433 MHz in indoor NLoS ceilings and floors_ scenario B

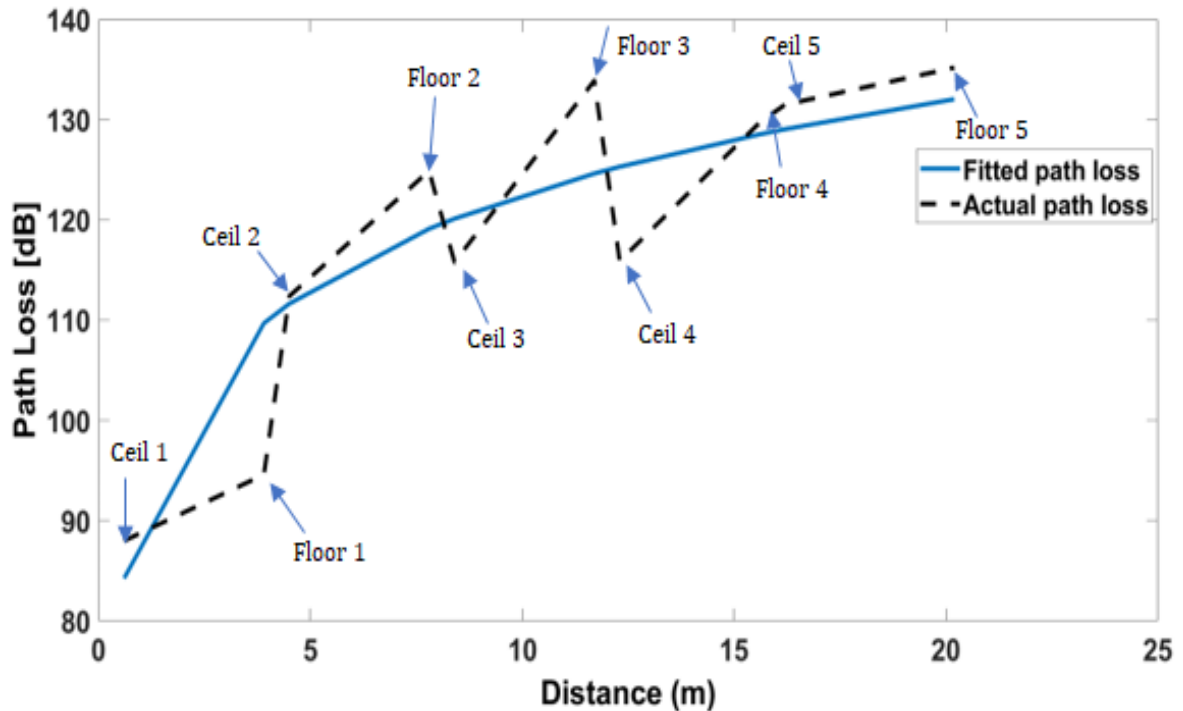


Figure 4-5: Averaged actual and fitted path loss at 868 MHz in indoor NLoS ceilings and floors_ scenario B

Figure 4-6 and Figure 4-7 show the impact of the emergency stairs, which are present on every floor of the building, on LoRa performance. As Rx move away from the Tx to form a NLoS communication, path loss increases due to the distance factor and the presence of stairs on the upper floors. There are also some variations in the path loss value that are occasionally caused by students using the stairs as an additional obstacle between the Tx and the Rx. These measurements were also carried out during a typical learning day.

As for the effect of walls, which was performed on a regular day at the university, it appears clearly in Figure 4-8 and Figure 4-9 for both frequencies. Where the loss increases with the increase in the number of walls separating Tx and Rx and forms a NLoS scenario. The reason behind the appearance of the measurements in this way is the presence of distance between these walls, which represent the walls of successive classrooms in Masri building, in addition to the presence of windows in these classrooms, which can cause the entry of the effect of multipath on the path loss.

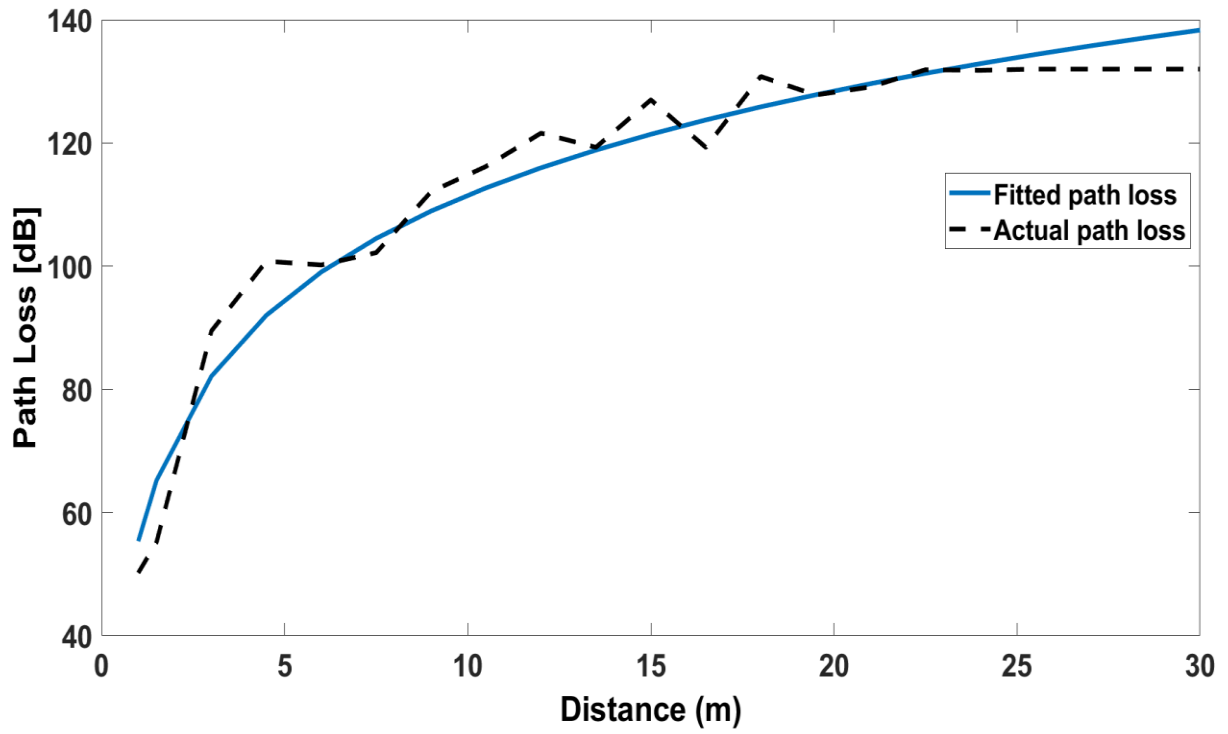


Figure 4-6: Averaged actual and fitted path loss at 433 MHz in indoor NLoS emergency stairs_ scenario C

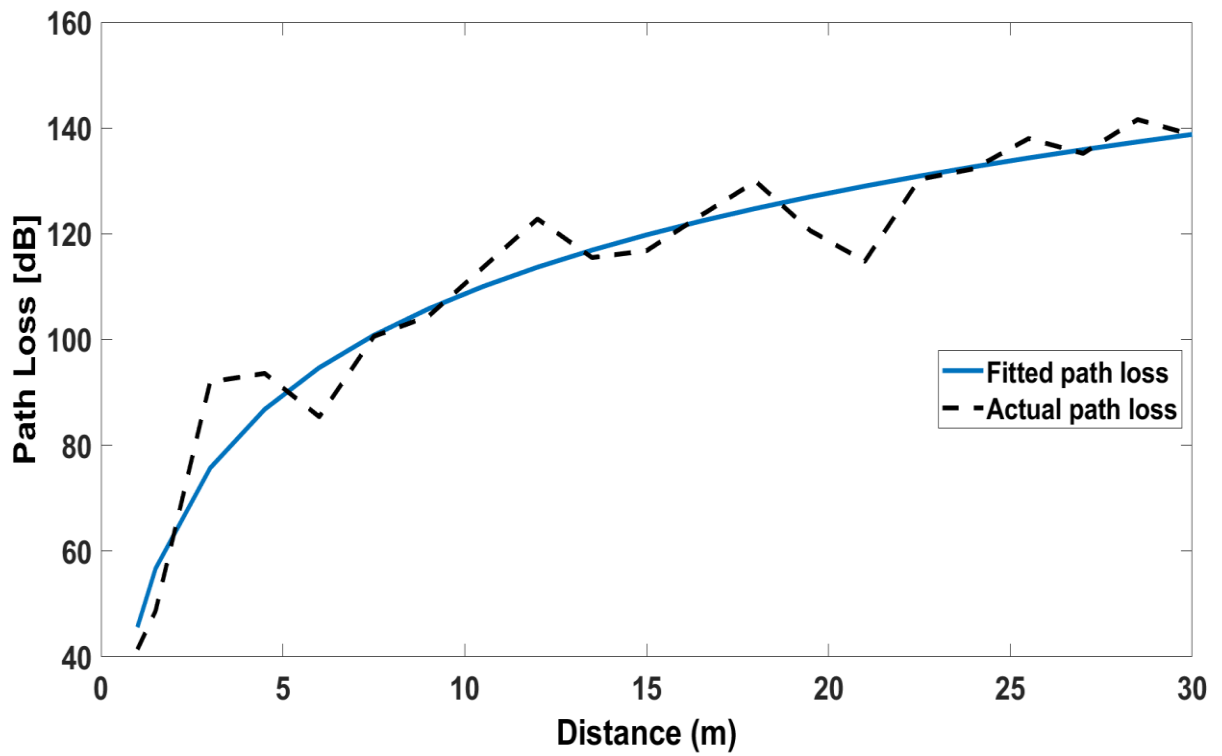


Figure 4-7: Averaged actual and fitted path loss at 868 MHz in indoor NLoS emergency stairs_ scenario C

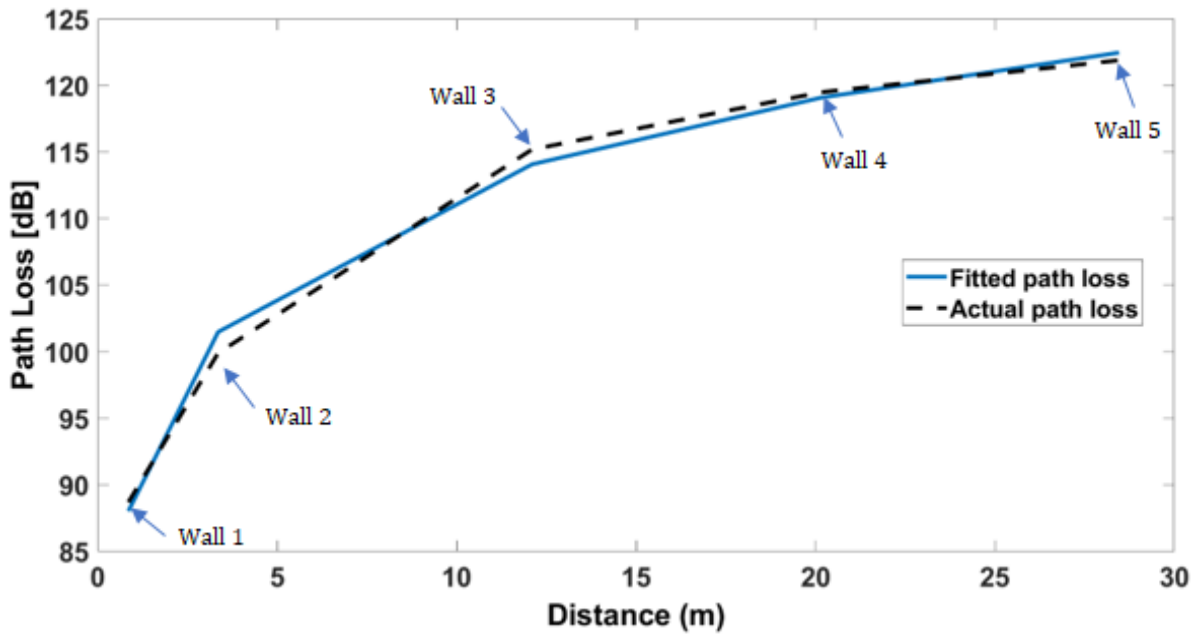


Figure 4-8: Averaged actual and fitted path loss at 433 MHz in indoor NLoS multiple walls_ scenario D

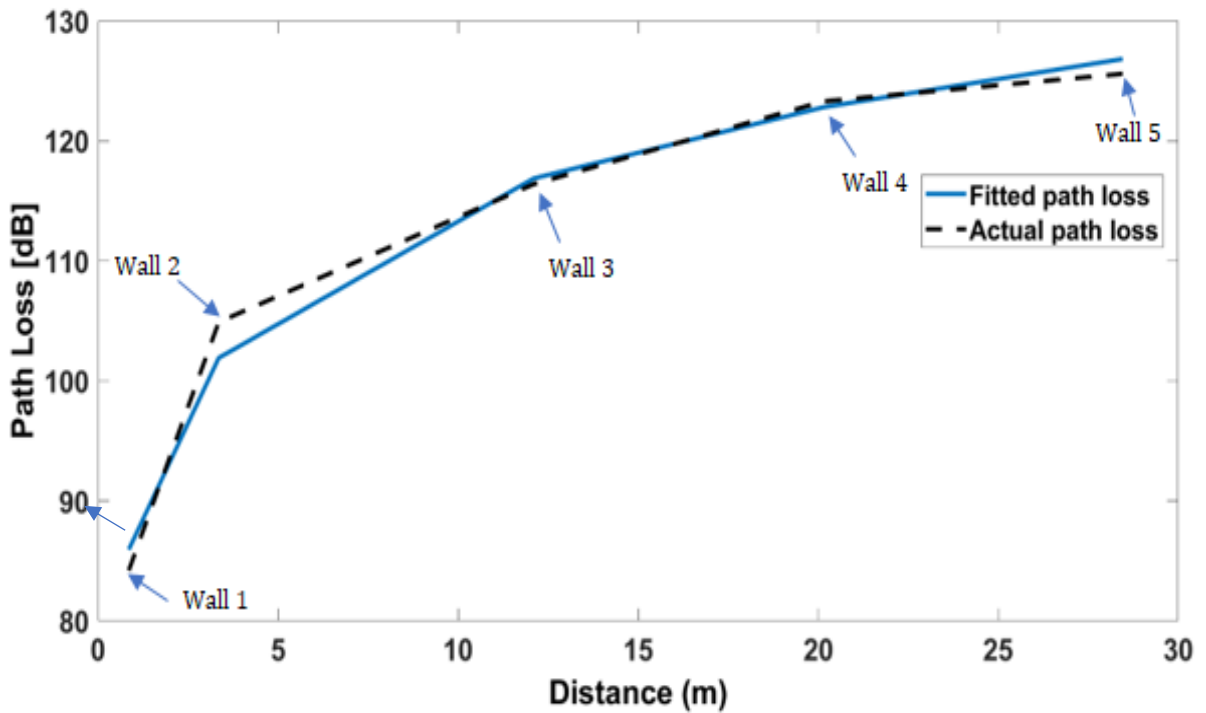


Figure 4-9: Averaged actual and fitted path loss at 868 MHz in indoor NLoS multiple walls_ scenario D

The last measurements in an indoor environment was carried out in a lecture theater without any students present, and its impact on the LoRa signal at frequencies of 433 MHz and 868 MHz is shown in Figure 4-10 and Figure 4-11. There is an increase in the path loss with increasing distance between the Tx and Rx, as well as the presence of obstructions

like student seats between them. Last but not least, leaving the hall and walking two meters outside caused a noticeable increase in the path loss at 18 m, which is an effect of the hall wall.

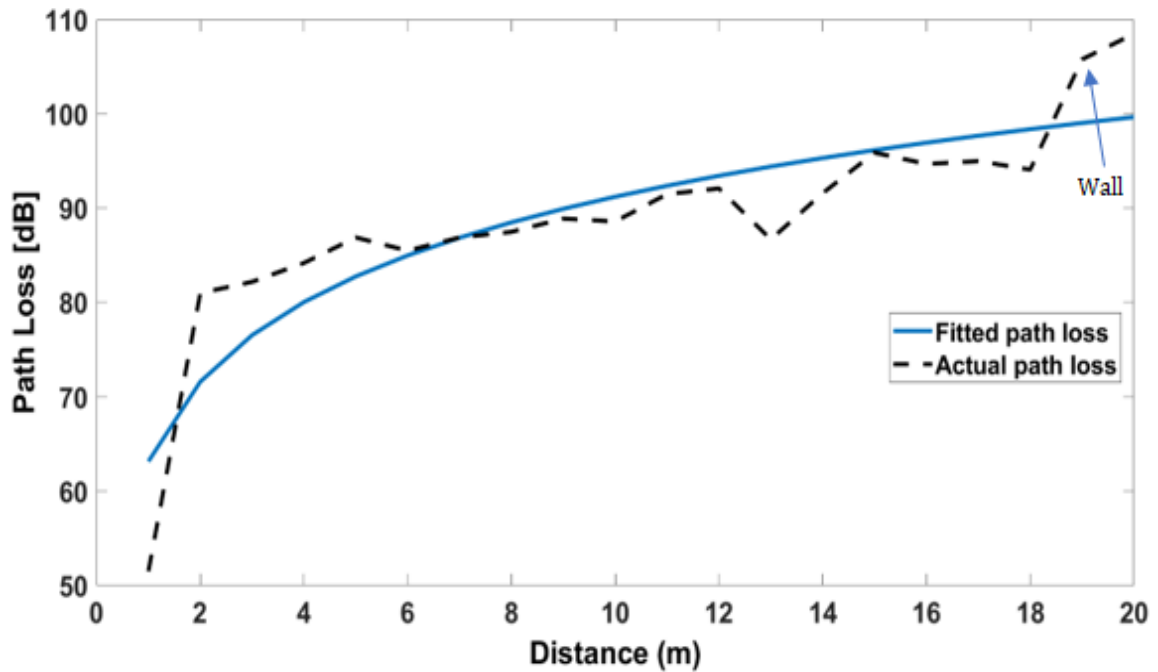


Figure 4-10: Averaged actual and fitted path loss at 433 MHz in indoor NLoS in theater lectures_scenario E

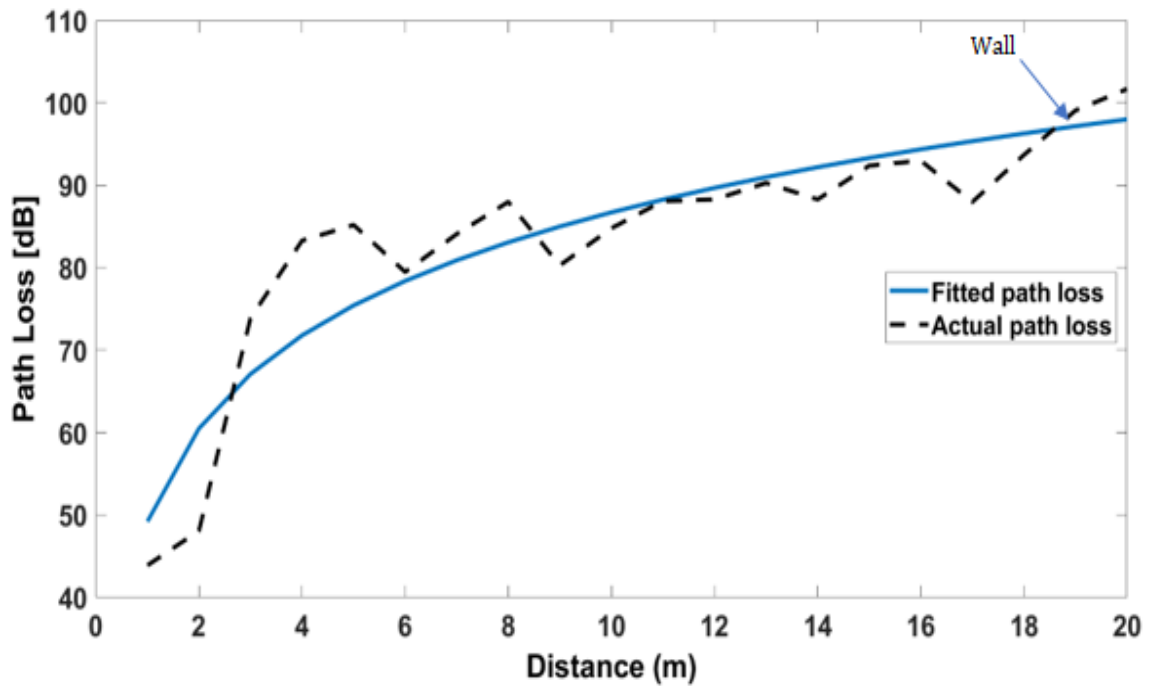


Figure 4-11: Averaged actual and fitted path loss at 868 MHz in indoor NLoS in theater lectures_scenario E

4.1.2 Outdoor Scenario

Based on the two strategies that were previously covered in section 3.4, Table 4.2 lists the suggested parameters of the path loss model in outdoor environments. The proposed parameters for each approach are shown in this table where A is the variation of path loss with accordance to distance, B represents the frequency dependent factor, and G represents the path loss intercept, along with their RMSE, scenario, environment, distance, and frequency. Based on the lower RMSE value, the best model for each scenario is chosen, and the measurement curve is plotted with the best-fit curve using MATLAB.

Figure 4-12 and Figure 4-13 illustrate how the LoRa signal performed at frequencies of 433 MHz and 868 MHz in an outdoor environment with tree leaves while the experiment was carried out on a typical learning day. As the number of successive trees between the Tx and Rx—which form an NLoS communication—increases, an increase in path loss is observed. The reason for the change in the path loss path was due to students passing while taking measurements between trees and their sitting occasionally, which had an impact on the strength of the received signal. The most important note here is the obstacles appear clearly at high frequencies, and the effect of the leaves becomes more obvious at a frequency of 868 MHz.

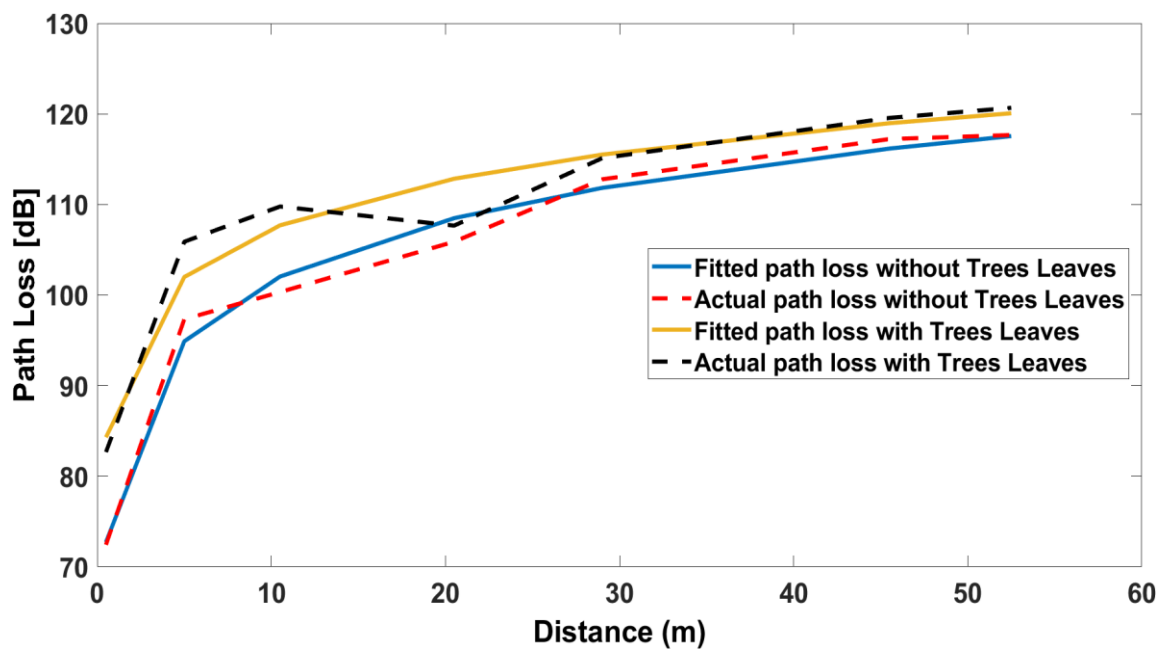


Figure 4-12: Averaged actual and fitted path loss at 433 MHz in outdoor NLoS and LoS for Trees' Leaves_ scenario A

Table 4.2: Proposed Parameters of the path loss model in the outdoor environment based on two approaches, scenario, environment, distance, frequency and their RMSE

Scenario	Environment	Distance Range (m)	Frequency Range (MHz)	A	B	G	RMSE
Trees' Leaves	NLoS	0.5-52.5	433	2.071	2	32.44	3.804
				1.77	2.169	32.44	3.155
			868	1.378	2	32.44	2.233
				1.363	2.007	32.44	2.442
Direct communication without Trees' Leaves	LoS	0.5-52.5	433	1.827	2	32.44	3.661
				2.218	1.781	32.44	1.883
			868	0.1607	2	32.44	19.82
				2.544	0.8016	32.44	2.459
Trees' Trunks	NLoS	1-25	433	2.021	2	32.44	3.938
				1.443	2.24	32.44	1.753
			868	1.581	2	32.44	2.091
				1.505	2.028	32.44	2.35
Direct communication without Trees' Trunks	LoS	1-25	433	1.966	2	32.44	2.654
				2.189	1.907	32.44	2.6
			868	-	2	32.44	24.45
				0.2497	0.5653	32.44	4.187
Complex Outdoor	LoS and NLoS	100-12000	433	1.103	2	32.44	47.08
				0.1748	3.686	32.44	3.294
			868	-	2	32.44	23.02
				0.1377	1.042	2.809	32.44

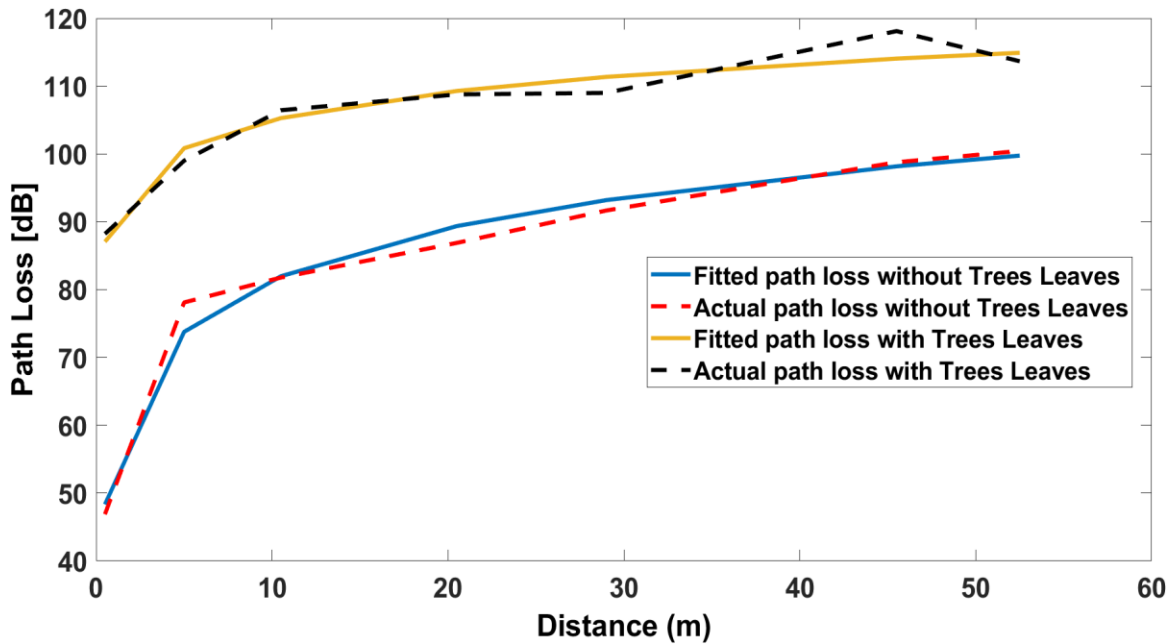


Figure 4-13: Averaged actual and fitted path loss at 868 MHz in outdoor NLoS and LoS for Trees' Leaves_ scenario A

In terms of the effect of trunks, it is evident in Figure 4-14 and Figure 4-15, where measurements were made outside to examine the impact of tree trunks on the LoRa signal at frequencies of 433 MHz and 868 MHz on a normal learning day. As the number of subsequent tree trunks between the Tx and Rx increases, the path loss increases, forming an NLoS communication. The nature of the vegetation in that area, where there are tall trees, big trunks, and grass that fill the place, as well as the sitting of some students during the measurements in the area between trees, all affected the strength of the receiving signal and caused the change that occurred in the path loss. As previously stated, the 868 MHz frequency is where the effect of the trunks appears to be more obvious because obstacles are more noticeable at high frequencies. The difficulty in taking measurements where most of the trees with wide trunks are randomly distributed throughout the area in university is worth mentioning.

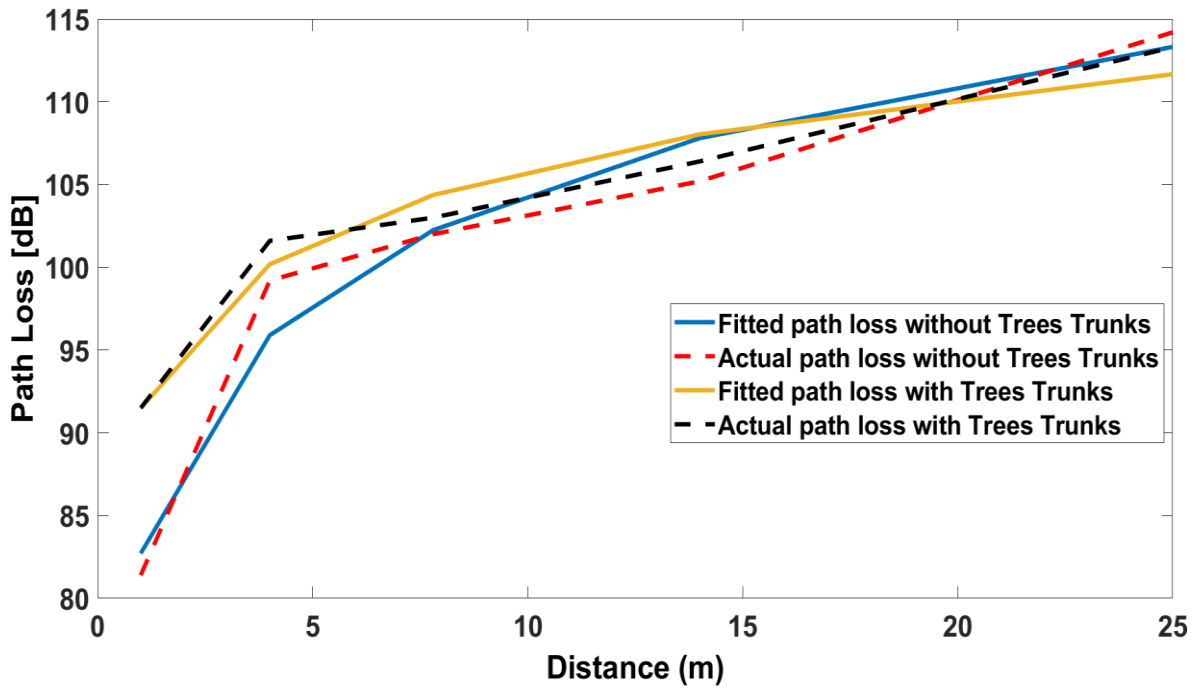


Figure 4-14: Averaged actual and fitted path loss at 433 MHz in outdoor NLoS and LoS for Trees' trunks_ scenario B

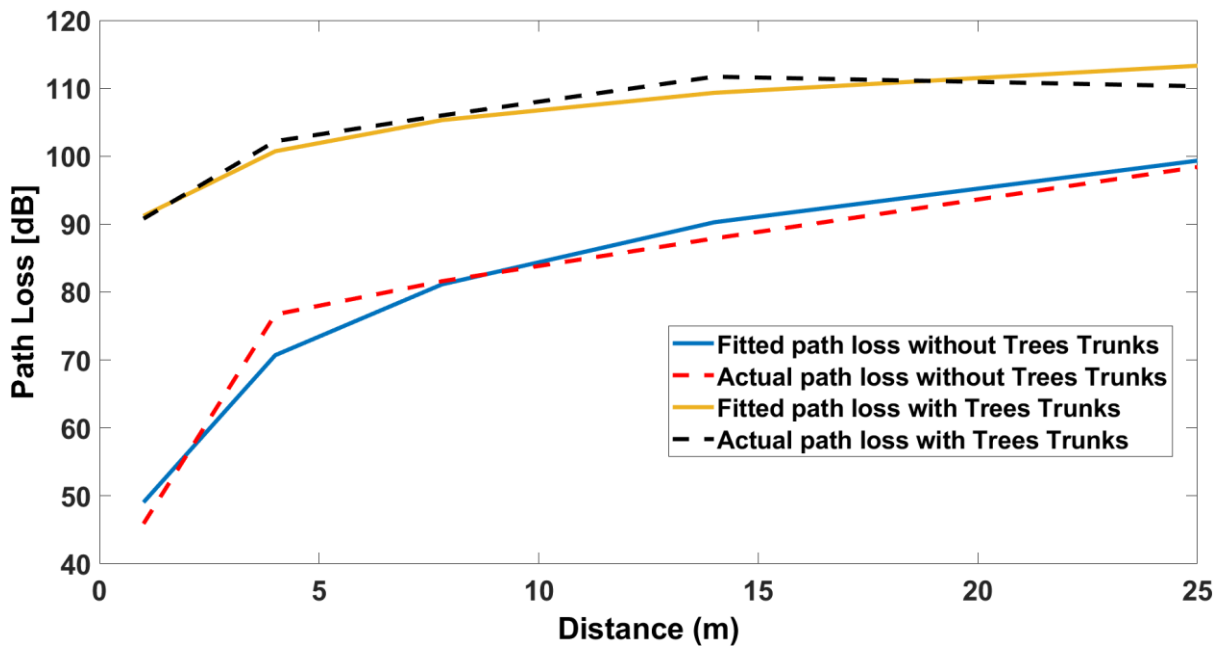


Figure 4-15: Averaged actual and fitted path loss at 868 MHz in outdoor NLoS and LoS for Trees' trunks_ scenario B

The last part of the measurement was carried out on a typical day in Birzeit, Rawabi, and Ramallah at both frequencies of 433 MHz and 868 MHz. This allowed to determine the coverage range of LoRa technology in the outdoor environment, which was the most significant scenario. Figure 4-16 and Figure 4-17 depict how the LoRa signal performs in

a complex scenario with the existence of various heights of buildings, trees, people, cars, distance, and multipath effects. In this scenario, a direct LoS communication is occasionally formed between the Tx and the Rx, and occasionally a NLoS communication is formed. It show that the loss increases with distance. However, it should be noted that the LoRa signal sometimes reaches the Rx along NLoS paths for a certain distance, the connection is broken, and then communication resumes after another distance, whether it be towards Rawabi or Ramallah. This is because of the nature of the areas, buildings, and other factors that affect communication. In terms of coverage, it extends over 10 km with LoS connection since LoRa signal could be picked up at the Al-Carmel Hotel in Al-Masyoun, Ramallah, with reasonable received signal strength. The unfortunate thing is the inability to go further distances because of the Israeli occupation.

At 433 MHz in Mazaya Mall, which is 3.4 Km away from the Tx, when the SF was changed from 12 to 10 to check the effect of changing SF, the message was received with lower SNR and it was disturbed and interrupted. However, when this variation was checked at Palestine Trade Tower, which is 8.7 Km away from the Tx, there was no connection between the Tx and the Rx. Finally, at the two places when SF is changed to 7, no connection between Tx and Rx achieved.

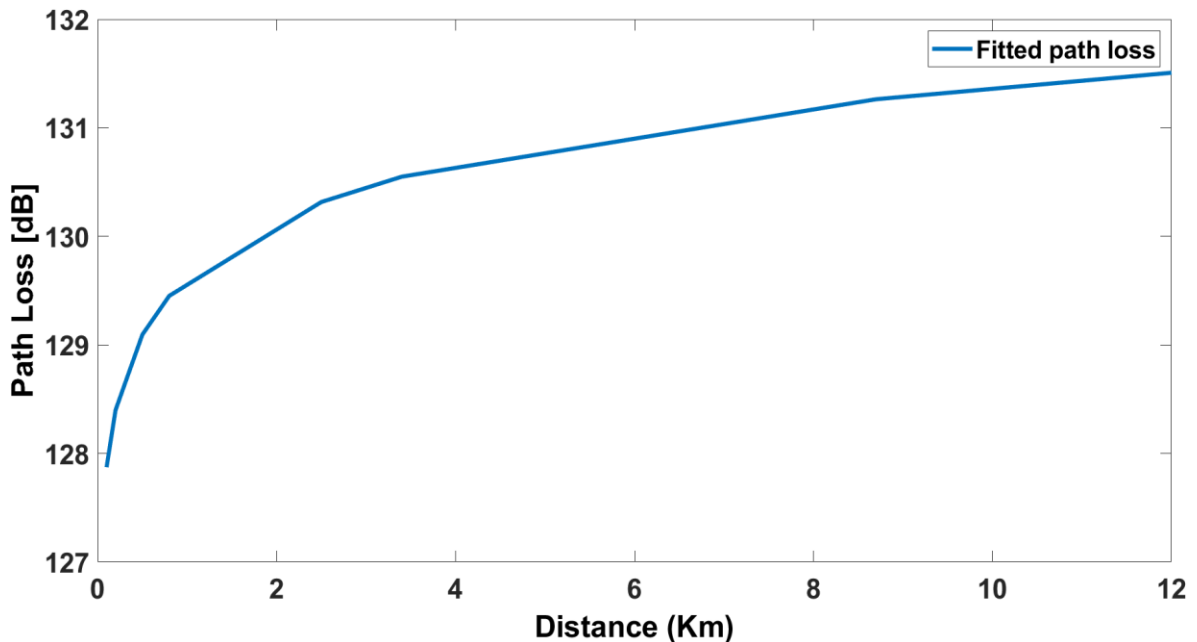


Figure 4-16: Averaged actual and fitted path loss at 433 MHz in outdoor NLoS and LoS for Complex Environment_ scenario C

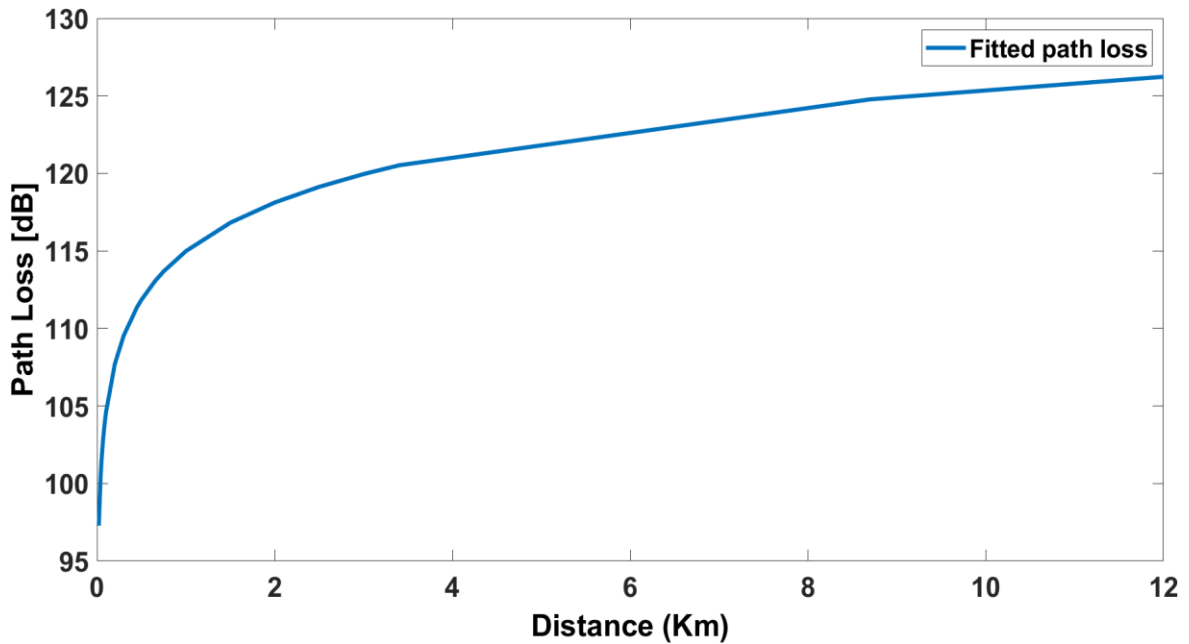


Figure 4-17: Averaged actual and fitted path loss at 868 MHz in outdoor NLoS and LoS for Complex Environment_ scenario C

4.2 Path Loss

This section compares various path loss models that have been previously discussed in the literature with the curve fitted for the measured data for both indoor and outdoor scenarios to evaluate these models' effectiveness and predictability under the various scenarios. Different factors, such as distance, multipath fading, and the effect of walls are taken into account for each scenario in this comparison.

4.2.1 Indoor Scenario

A comparison between the FreeSpace model and other models that have been mentioned and discussed in the literature is provided. This comparison offers a clear understanding and perception of these models' abilities and performance to accurately predict how the indoor environment affects signal strength. Figure 4-18 and Figure 4-19 show LoS scenarios for frequencies of 433 MHz and 868 MHz. The Figures illustrated that in the case of LoS connection at both frequencies, the performance of the 3GPP model and FreeSpace is comparable, whereas the other models—ITU-R2318, IEEE802.11, COST231 and WINNER II—overestimated the free space path loss.

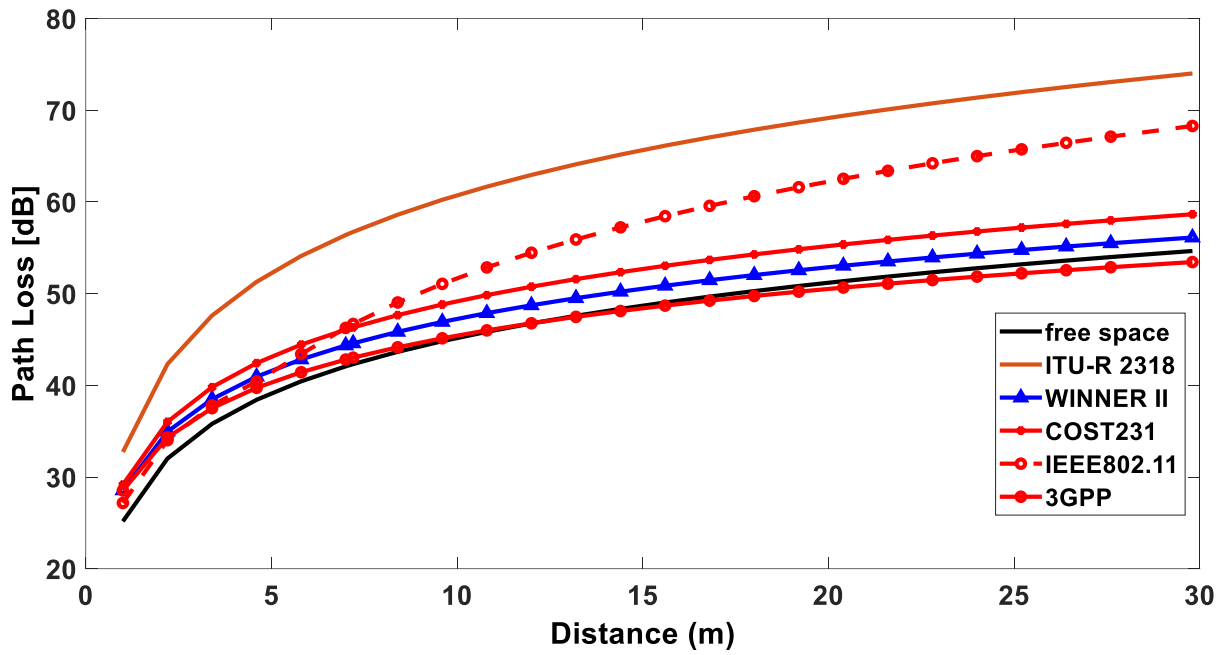


Figure 4-18: Estimated path loss as a function of distance at 433 MHz.

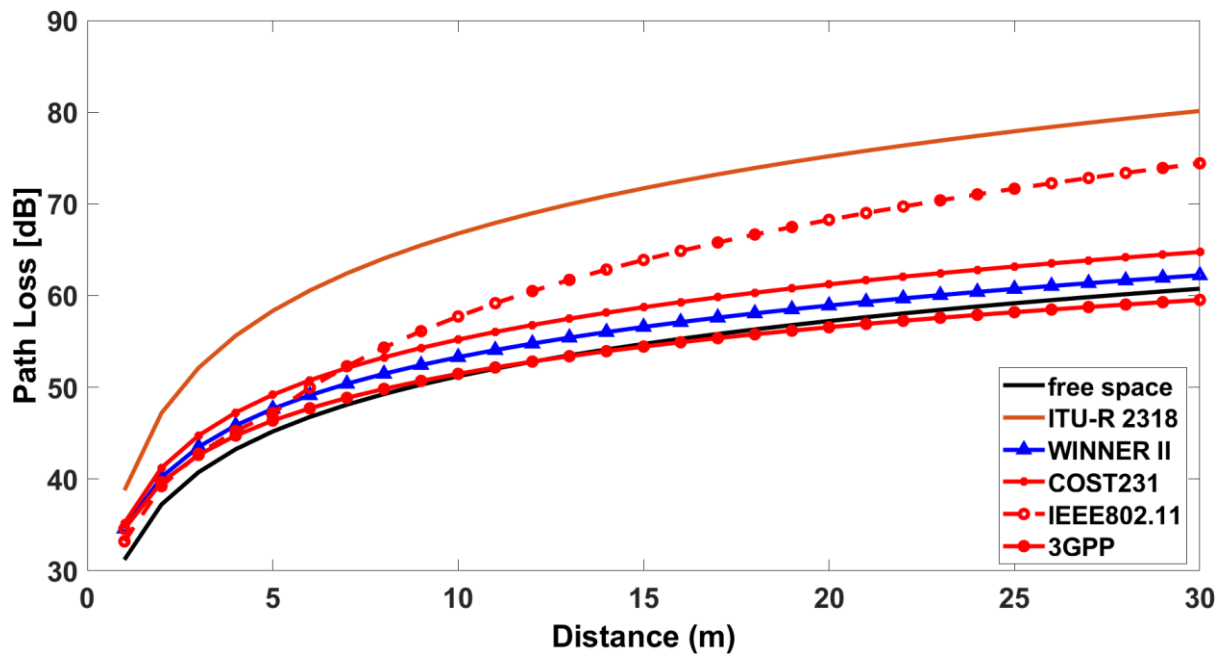


Figure 4-19: Estimated path loss as a function of distance at 868 MHz.

Figure 4-20 and Figure 4-21 provide a comparison between the curve fitted for the measured data in LoS scenarios and the other models at 433 MHz and 868 MHz. It is important to note that none of the various models consistently matches the fitted path loss, and all models underestimate the path loss. However, it is clearly noted that ITUR is the

closest model on the fitted path loss, followed by IEEE 802.11, COST231, WINNER II and finally 3GPP, respectively in both frequencies.

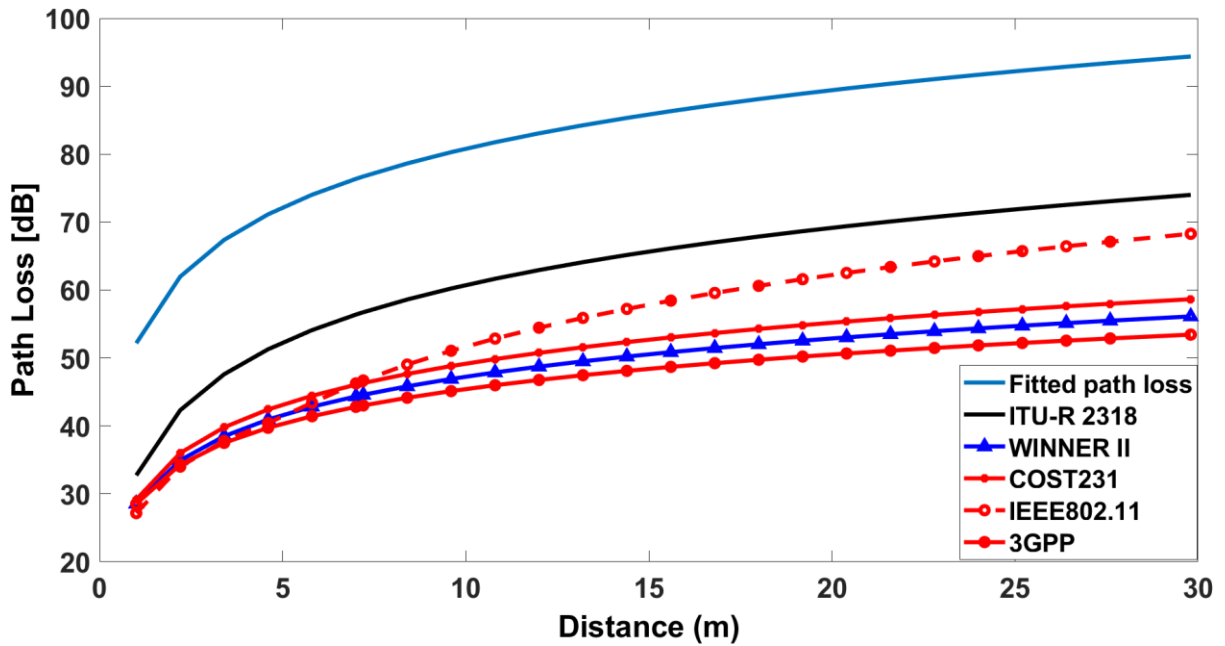


Figure 4-20: Models and fitted path loss at 433 MHz in indoor LoS_scenario A

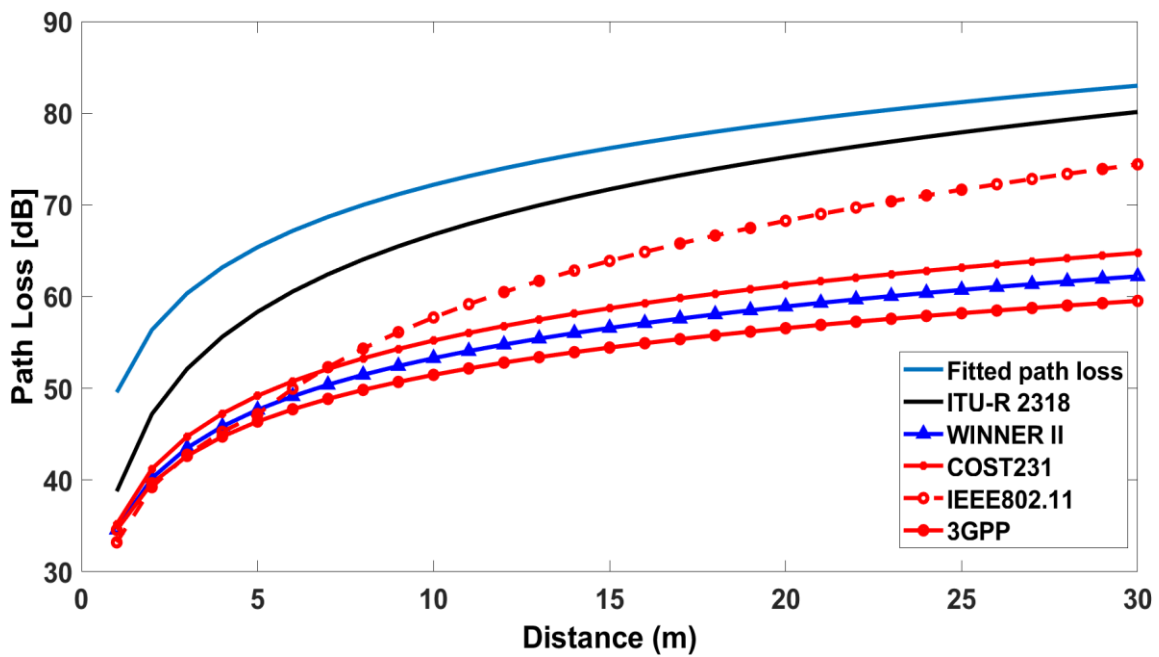


Figure 4-21: Models and fitted path loss at 868 MHz in indoor LoS_scenario A

Figure 4-22 and Figure 4-23 show how the ceiling and floors affect the strength of the signal received, and it is clear that the loss increases as LoRa Rx descends to lower floors

farther away from the LoRa Tx. Here, it is important to note the influence of vertical distance, the presence of staff and students, and the multipath produced by the building's windows. Despite the fact that all of the models clearly take ceilings and floors into account, none of them generally match the fitted path loss model. However, ITUR is the closest one to the model based on the new parameters for distances less than 3.9 m, in addition to distances greater than 8.4 m at both frequencies, and it is noted that it matches the fitted curve at 868 MHz at a distance greater than 16.2m. WIINER II, in the middle of the mentioned distance, comes the closest to the suggested model. It is remarkable to note the performance of the IEEE 802.11 model, which does not take into account the presence of ceilings and floors but is limited to the interaction of the signal with the indoor environment only and does not represent the measured data.

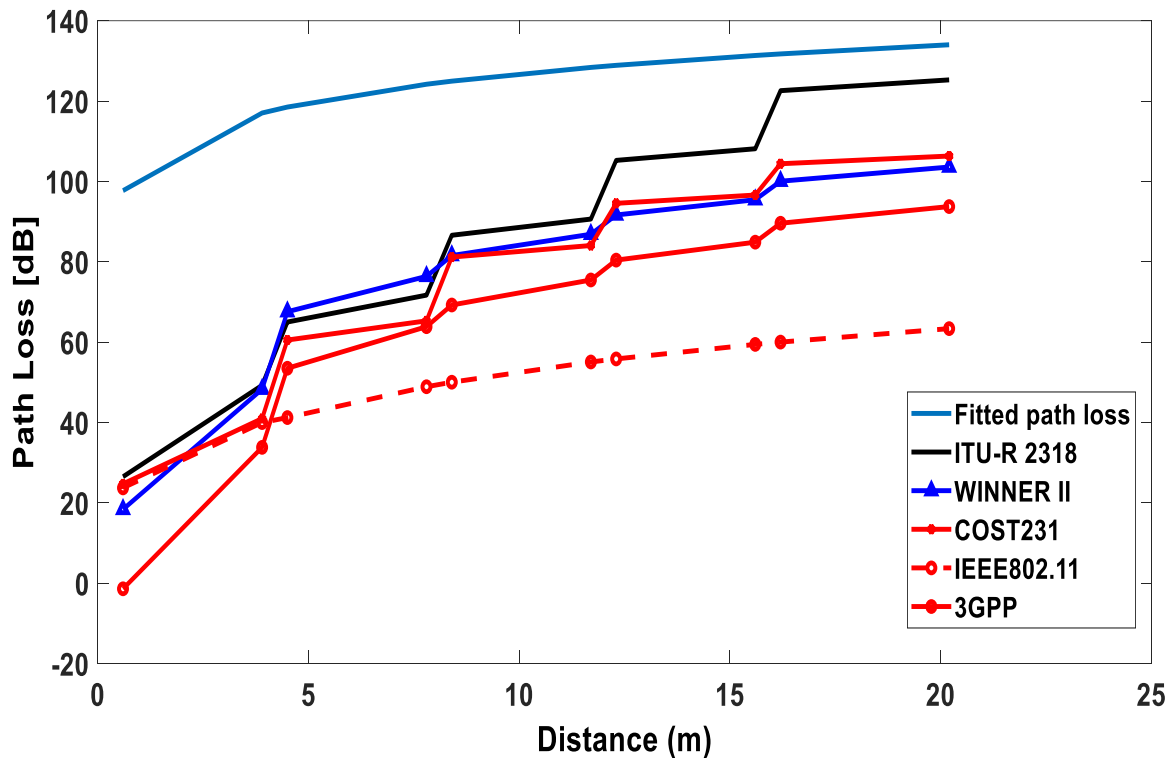


Figure 4-22 : Models and fitted path loss at 433 MHz in indoor NLoS ceilings and floors_ scenario B

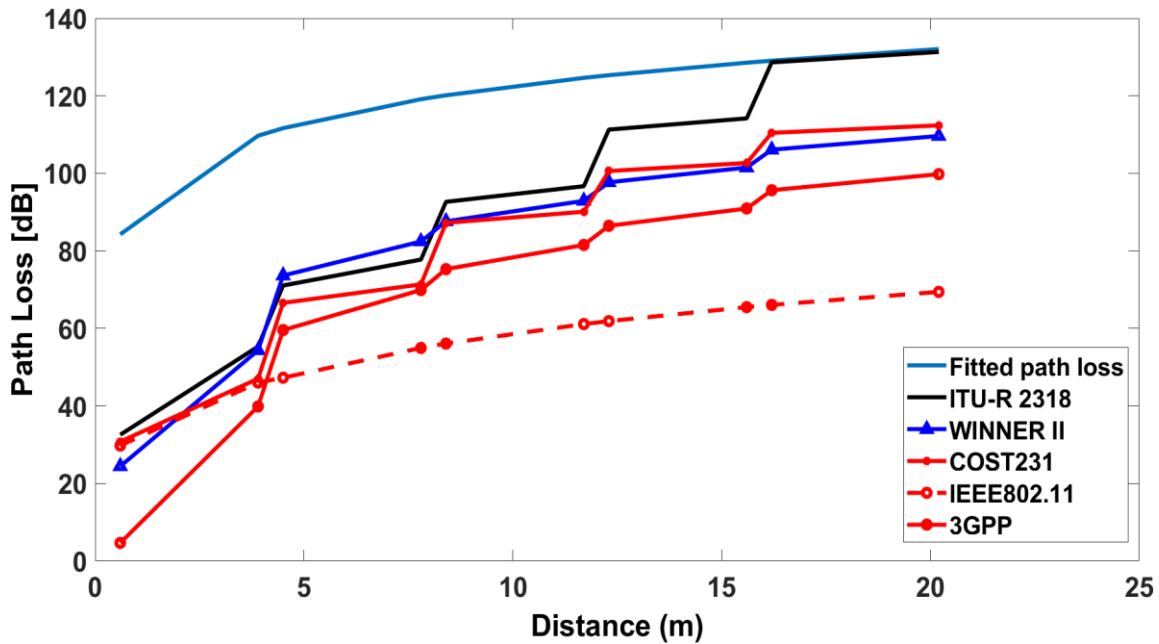


Figure 4-23: Models and fitted path loss at 868 MHz in indoor NLoS ceilings and floors_ scenario B

Figure 4-24 and Figure 4-25 depict how the LoRa signal performed at the two investigated frequencies on the emergency stairs. The path loss increases as the distance between the Tx and Rx along the stairs connecting all floors of the Masri building increases, as is to be expected. The proposed path loss model is underestimated by all models, but Winner II is the closest, followed by COST231, ITU-R 2318, IEEE 802.11, and 3GPP, respectively in both studied frequencies.

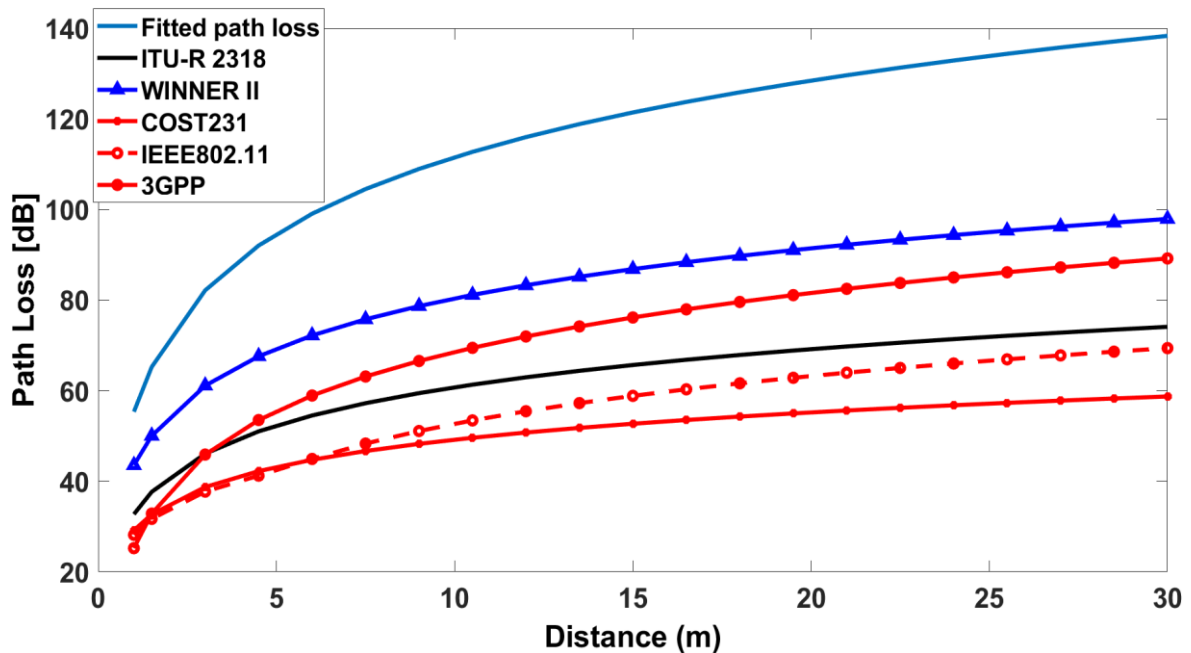


Figure 4-24: Models and fitted path loss at 433 MHz in indoor NLoS Emergency stairs_ scenario C

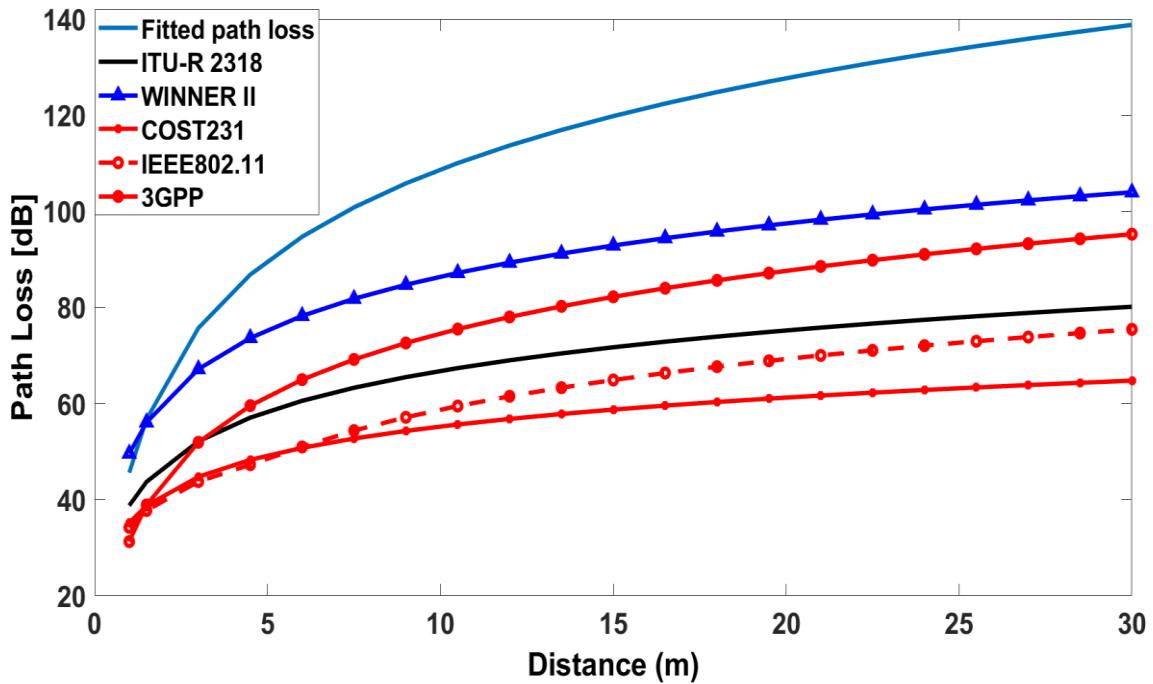


Figure 4-25: Models and fitted path loss at 868 MHz in indoor NLoS Emergency stairs_ scenario C

The impact of walls can be seen in Figure 4-26 and Figure 4-27, where the loss rises as the number of walls between the Tx and Rx increases. The loss after the first wall at a frequency of 868 MHz reached 84.2 dB, while it reached 88.7 dB at 433 MHz, and then it started to rise as a result of increasing the number of walls, reaching a total of five consecutive walls, in addition to the distance between these walls and the multipath effect arising from the presence of classroom windows. Regarding the other models, the effect of the walls is visible in 3GPP, COST231 and WINNER II, but is not taken into account by IEEE 802.11 and ITU-R2318. In comparison to the fitted curve, the path loss was underestimated by the WINNER II, ITU-R2318, and IEEE802.11 models. COST231 initially underestimated the path loss before changing to an overestimation at 27.85m. The loss was also underestimated by 3GPP until a distance of 11.85 m, after which it overestimated. Other models perform similarly at the previous frequency of 868 MHz, with the exception of 3GPP and COST231. 3GPP approximately reaches the fitted curve of the measured data from 12.85 m to 19.85 m, and COST231 approximately reaches it from 20.85 m to 28.85 m.

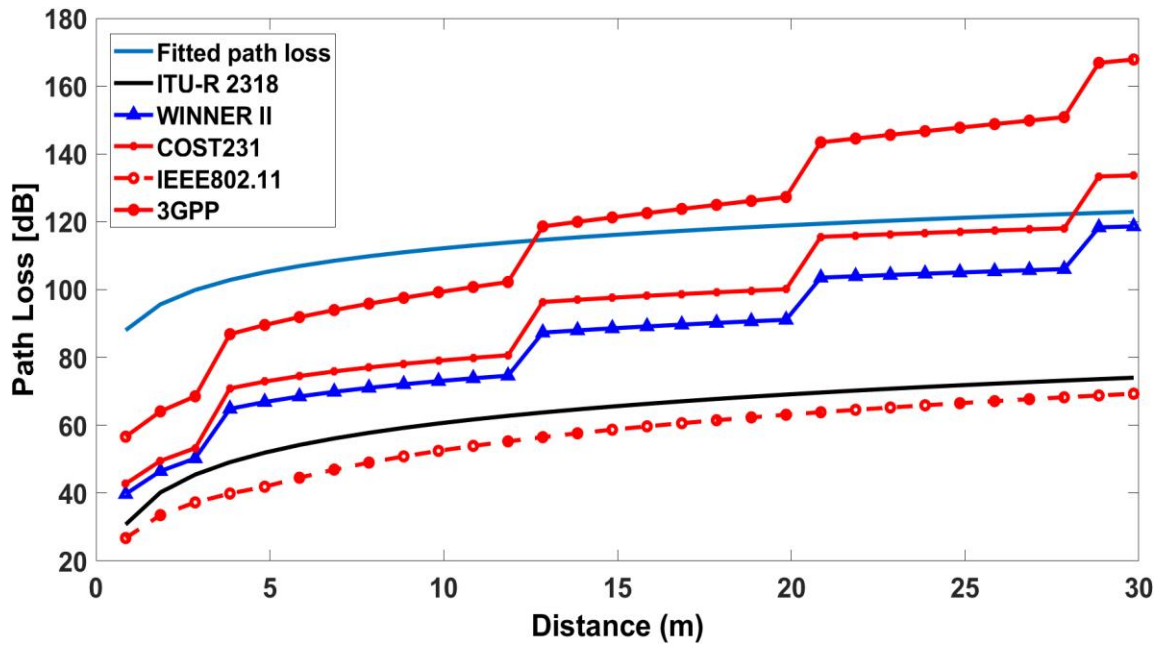


Figure 4-26: Models and fitted path loss at 433 MHz in indoor NLoS multiple walls_ scenario D

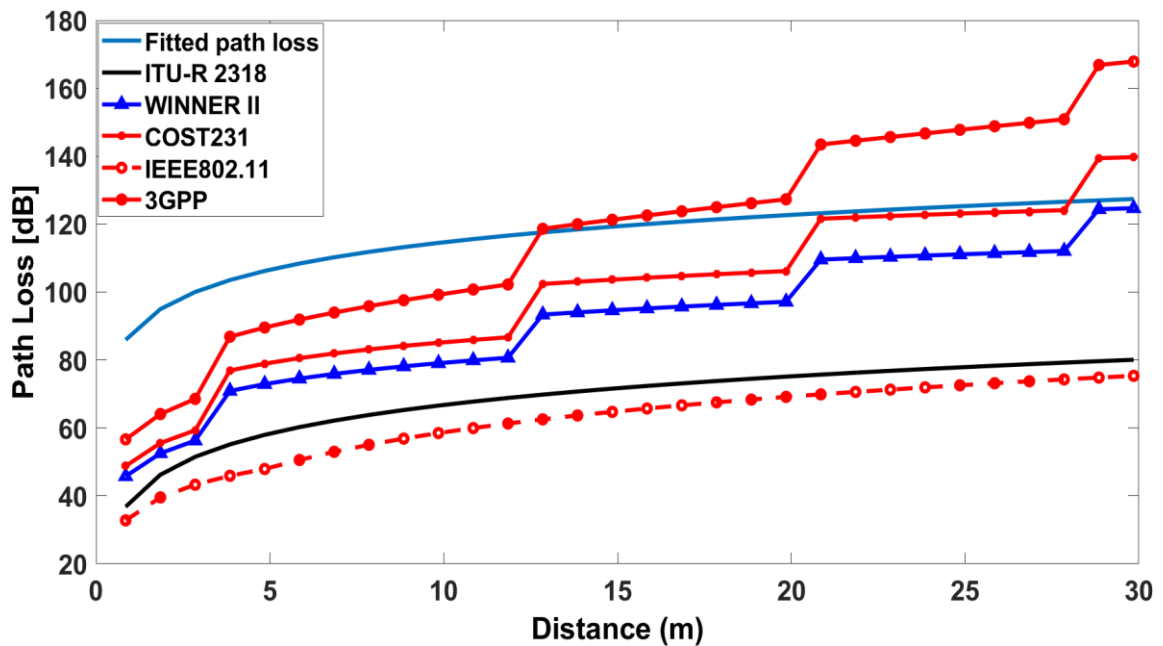


Figure 4-27: Models and fitted path loss at 868 MHz in indoor NLoS multiple walls_ scenario D

Another scenario was conducted in the lecture theater to examine how the LoRa signal performed there, where there are student seats and large windows that contribute to multipath in addition to the effect of Tx and Rx separation distance. The signal performance demonstrates an increase in path loss with distance, in addition to the presence of additional losses at 18 m caused by going outside the lecture theater and the presence of the wall as

an obstacle between the Tx and the Rx as shown in Figure 4-28 and Figure 4-29 . As for the performance of other models, an increase in the path loss was installed in all models with the increase in distance, and the effect of the wall appears in WINNER II, COST231, and 3GPP, while ITU-R2318 and IEEE802.11 do not take this effect into account. Up to 5m, ITU-R2318 has the best fit to the curve, but after that point, WINNER II overtakes it and is the closest at both frequencies. One interesting finding was that the path loss at 433 MHz and 868 MHz was underestimated by all models except WINNER II. At a distance of 19 m and an operating frequency of 868 MHz, WINNER II matches the fitted data curve. Regarding the impact of the wooden door on the signal strength alone, it resulted in a loss of about 8 dB. This loss was cut to 5 dB by the glass door at both frequencies.

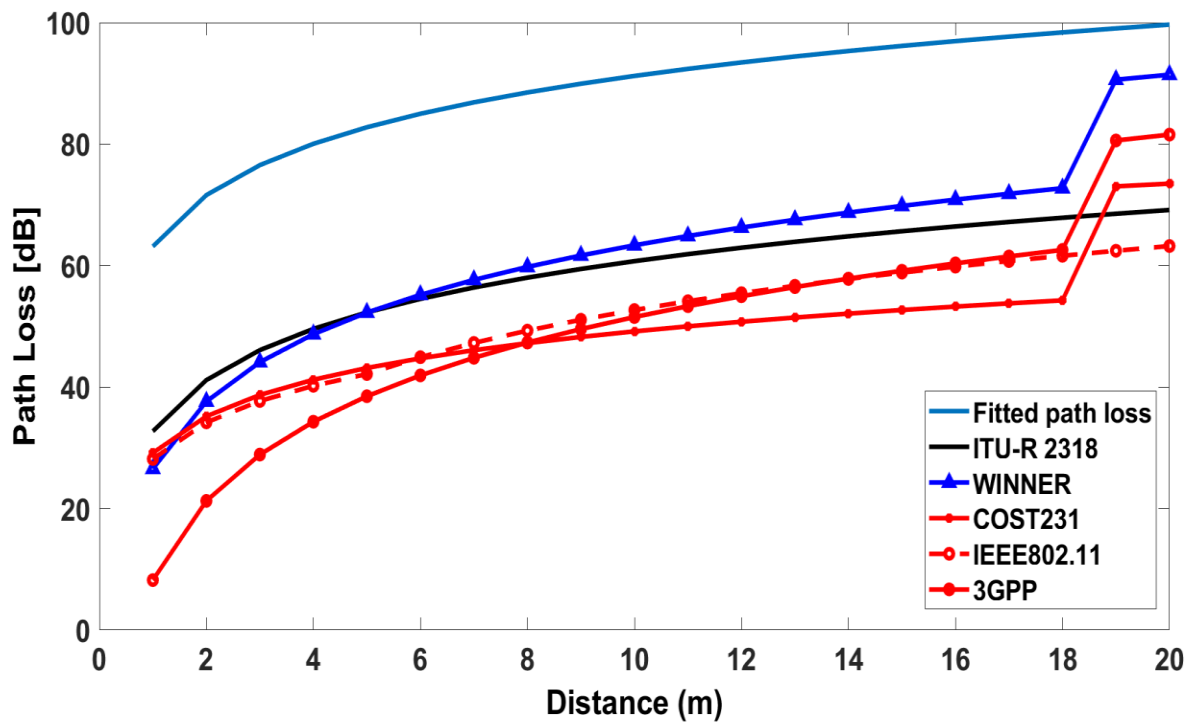


Figure 4-28: Averaged actual and fitted path loss at 433 MHz in indoor NLoS in Theater Lectures_ scenario E

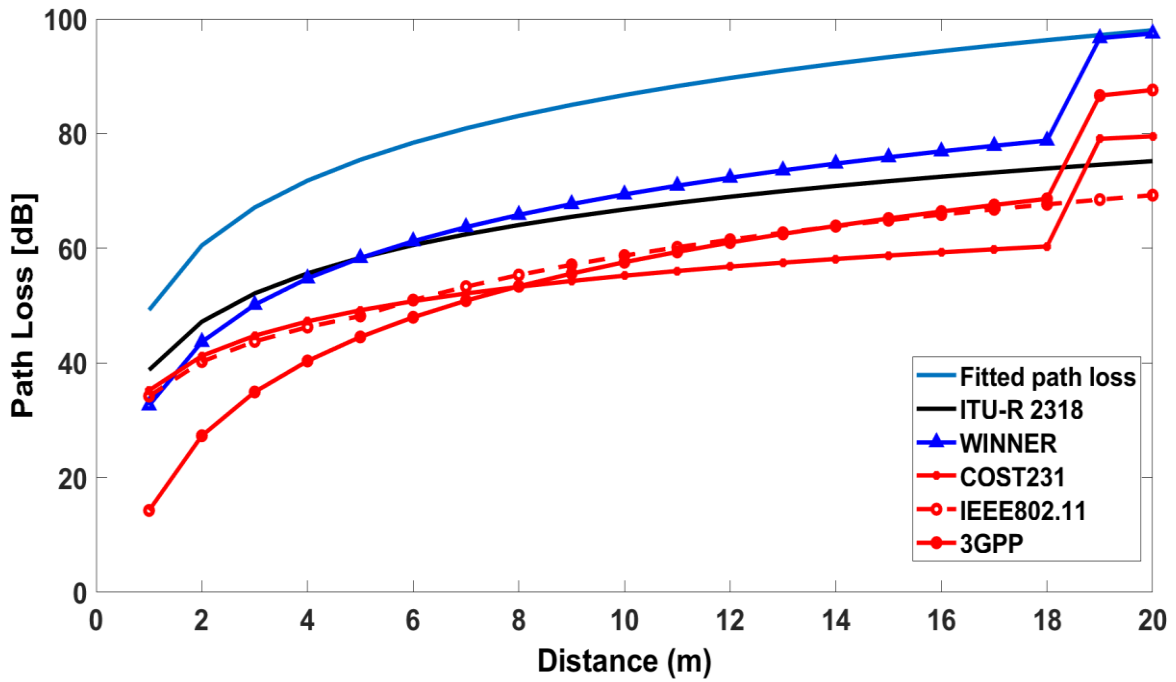


Figure 4-29: Averaged actual and fitted path loss at 868 MHz in indoor NLoS in Theater Lectures_ scenario E

4.2.2 Outdoor Scenario

This section continues to compare the results with models in the literature but in an outdoor environment. Figure 4-30 and Figure 4-31 show the performance of the LoRa signal in an outdoor environment in the presence of trees' leaves, where we notice an increase in path loss with the increase in the number of trees separate Tx and Rx. The performance of LoRa in the same location without these trees is also clear from the figures. While other models such as WINNER II, COST231, IEEE802.11, 3GPP, and Free space underestimated the path loss at both frequencies of 868 MHz and 433 MHz, fitted curve with trees' leaves is relatively close to the Lee model as same observations were obtained in [66],[67],[68]. Despite the fact that the experiment was conducted under the same conditions and at the same location, the effect of the loss was much more noticeable at 868MHz than it was at 433MHz. Due to the fact that high frequencies cover lower distances than low frequencies, they tend to show obstacles more clearly.

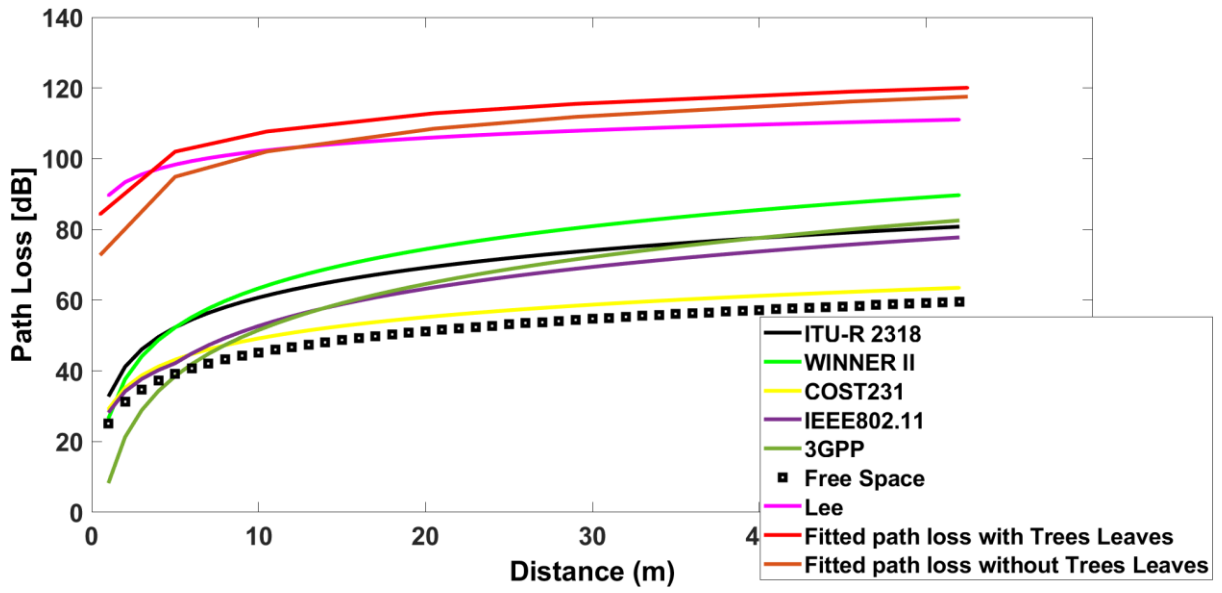


Figure 4-30: Averaged actual and fitted path loss at 433 MHz for outdoor NLoS and LoS for Trees' Leaves_ scenario A

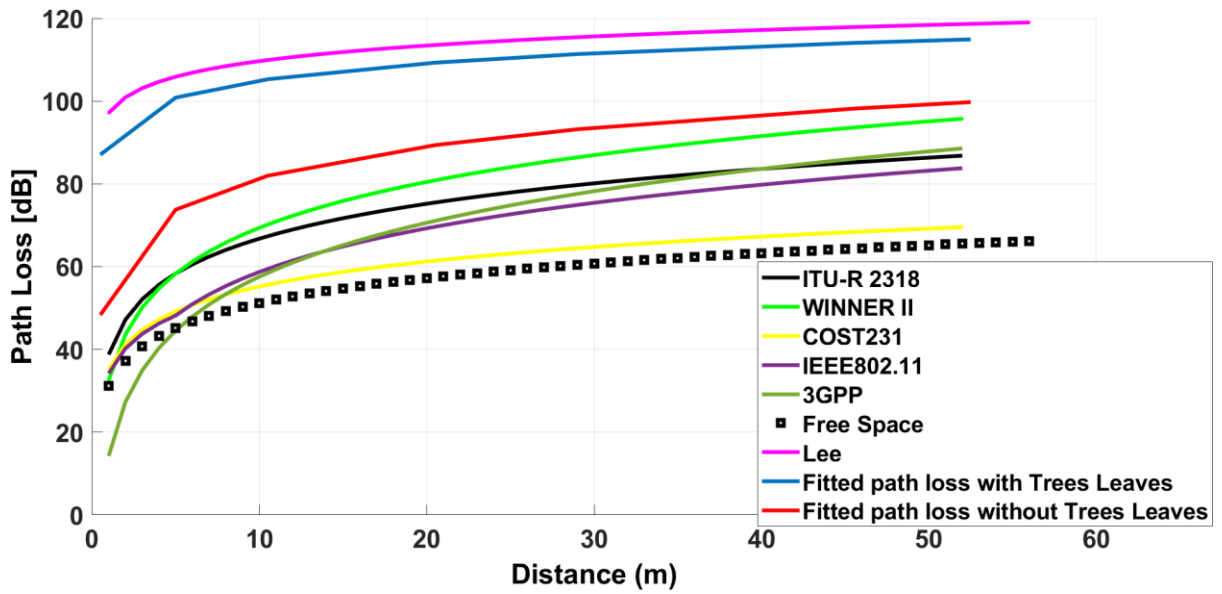


Figure 4-31: Averaged actual and fitted path loss at 868 MHz for outdoor NLoS and LoS for Trees' Leaves_ scenario A

Following a study on how trees' leaves affect LoRa signal performance, Figure 4-32 and Figure 4-33 show how trees' trunks effect on the LoRa signal. The findings show that as the number of trees' trunks that block the LoRa signal increases, the path loss also increases. In addition, the LoRa signal's performance in an environment without trunks, where the path loss was lower, is shown in the same figures also.

As can be seen, the path loss model based on the proposed parameters performs nearly as well as the Lee model when there are trunks present, same observations were obtained in [66],[67],[68]. However, path loss was underestimated by models like WINNER II, COST231, IEEE 802.11, 3GPP, and Free Space at both frequencies of 433 MHz and 868 MHz. Because higher frequencies have a tendency to show obstacles more clearly, it is important to note how clearly the influence of tree trunks can be seen at 868 MHz.

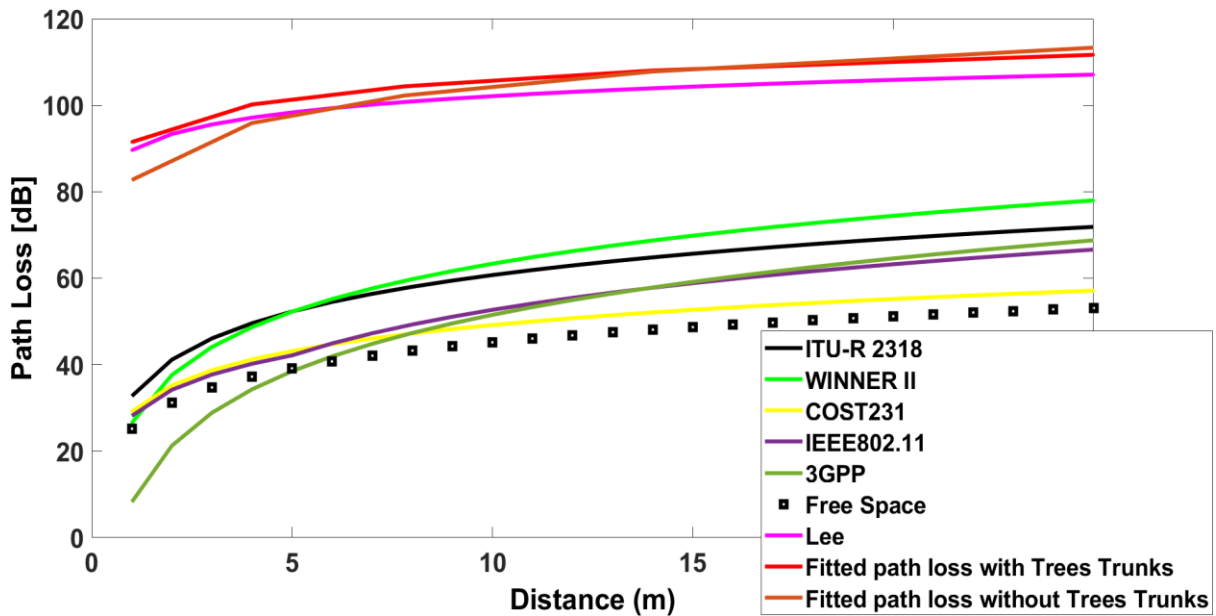


Figure 4-32: Averaged actual and fitted path loss at 433 MHz in outdoor NLoS and LoS for Trees' Trunks_ scenario B

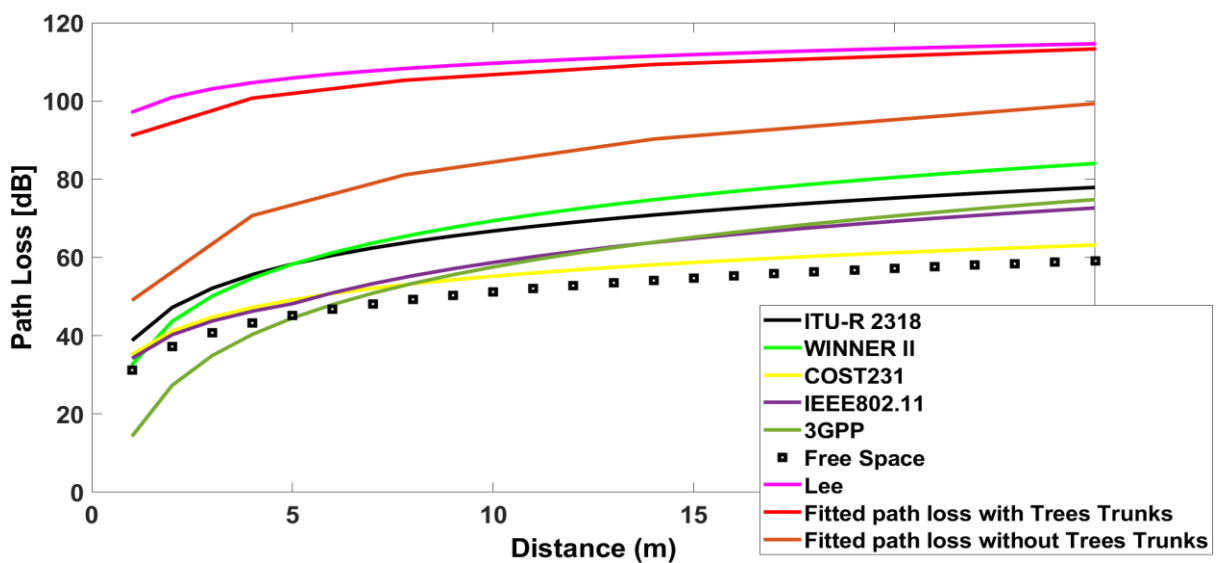


Figure 4-33: Averaged actual and fitted path loss at 868 MHz in outdoor NLoS and LoS for Trees' Trunks_ scenario B

Figure 4-34 and Figure 4-35 continue the discussion of LoRa's performance over long distances of up to 12 km in a challenging outdoor environment with varying-height buildings, trees, streets, traffic flow, and LoS and NLoS connections. The results show that although the experiment was carried out under identical conditions at both frequencies, at the frequency of 433 MHz and at a distance of 2 km up to 12 km, the performance of the fitted curve is close to that of the LEE model and same observations were obtained in [66],[67],[68], while at the frequency of 868 MHz, the performance of the fitted curve was matched to the LEE model at a distance of 2 km up to 12 km. Regarding the other models, ITU-R2318, SUI, COST 231, and Okumura Hata all significantly overestimated the path loss, while Free Space significantly underestimated the expected path loss at the two frequencies.

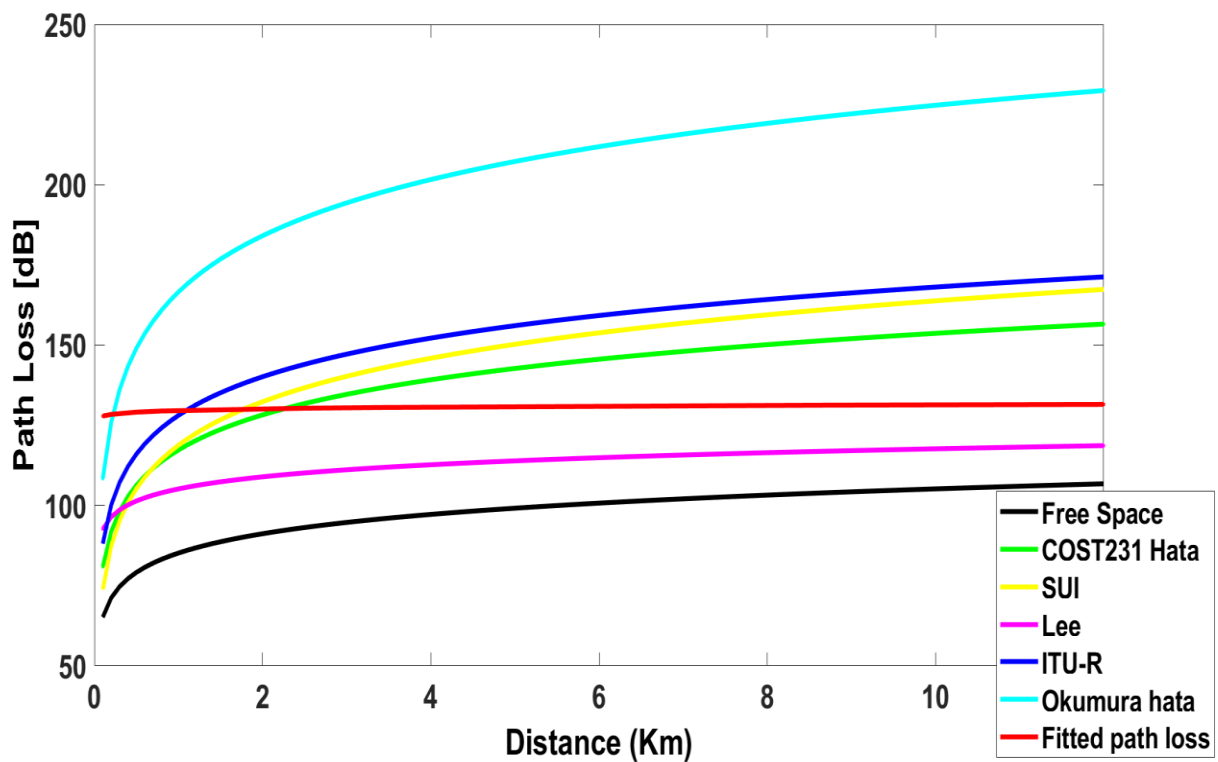


Figure 4-34: Averaged actual and fitted path loss at 433 MHz in NLoS and LoS complex outdoor_ scenario C

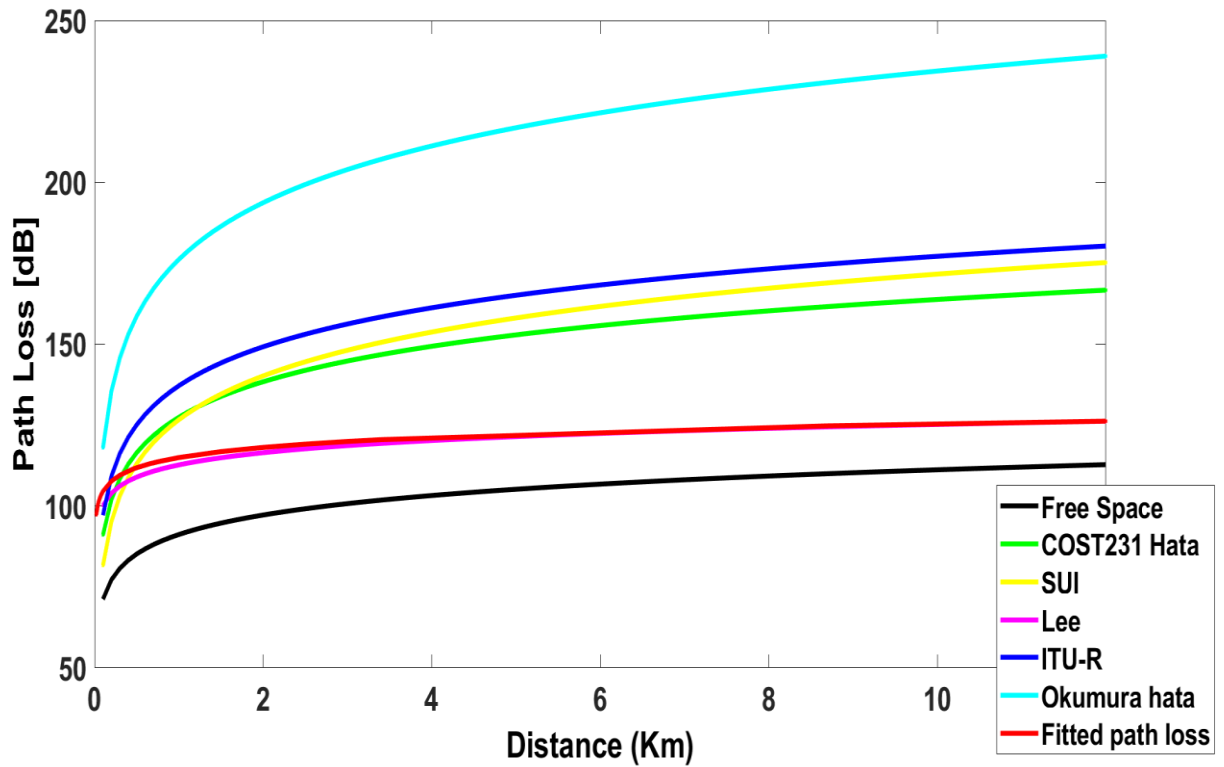


Figure 4-35: Averaged actual and fitted path loss at 868 MHz in NLoS and LoS complex outdoor_ scenario C

4.3 Model Validation

Firstly, the measurements were re-measured for two scenarios, one indoor and the other outdoor, at the frequencies of 868 MHz and 433 MHz after a month for validation, and the path loss were as in the Figure 4-38 to Figure 4-41 and this applied to all scenarios.

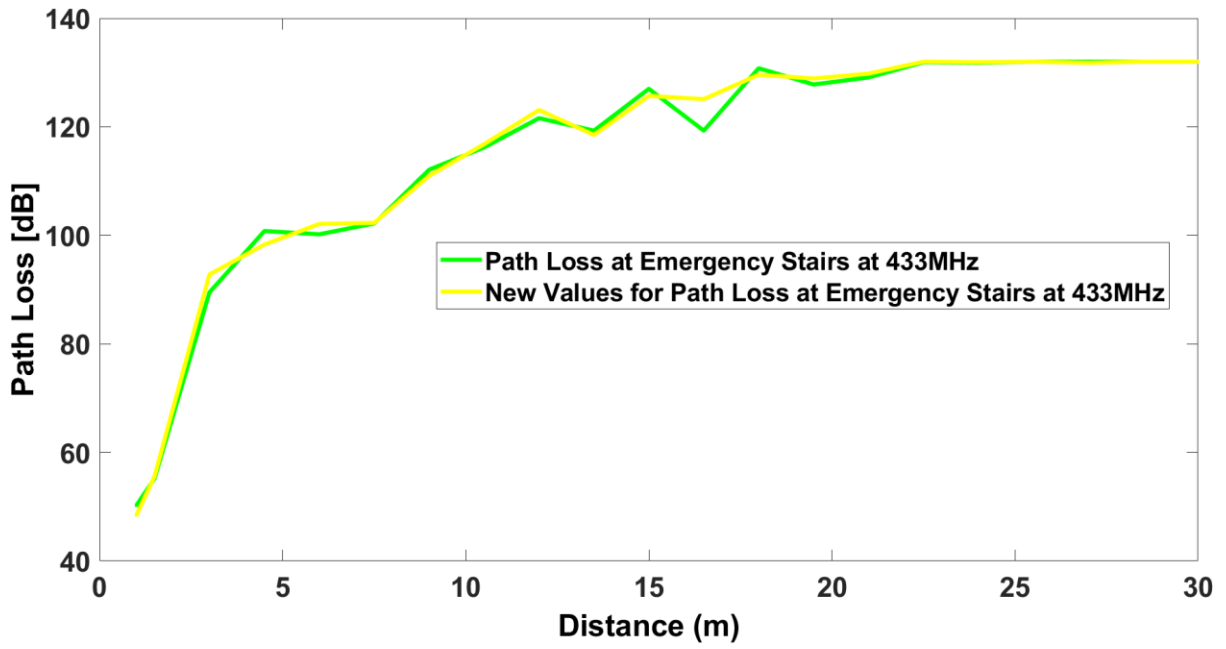


Figure 4-36: Path loss at emergency stairs at 433MHz and new path loss based on new measurements

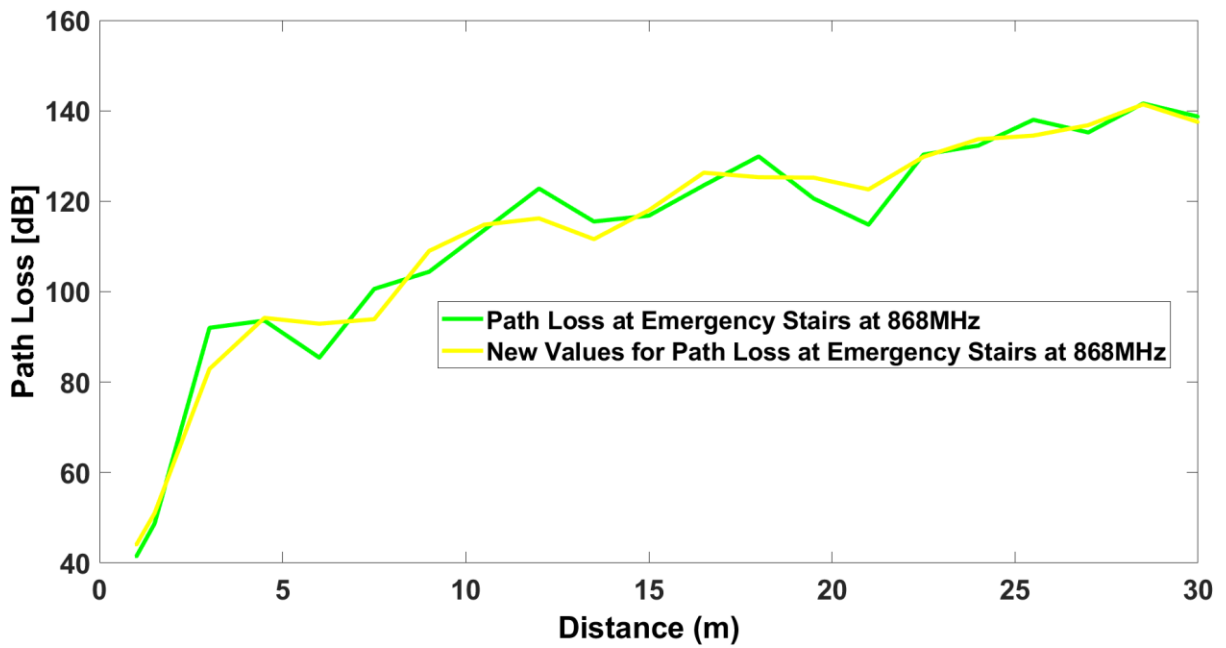


Figure 4-37: Path loss at emergency stairs at 868MHz and new path loss based on new measurements

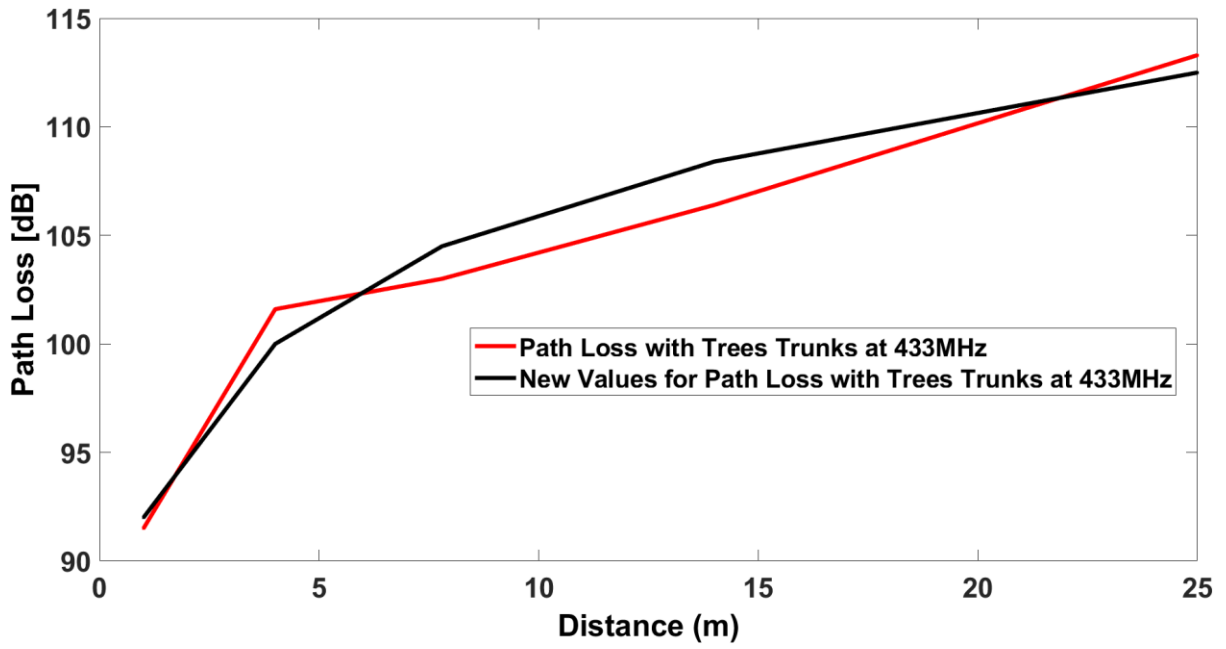


Figure 4-38: Path loss with trees trunks at 433MHz and new path loss based on new measurements

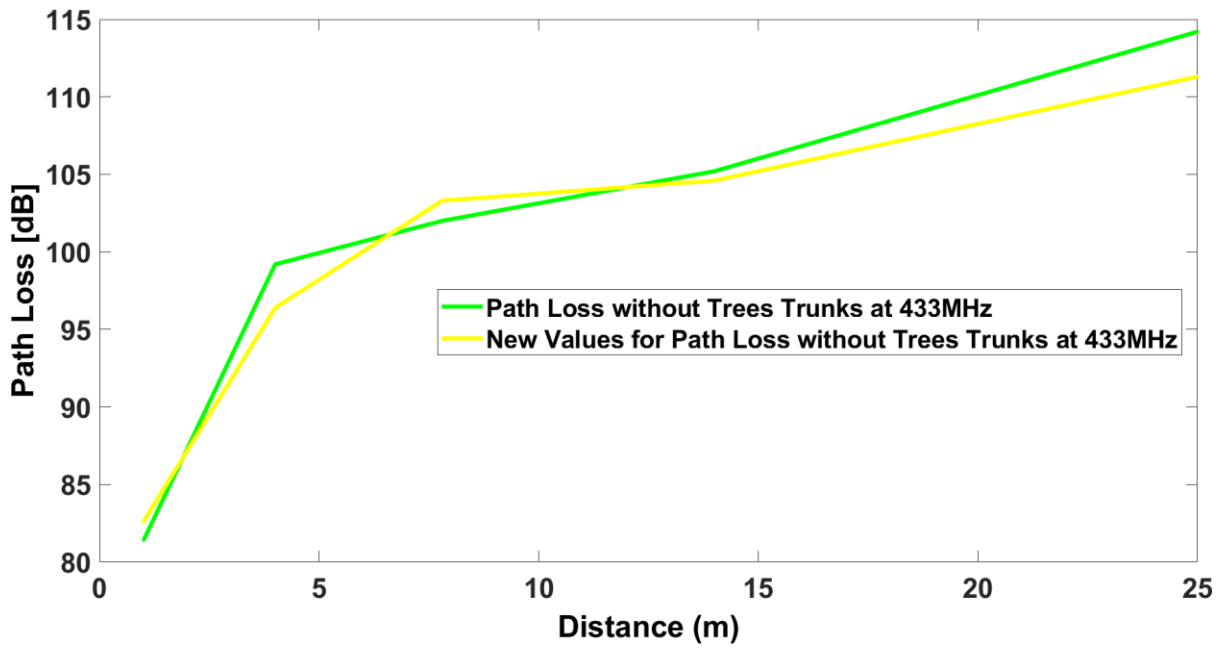


Figure 4-39: Path loss without trees trunks at 433MHz and new path loss based on new measurements

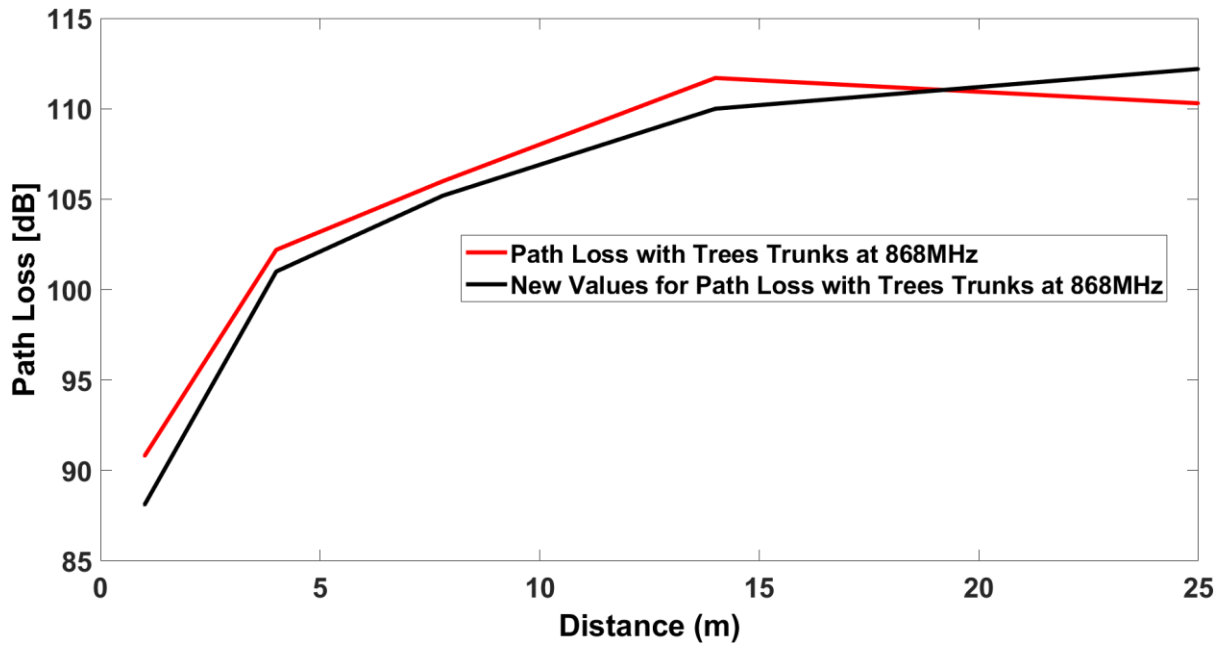


Figure 4-40: Path loss with trees trunks at 868MHz and new path loss based on new measurements

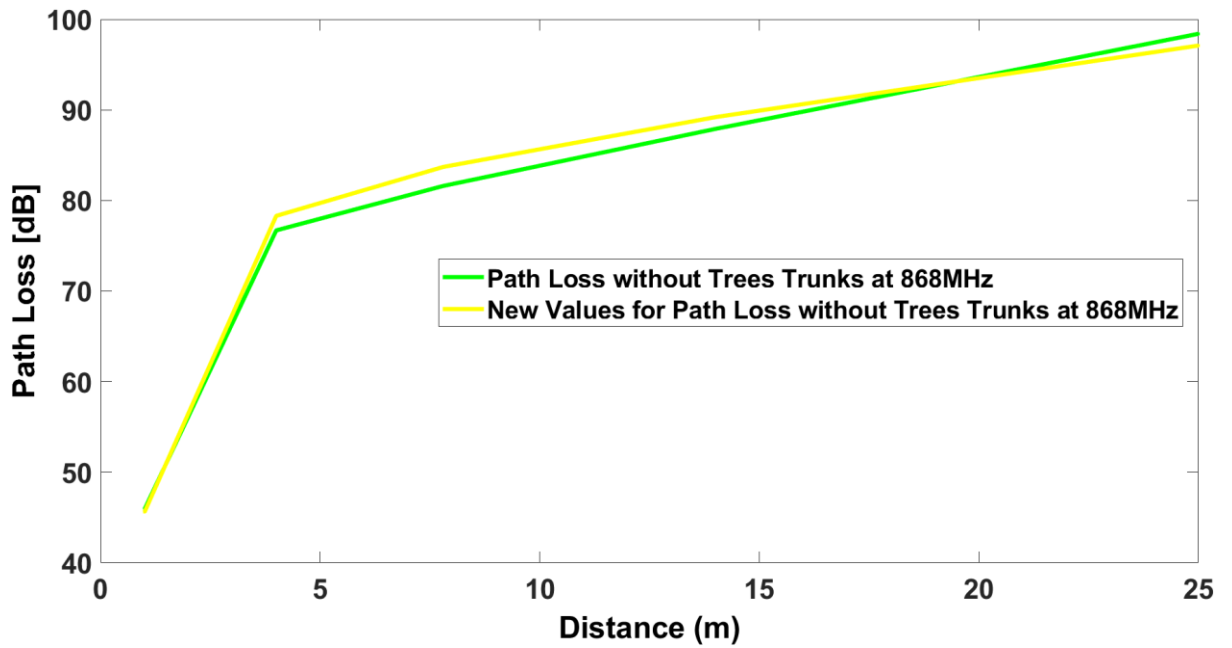


Figure 4-41: Path loss without trees trunks at 868MHz and new path loss based on new measurements

Table 4.3: RMSE between previous and new path loss calculated based on measurements for two scenarios indoor and outdoor for validation

Scenario	RMSE
Path Loss for emergency stairs at 433MHz	1.7881
Path Loss for emergency stairs at 4868MHz	4.4114
Path Loss with trees Trunks at 433MHz	1.3928
Path Loss without trees Trunks at 433MHz	1.9869
Path Loss with trees Trunks at 868MHz	1.7815
Path Loss without trees Trunks at 868MHz	1.4449

In various indoor and outdoor scenarios, RMSE is used to assess the accuracy between the fitted path loss model based on the proposed parameters and the path loss model based on measurements. RMSE is also used to evaluate the accuracy and find the difference between the new proposed parameters for path loss model and the previous models in the literature, as illustrated in Table 4.4 to Table 4.6. The Tables show that the new proposed parameters for path loss models in both indoor and outdoor environments fit the measured data better than the other models based on their lowest RMSE values, while the performance of the other models varies according to the types of scenarios they can handle.

Table 4.4: RMSE for path loss model based on the proposed parameters and different models in the literature in indoor scenarios

Scenario	Model based on the Proposed parameters	RMSE				
		ITU-R 2318	WINNER II	COST231	IEEE802.11	3GPP
Corridor LoS 433MHz	7.62	20.11	34.29	32.26	28.05	36.27
Corridor LoS 868MHz	6.42	5.36	19.27	17.22	13.13	21.29
Ceilings and floors 433MHz	5.98	44.08	49.10	50.71	73.94	61.98
Ceilings and floors 868MHz	6.97	33.06	37.45	39.23	62.70	50.30
Emergency stairs 433MHz	4.78	53.274	32.97	65.60	59.72	43.87
Emergency stairs 868MHz	6.51	45.74	25.77	58.07	51.99	35.89
Walls 433MHz	0.970	51.13	31.04	25.23	57.93	22.03
Walls 868MHz	1.66	47.79	27.47	21.82	54.58	20.26
Lectures theater 433MHz	5.14	29.39	27.72	39.91	37.02	40.13
Lectures theater 868MHz	5.55	18.30	16.36	29.01	25.86	28.58

Table 4.5: RMSE for path loss model based on the proposed parameters and different models in the literature in vegetation outdoor scenarios

Scenario	Model based on the Proposed parameters	RMSE							
		Free Space	Lee	ITU-R 2318	WINNER II	COST231	IEEE802.11	3GPP	Fitted LoS path loss
Trees' Leaves 433MHz	2.66	61.45	7.09	43.62	38.82	57.45	49.25	48.95	4.70
Trees' Leaves 868MHz	2.067	51.74	4.26	34.30	29.89	47.93	39.99	40.02	20.48
Trees' Canopies 433MHz	1.35	60.74	3.89	45.35	43.14	56.74	52.52	55.13	2.93
Trees' Canopies 868MHz	1.87	55.79	2.86	40.38	38.20	51.79	47.56	50.19	22.98

Table 4.6: RMSE for path loss model based on the proposed parameters and different models in the literature in complex outdoor scenarios

Scenario	Model based on the Proposed parameters	RMSE					
		Free Space	COST231 Hata	SUI	LEE	ITU-R	Okumura hata
Complex Outdoor 433MHz	2.85	33.98	18.79	26.11	18.34	28.87	77.31
Complex Outdoor 868MHz	6.72	18.49	31.67	37.80	1.45	43.43	94.32

4.4 Shadow Fading

The received signal's variation around its average is known as “shadow fading” [50]. This shadowing occurs in indoor environments as a result of the signal's interaction with the walls, furniture, floors, and ceilings while it occurs in outdoor environments as a result of multipath, buildings, trees, movement of people and cars, and weather factors. For each of the measured scenarios, shadow fading was estimated in both indoor and outdoor environments.

4.4.1 Indoor Scenario

The Probability Density Functions(PDF) and Cumulative Density Function(CDF) for all scenarios discussed previously for indoor environment are presented in

Figure 4-44 to Figure 4-55 using MATLAB tool called “distributionFitter”, while Table 4.7 presents the mean and the standard deviation for the shadow fading.

First of all, to plot PDF using “distributionFitter” a histogram for path loss based on measured data was produced by this MATLAB tool for the studied scenario as shown in Figure 4-42, and then a fitted PDF was generated for the plotted histogram as in Figure 4-43. This tool is able to plot many distribution functions as CDF, so a CDF also is plotted for the studied scenarios using this tool as shown in Figure 4-45 and

Figure 4-46.

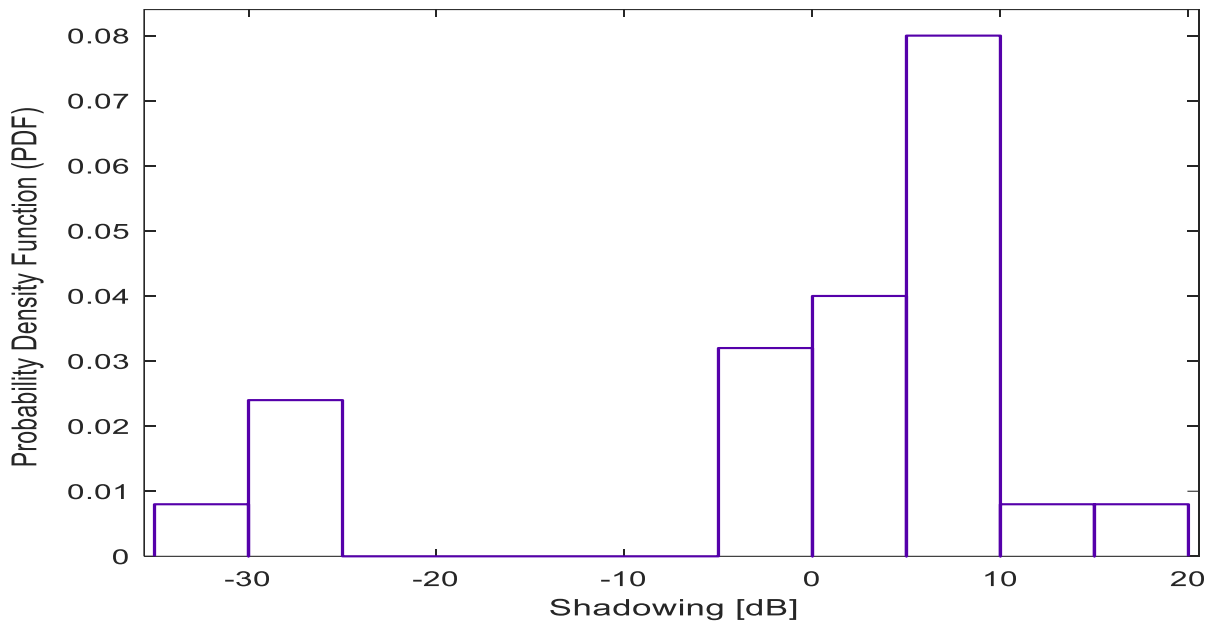


Figure 4-42: Histogram for path loss based on measured data at 433 MHz in indoor LoS_scenario A

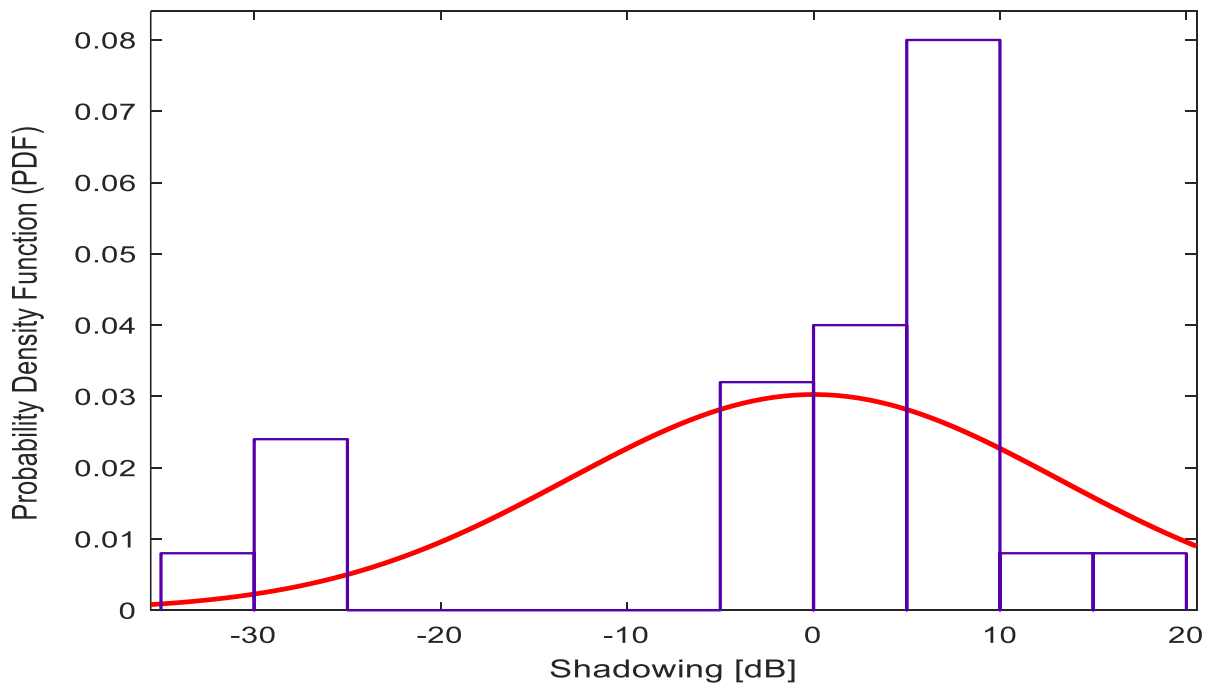


Figure 4-43: Fitted PDF generates for the plotted histogram at 433 MHz in indoor LoS_scenario A

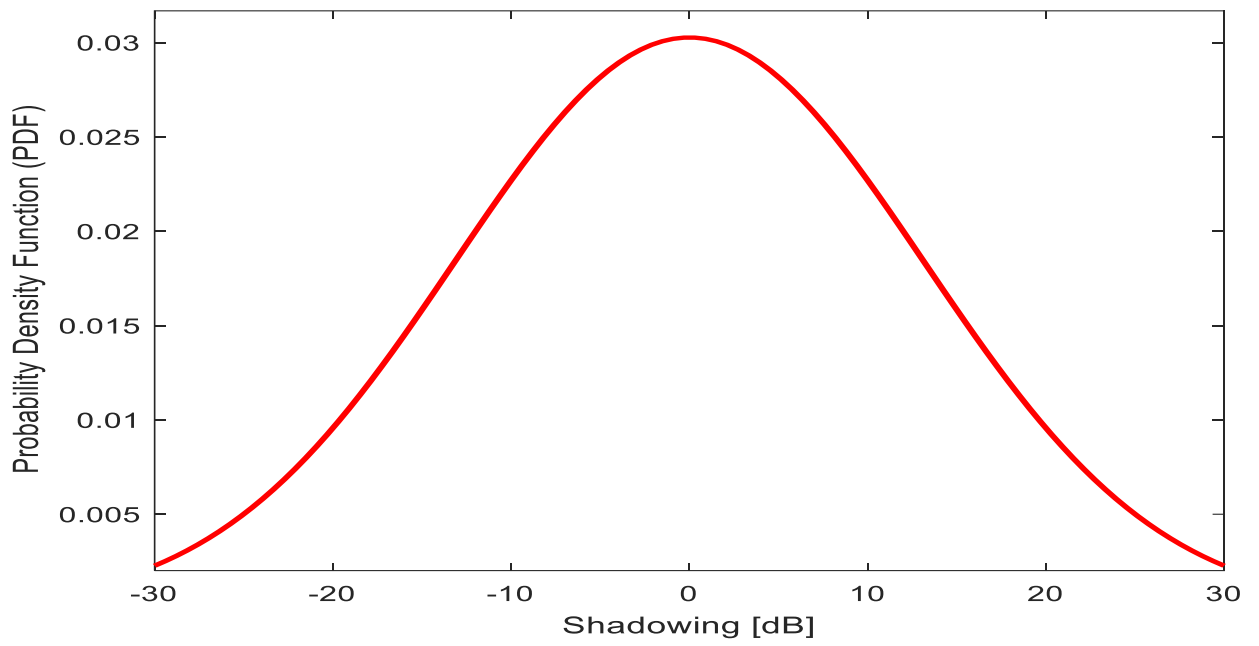


Figure 4-44: Fitted PDF when histogram hides at 433 MHz in indoor LoS_scenario A

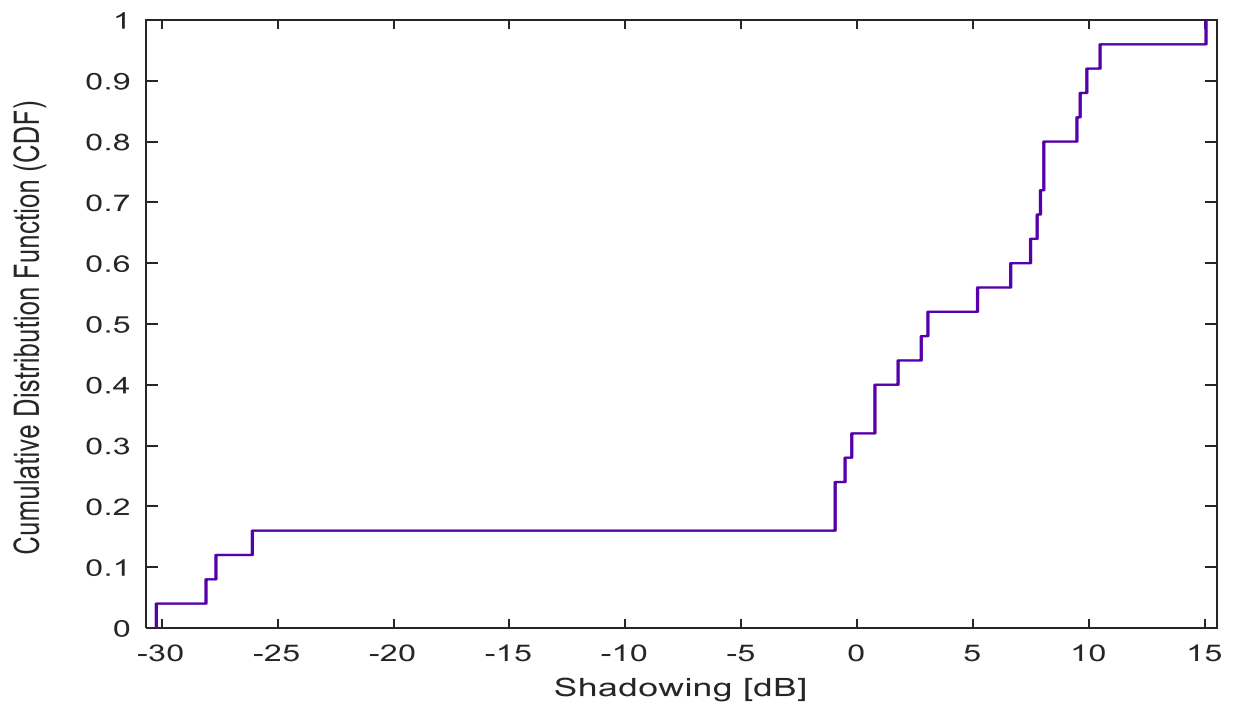


Figure 4-45: CDF vs shadowing at 433 MHz in indoor LoS_scenario A

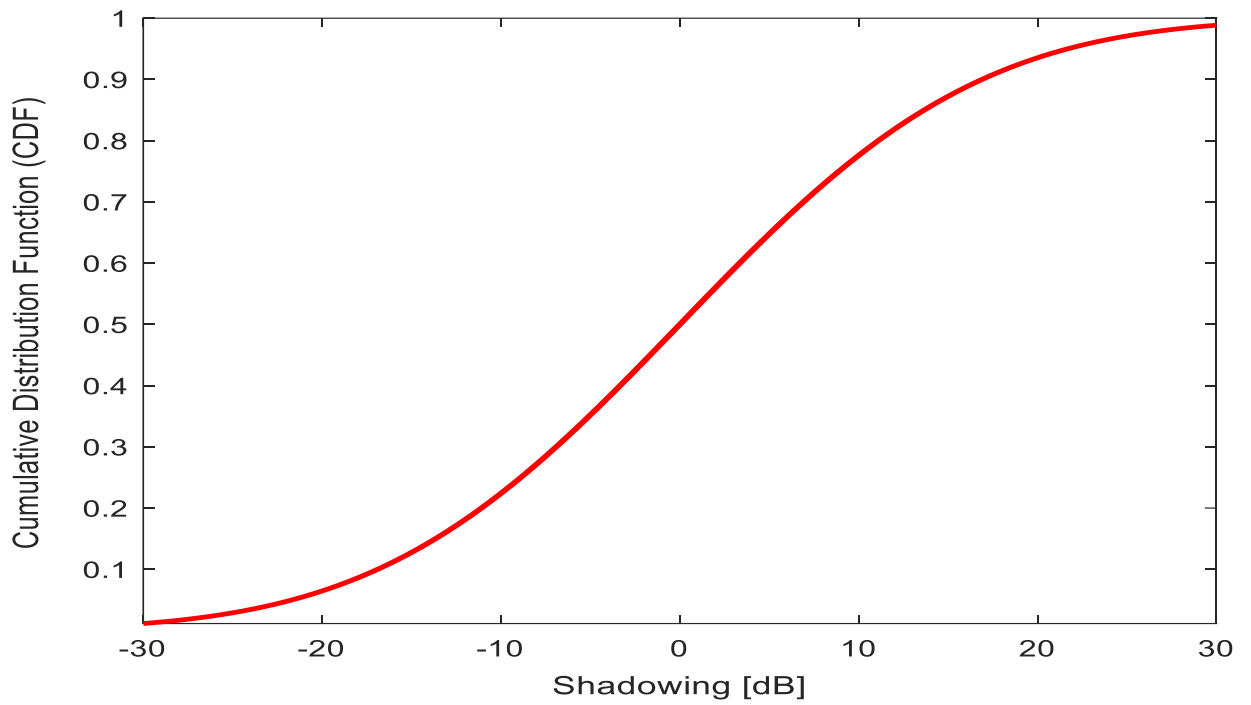


Figure 4-46: Fitted CDF vs shadowing at 433 MHz in indoor LoS_scenario A

The following figures presents PDF and CDF as discussed in the previous steps in the above figures for the rest of scenarios.

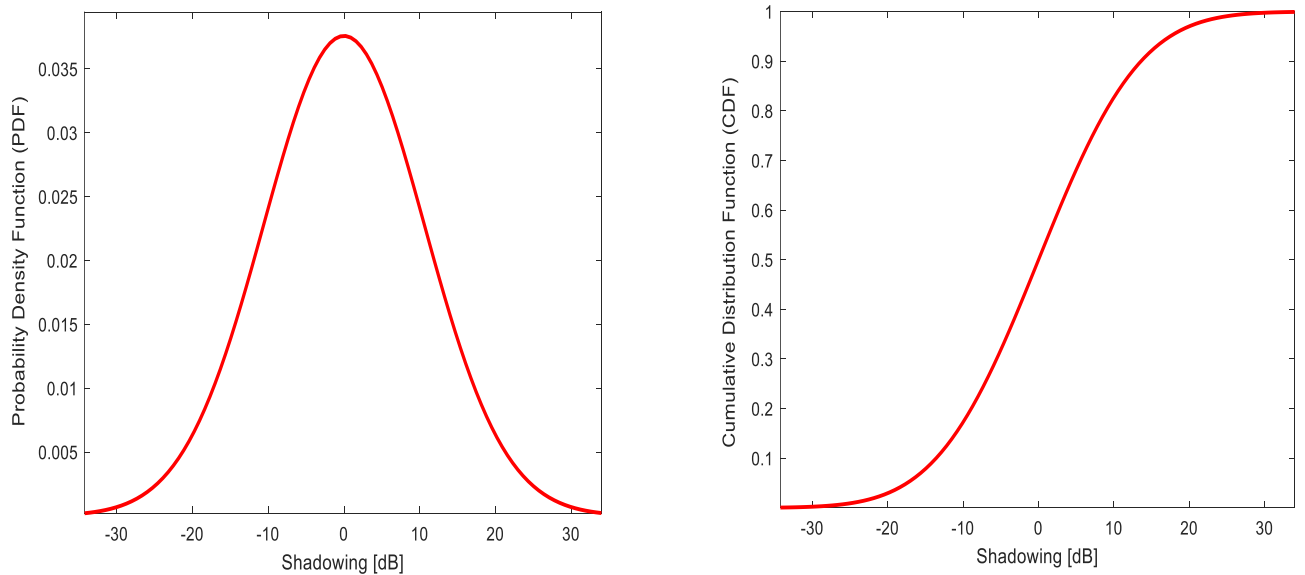


Figure 4-47: PDF and CDF for indoor LoS at 868 MHz_scenario A

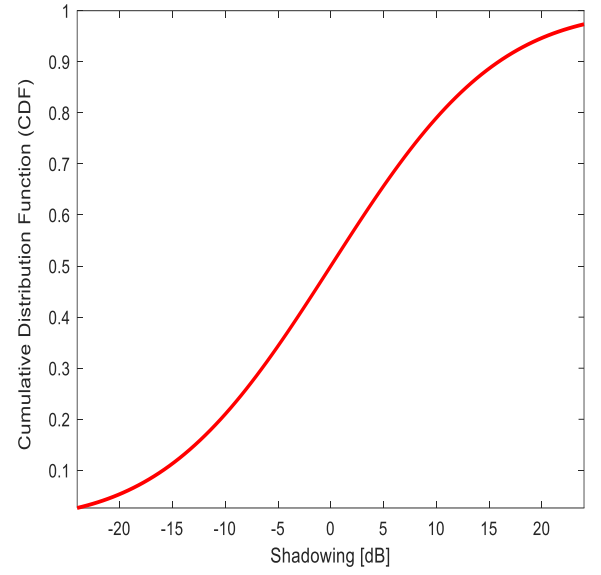
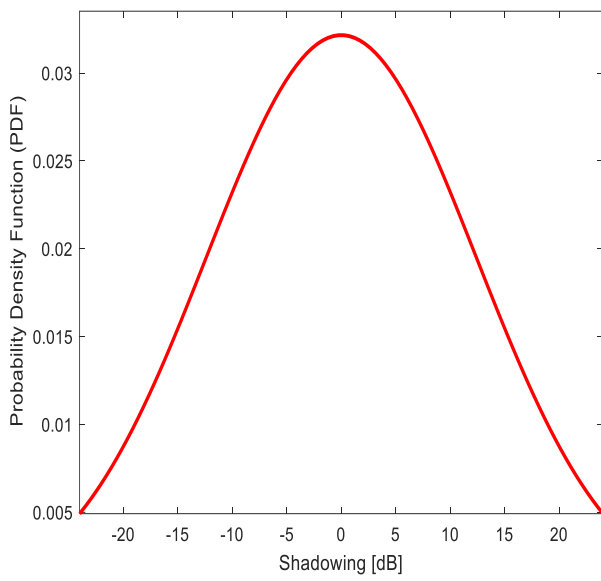


Figure 4-48: PDF and CDF for indoor NLoS ceilings and floors at 433 MHz _ scenario B

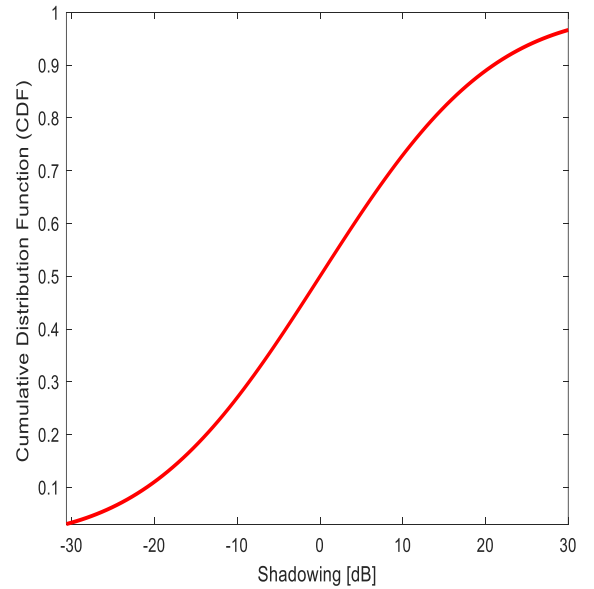
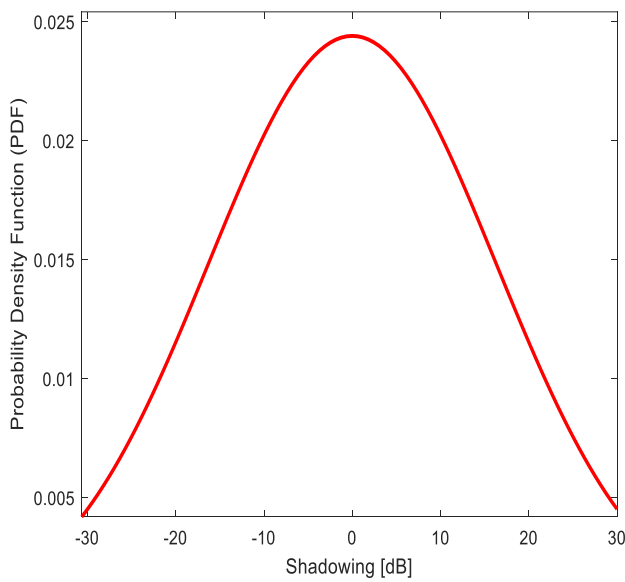


Figure 4-49: PDF and CDF for indoor NLoS ceilings and floors at 868 MHz _ scenario B

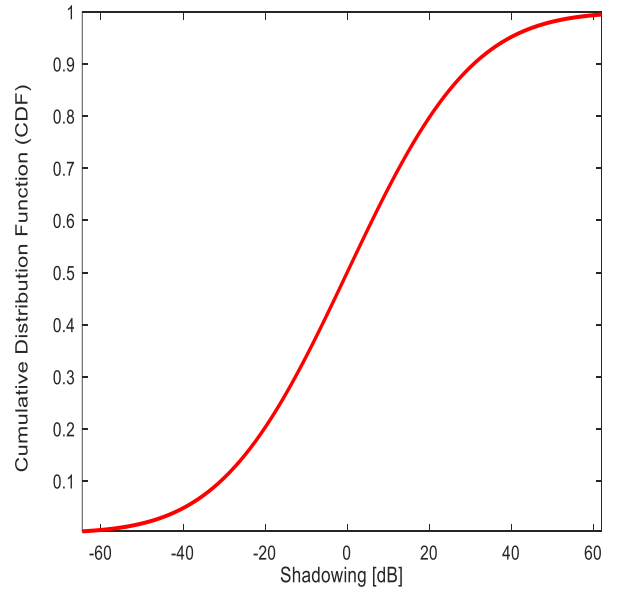
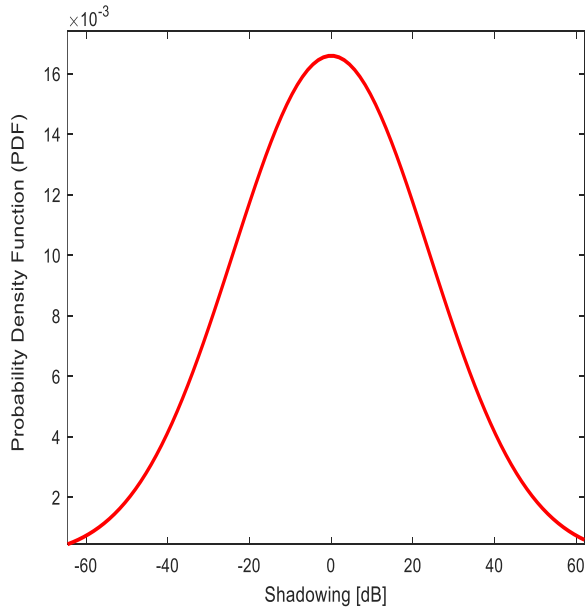


Figure 4-50: PDF and CDF for indoor NLoS emergency stairs at 433 MHz _ scenario C

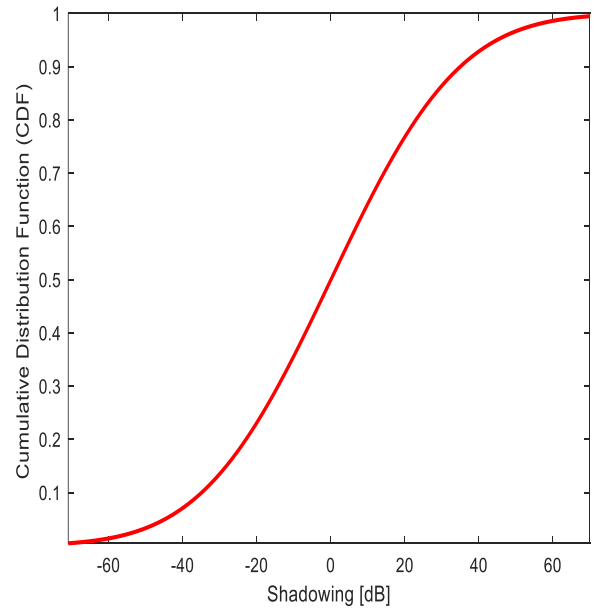
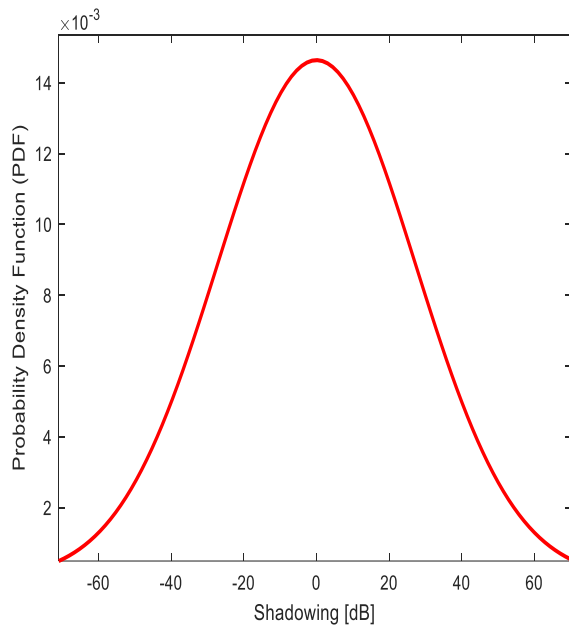


Figure 4-51: PDF and CDF for indoor NLoS emergency stairs at 868 MHz _ scenario C

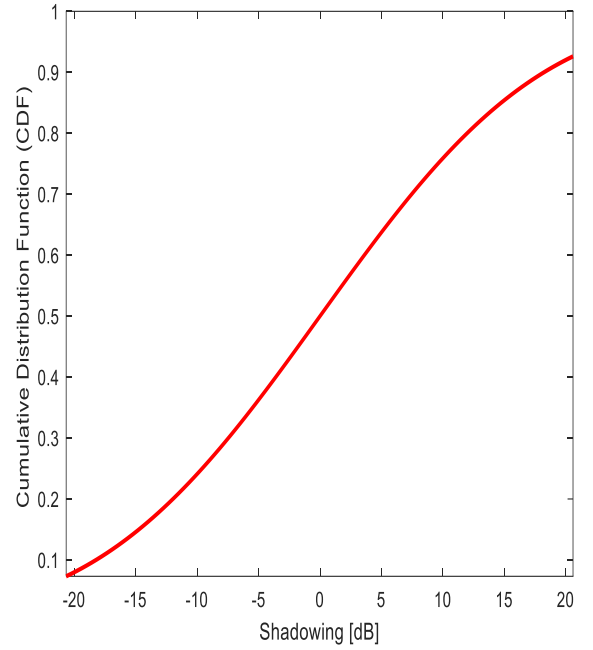
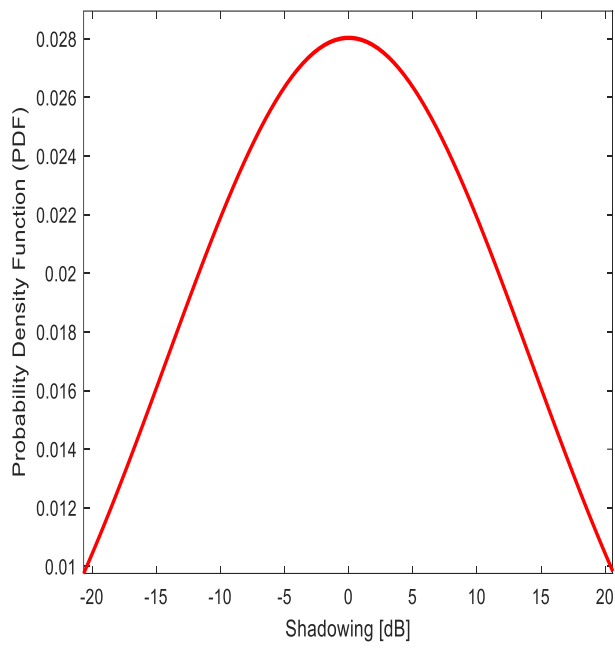


Figure 4-52: PDF and CDF for indoor NLoS multiple walls at 433 MHz _ scenario D

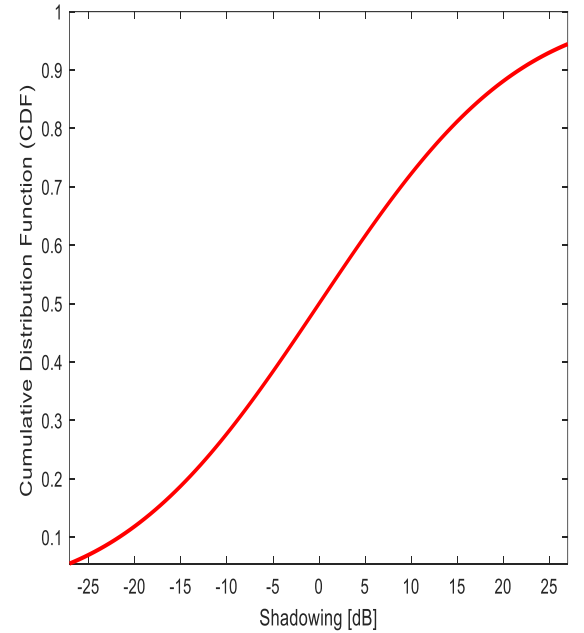
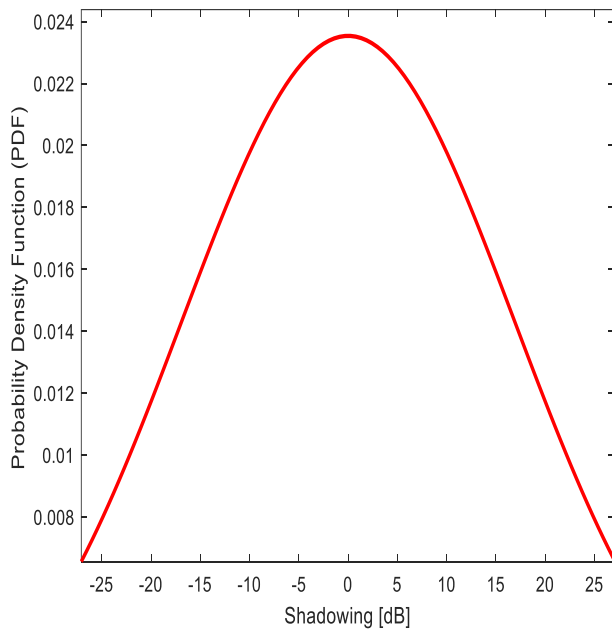


Figure 4-53: PDF and CDF for indoor NLoS multiple walls at 868 MHz _ scenario D

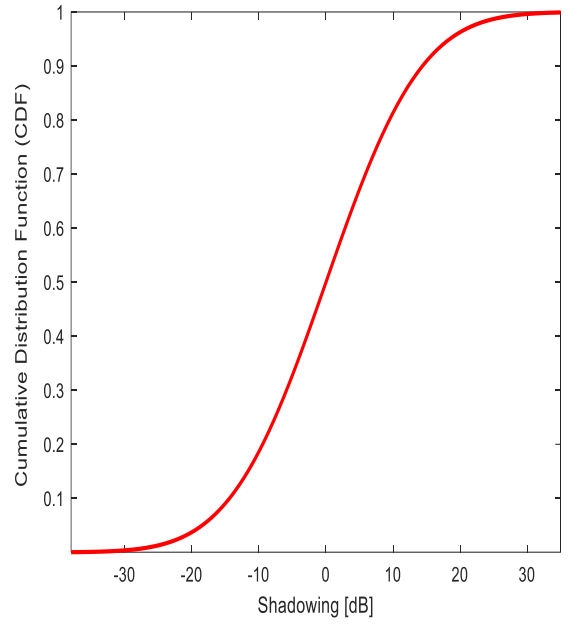
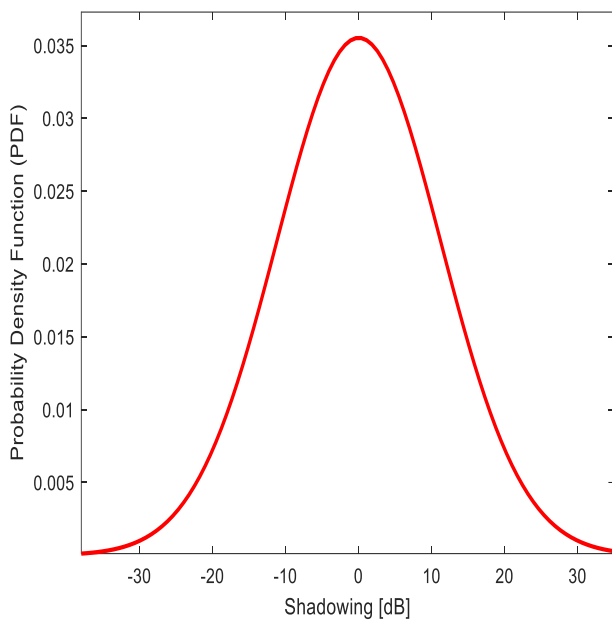


Figure 4-54: PDF and CDF for indoor NLoS theater lecture at 433 MHz _ scenario E

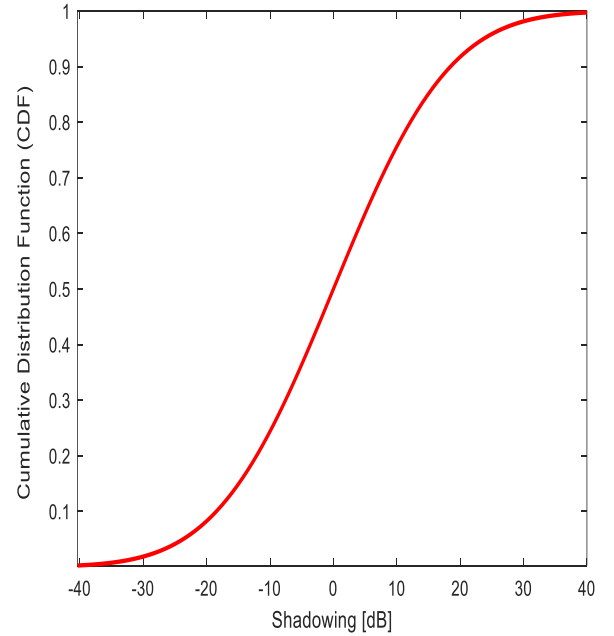
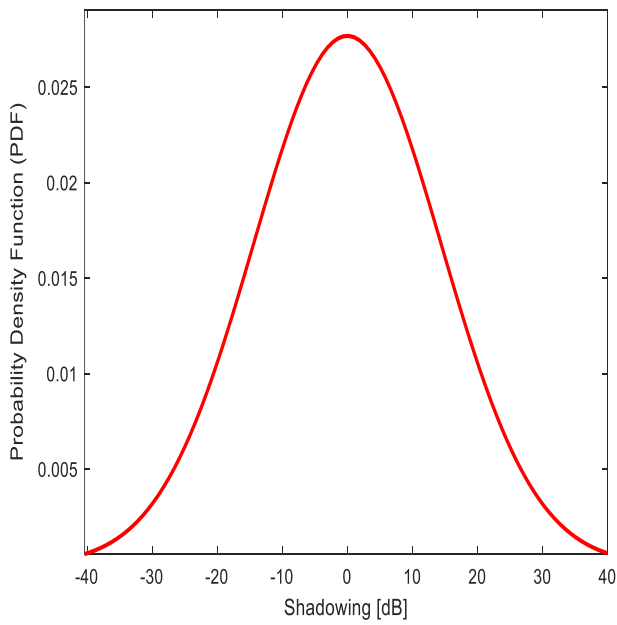


Figure 4-55: PDF and CDF for indoor NLoS theater lecture at 868 MHz _ scenario E

Table 4.7: Mean and standard deviation for the shadow fading in indoor scenarios

Scenario	Mean (μ)	Sigma (σ)
LoS corridor at 433 MHz	-8.52651e-15	13.1797
Theater lectures at 433 MHz	2.13163e-15	11.2285
Emergency stairs at 433 MHz	2.03012e-15	24.0389
Ceilings and floors at 433 MHz	1.98952e-14	12.4044
Multiple walls at 433 MHz	-2.84217e-15	14.2302
LoS corridor at 868 MHz	-1.84741e-14	10.6124
Theater Lectures at 868 MHz	-3.55271e-15	14.4112
Emergency stairs at 868 MHz	3.38354e-14	27.2554
Ceilings and floors at 868 MHz	1.56319e-14	16.3408
Multiple walls at 868 MHz	5.68434e-15	16.9484

4.4.2 Outdoor Scenario

Figure 4-56 to Figure 4-65 show the PDF for each of the scenarios for an outdoor environment that are previously discussed using “distributionFitter” MATLAB tool and Table 4.8 shows the mean and the standard deviation for these fitted curves.

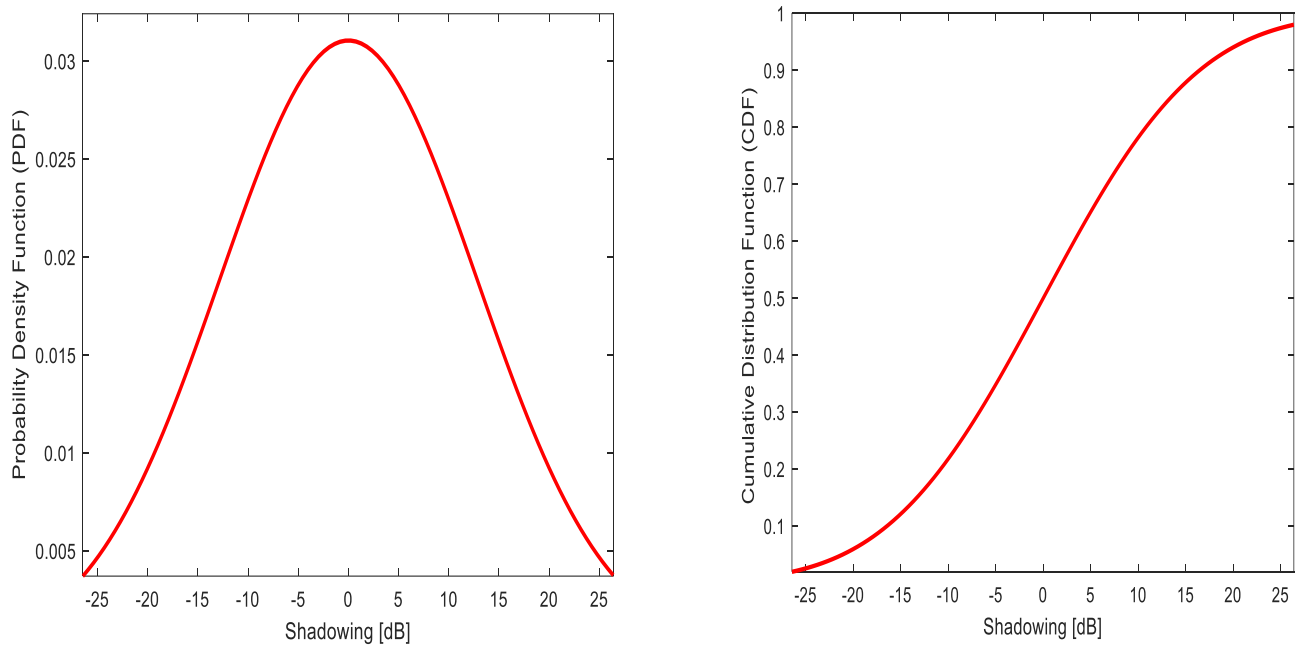


Figure 4-56: PDF and CDF for outdoor NLoS with trees' leaves at 433MHz_ scenario A

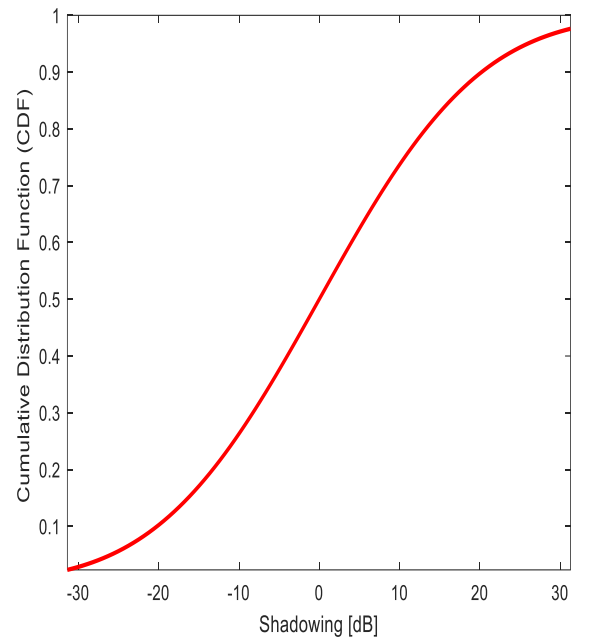
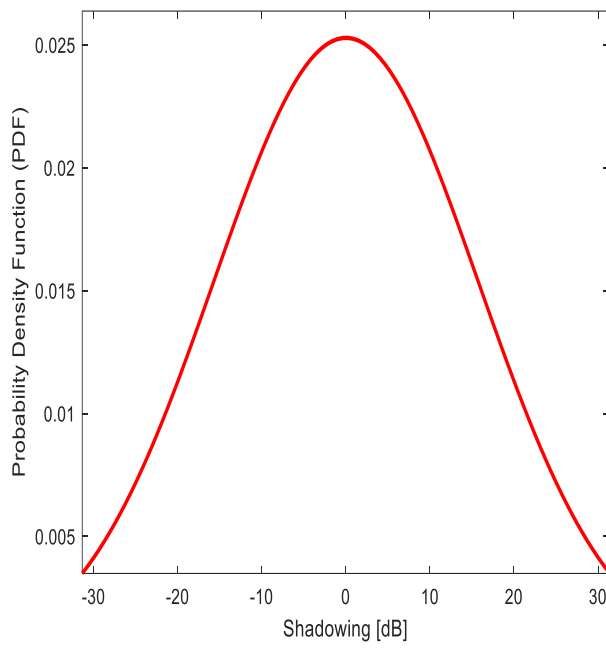


Figure 4-57: PDF and CDF for outdoor NLoS without trees' leaves at 433MHz _ scenario A

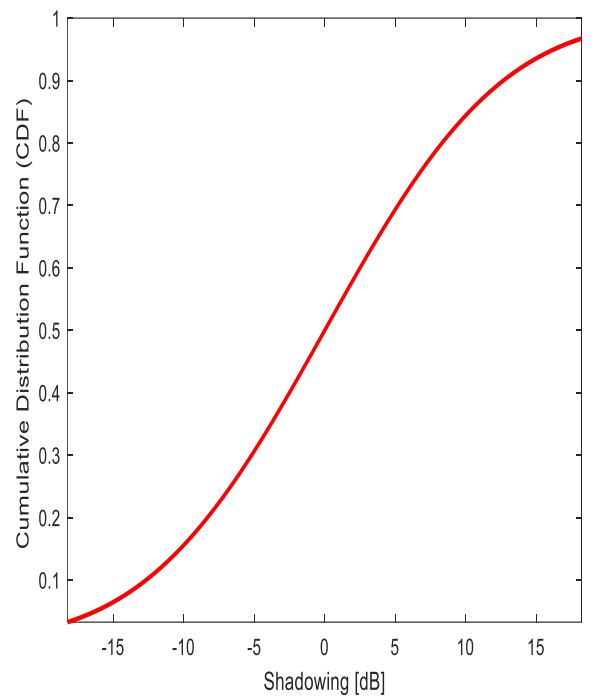
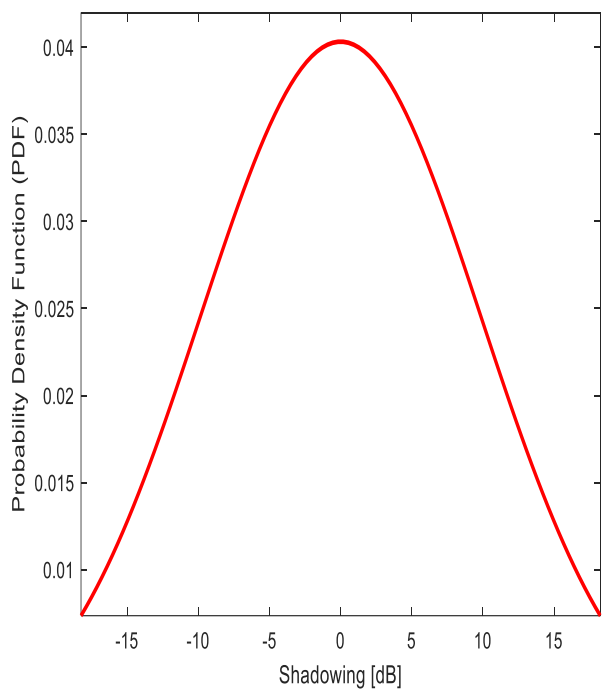


Figure 4-58: PDF and CDF for outdoor NLoS with trees' leaves at 868 MHz _ scenario A

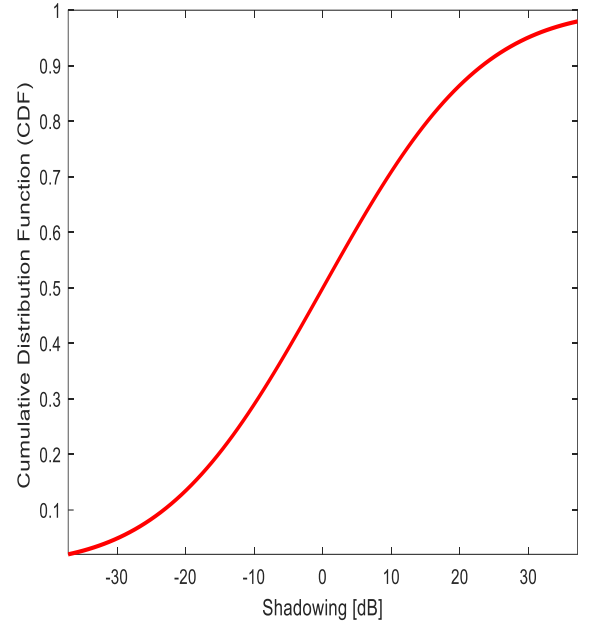
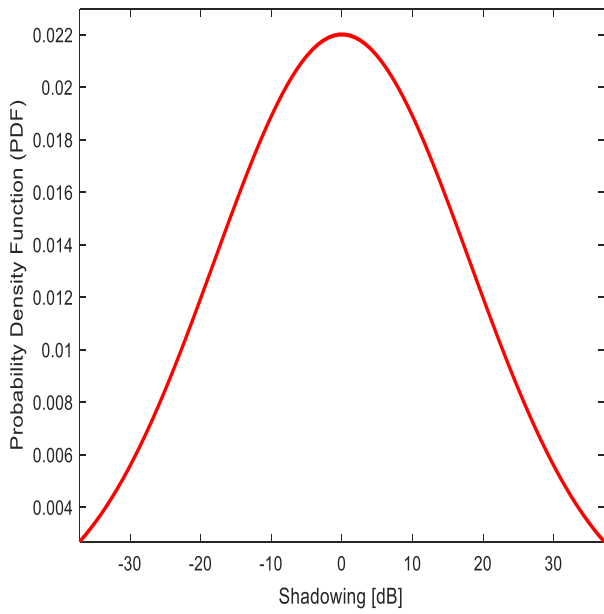


Figure 4-59: PDF and CDF for outdoor NLoS without trees' leaves at 868MHz_ scenario A

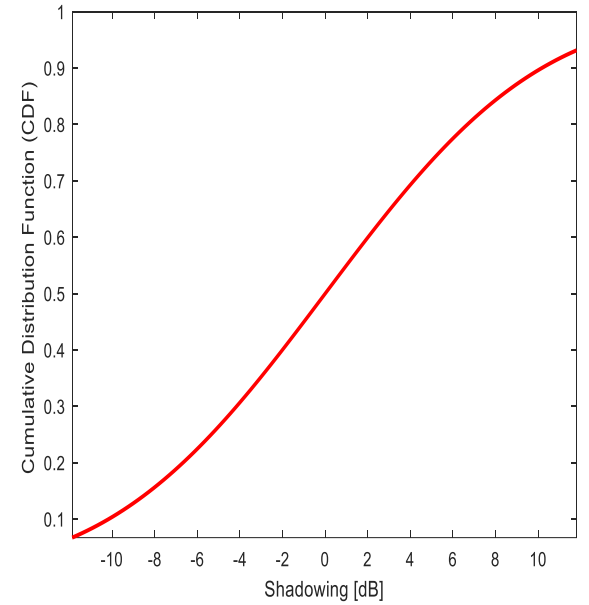
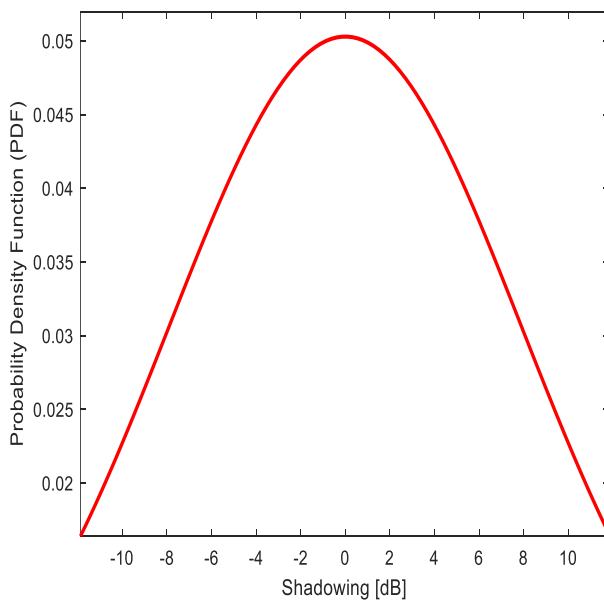


Figure 4-60: PDF and CDF for outdoor NLoS with trees' trunks at 433MHz_ scenario B

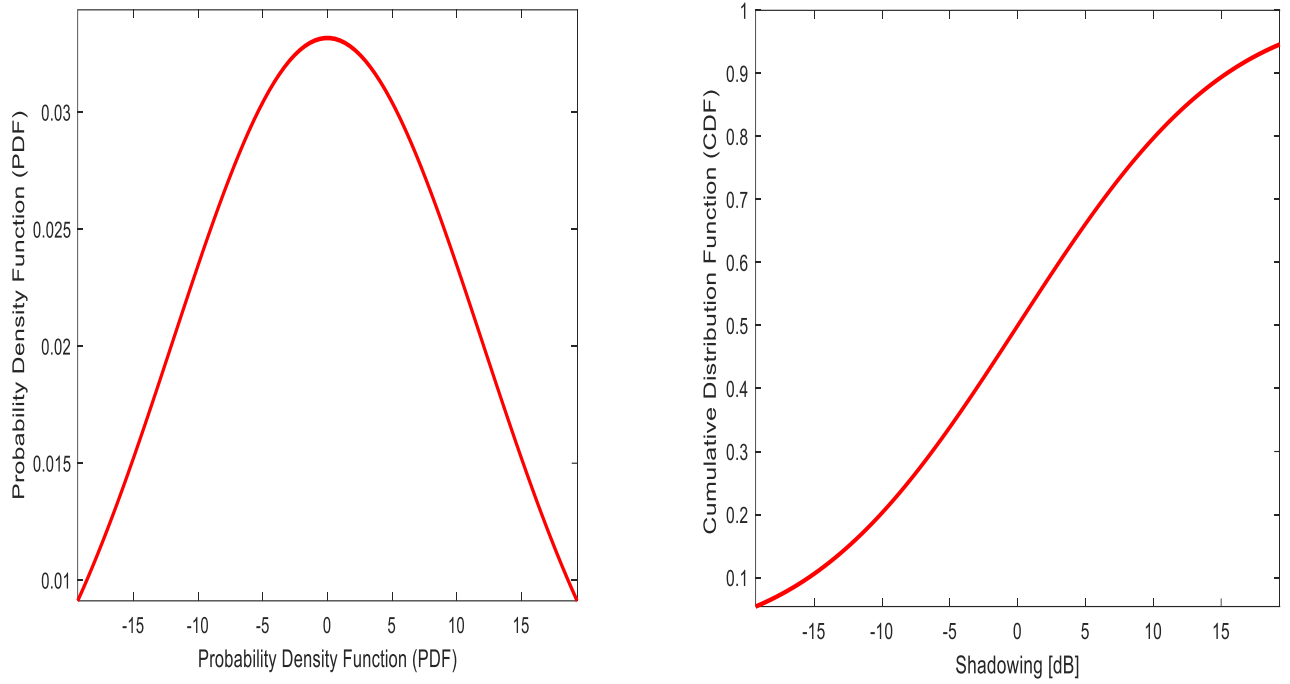


Figure 4-61: PDF and CDF for outdoor NLoS without trees' trunks at 433MHz_scenario B

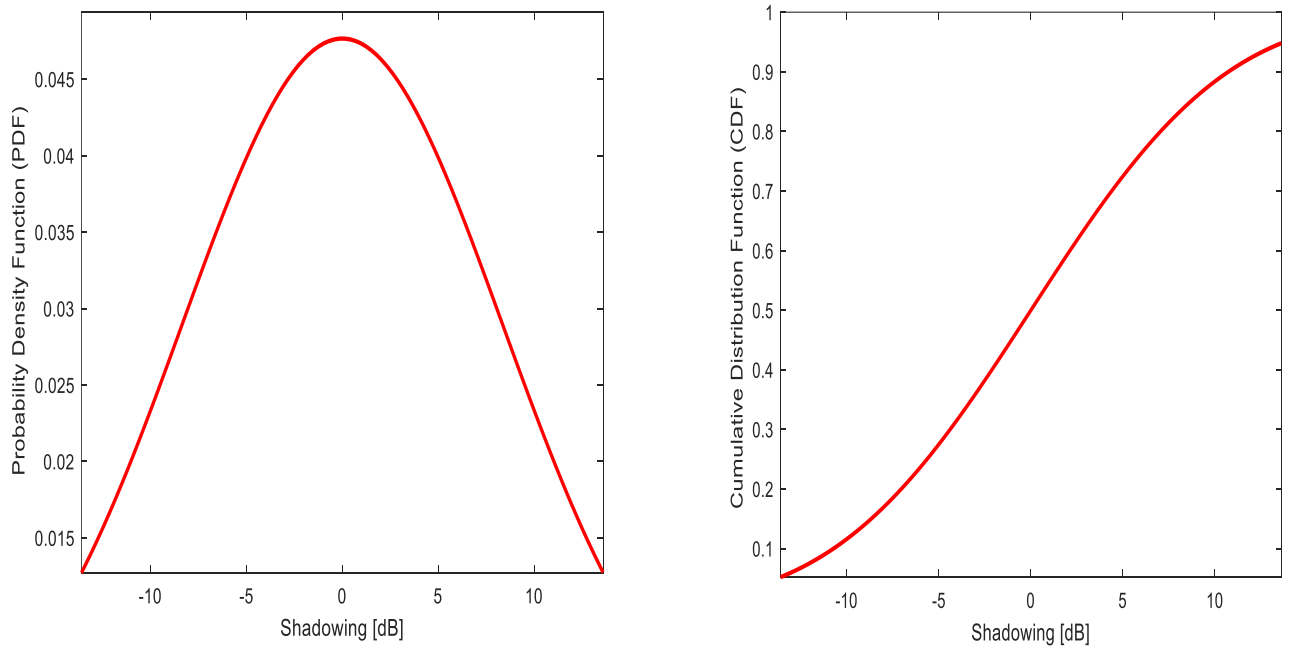


Figure 4-62: PDF and CDF for outdoor NLoS with trees' trunks at 868MHz_scenario B

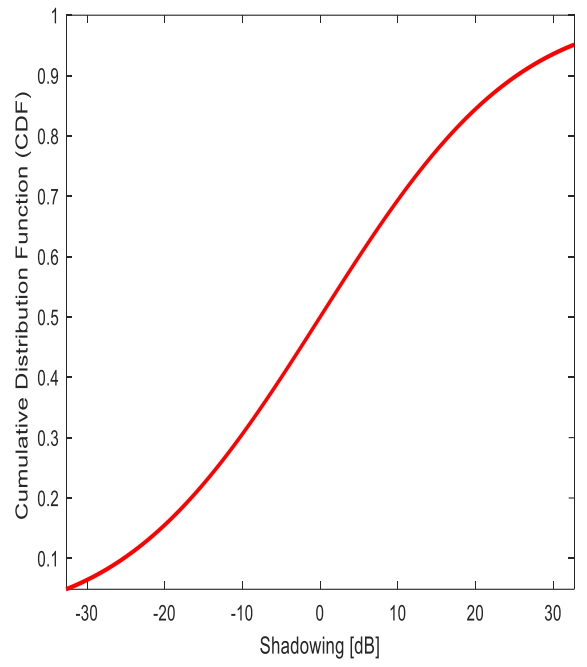
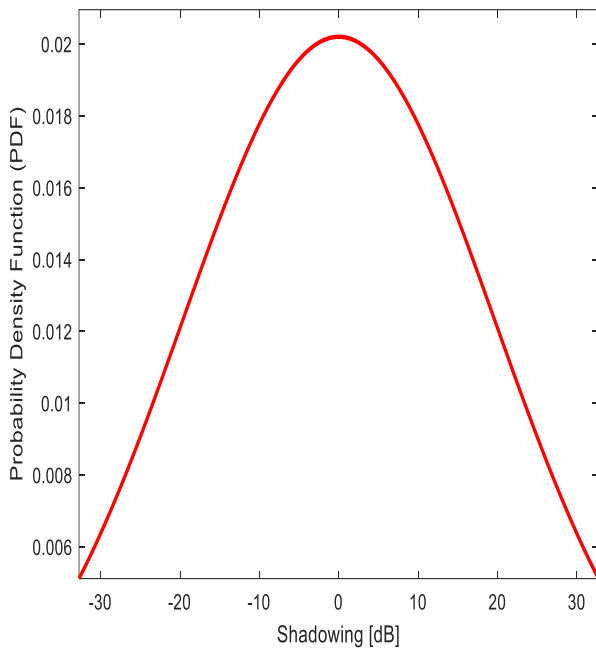


Figure 4-63: PDF and CDF for outdoor NLoS without trees' trunks at 868MHz_ scenario B

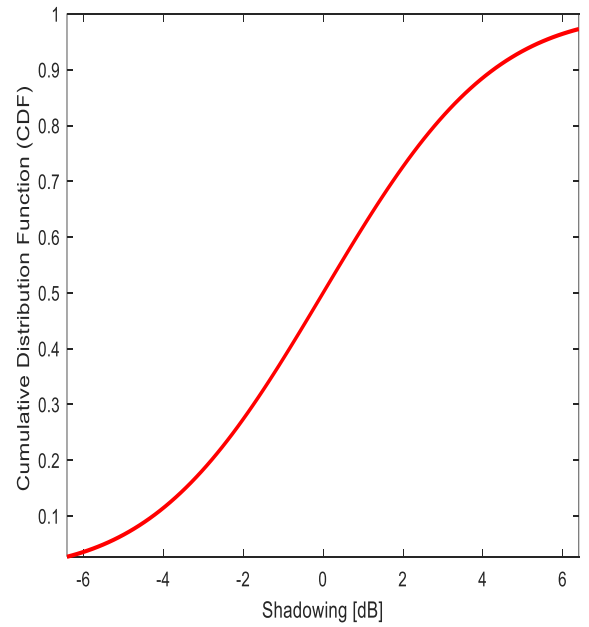
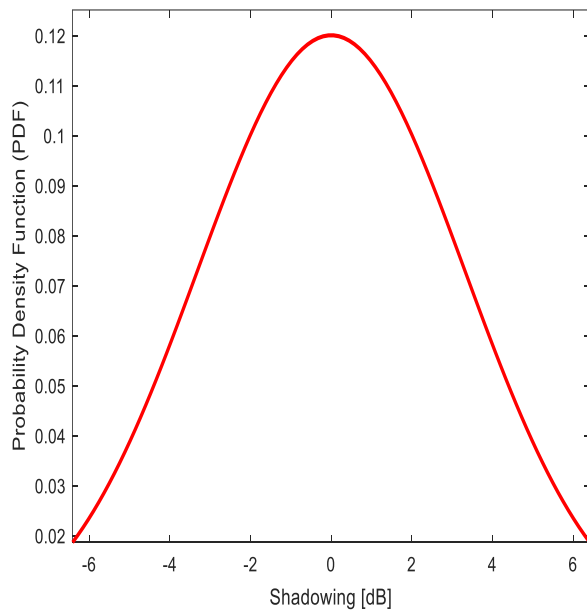


Figure 4-64: PDF and CDF for outdoor NLoS and LoS complex outdoor environment at 433 MHz_ scenario C

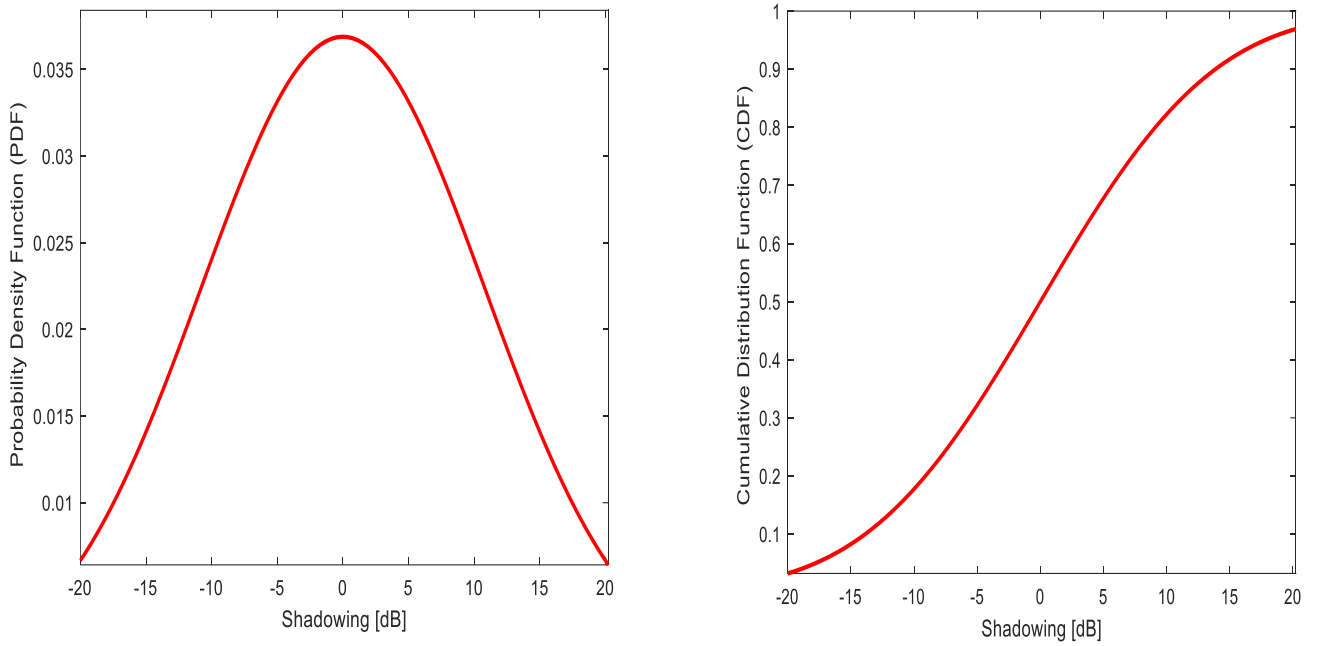


Figure 4-65: PDF and CDF for outdoor NLoS and LoS complex outdoor environment at 868 MHz_ scenario C

Table 4.8: Mean and standard deviation for the shadow fading in outdoor scenarios

Scenario	Mean (μ)	Sigma (σ)
Trees' leaves at 433 MHz	2.03012e-15	12.844
Without trees' leaves at 433 MHz	-1.42109e-14	15.7769
Trees' leaves at 868 MHz	-2.03012e-15	9.89349
Without trees' leaves at 868 MHz	0	18.1246
Trees' trunks at 433 MHz	2.84217e-15	7.93303
Without trees' trunks at 433 MHz	-2.84217e-15	12.0258
Trees' trunks at 868 MHz	-2.84217e-15	8.37048
Without trees' trunks at 868 MHz	7.10543e-15	19.7432
NLoS and LoS for complex outdoor Environment at 433 MHz	-1.06581e-14	3.32265
NLoS and LoS for complex outdoor Environment at 868 MHz	1.74406e-14	10.8143

All of our findings in both indoor and outdoor environments are consistent with the definition of shadowing, which calls for a distribution that resembles the normal distribution, a mean that is close to zero, and data dispersion to the right and left of the mean.

Chapter 5 Conclusion and Future Works

5.1 Conclusion

LoRa technology is a promising technology for IoTs networks because it provides long-range communications at low data rates with low power consumption and cost effectiveness, meeting the essential requirements of IoTs applications. This work suggested using LoRa technology in order to understand channel behavior and provide realistic, and reliable empirical new parameters for path loss propagation model for LoRa in the city of Birzeit, Palestine. This would allow for the measurement of received signal strength and the prediction of path loss parameters', which would reveal the dependability of this promising technology for long-range IoTs communications.

This study used a variety of scenarios to examine how the LoRa technology performed in both indoor and outdoor environments, including the impact of stairs, floors, walls, tree leaves, and trunks, in addition to a more complicated outdoor scenario. After that, the measured received power was averaged, and the parameters of path loss model were extracted from the measurements. The path loss based on the proposed parameters was compared with the earlier path loss models. The most important finding is that, in all outdoor scenarios, the data fitted curve was approaching Lee model as the same observation were obtained in the literature, whereas, in indoor scenarios, the closest curve of the data fitted curve varied depending on the scenario's nature and the variables that the model prioritizes. However, the model based on the proposed parameters in the different scenarios were closest to the path loss model based on measured readings and had the least RMSE compared to the other models. In the future, when deploying IoT applications and using LoRa technology here in Palestine, these empirical parameters for propagation models in Birzeit city will help to optimize the network parameters in order to achieve the best connection and deliver a high level of quality of experience in this area to the users.

5.2 Contributions

Thesis contributions are:

- Extensive measurements at five different indoor environment scenarios and three different outdoor environment scenarios at 433 MHz and 868 MHz were conducted. More than 15000 readings were measured across 16 different scenarios.
- Understanding the channel behavior for LoRa technology based on the received signal strength
- New proposed parameters for the path loss model suggested for LoRa technology.
- Provide precise empirical parameters for path loss propagation model in Birzeit city based on measurements made with LoRa modules Tx and Rx in the real world.

5.3 Research Limitations

- Finding LoRa Tx and Rx modules locally was challenging, so we had to order them from outside sources and wait a long time for them to arrive before we could start our measurements.
- The absence of a clear manual from the manufacturer on how to use and connect the LoRa modules that received make it take longer time to get them working properly.
- The presence of the Israeli occupation imposes many challenges, as one of pieces was confiscated before it reached, in addition to inability during our outdoor measurements, to reach distances greater than 10 km due to the presence of settlements and checkpoints.

5.4 Future Works

The suggested models need to be expanded to include other frequencies in future work since the research was restricted to the frequencies of 433 MHz and 868 MHz only. One of the other recommendations for future work is to conduct additional measurements for additional scenarios in different environments.

References

- [1] R. El Chall, S. Lahoud, and M. El Helou, "LoRaWAN Network: Radio Propagation Models and Performance Evaluation in Various Environments in Lebanon," *IEEE Internet of Things Journal*, vol. 6, no. 2, pp. 2366-2378, 2019.
- [2] R. Liang, L. Zhao, and P. Wang, "Performance Evaluations of LoRa Wireless Communication in Building Environments," *Sensors*, vol. 20, no. 14, 2020.
- [3] A. M. Abdul Rahman, F. H. K. Zaman, and S. A. C. Abdullah, "Performance Analysis of LPWAN using LoRa Technology for IoT Application," *International Journal of Engineering and Technology(UAE)*, vol. 7, pp. 212-216, 2018.
- [4] A. Valcarce, G. De La Roche, A. Juttner, D. Lopez-Perez, and J. Zhang, "Applying FDTD to the Coverage Prediction of WiMAX Femtocells", *EURASIP Journal on Wireless Communications and Networking*, pp.1-13, vol. 2009, 2009.
- [5] J Sosa, S Coss, A Rodríguez, L Rodríguez, M Galaz, E Ramírez, and M Enciso, "Indoor 2.4 GHz Microwave Propagation Study Using 3D FDTD Approach", *Electronics Letters*, vol. 47, no. 24, pp. 1308 – 1309, 2011.
- [6] A. Zyoud, J. Chebil, M. Habaebi, Md. Islam, and A. Lwas, "Investigation of Three Dimensional Empirical Indoor Path Loss Models for Femtocell Networks", In *IOP Conference Series: Materials Science and Engineering*, vol. 53, no. 1, pp. 012021, 2013.
- [7] S. Sun, T. S. Rappaport, S. Rangan, T. A. Thomas, A. Ghosh, I. Z. Kovacs, and J. Jarvelainen, "Propagation Path Loss Models for 5G Urban Micro-and Macro-Cellular Scenarios", In *2016 IEEE 83rd Vehicular Technology Conference (VTC Spring)*, pp. 1-6, 2016.
- [8] W. Xu, J. Y. Kim, W. Huang, S. Kanhere, S. Jha, and W. Hu, "Measurement, Characterization and Modeling of LoRa Technology in Multi-Floor Buildings," *IEEE Internet of Things Journal*, vol. 7, no.1, pp. 298-310, 2020.
- [9] T. Janssen, N. BniLam, M. Aernouts, R. Berkvens, and M. Weyn, "LoRa 2.4 GHz Communication Link and Range," *Sensors*, vol. 20, 2020.
- [10] P. Kulkarni, Q. A. Hakim, and A. Lakas, "Experimental Evaluation of a Campus-Deployed IoT Network Using LoRa," *IEEE Sensors Journal*, vol. 20, pp. 2803-2811, 2020.
- [11] S. -Y. Wang, Y. -R. Chen, T. -Y. Chen, C. -H. Chang, Y. -H. Cheng, C. -C. Hsu, and Y. -B. Lin, "Performance of LoRa-Based IoT Applications on Campus," *2017 IEEE 86th Vehicular Technology Conference (VTC-Fall)*, pp. 1-6, 2017.
- [12] J. Liando, A. Jg, A. Tengourtius, and M. Li, "Known and Unknown Facts of LoRa: Experiences from a Large-scale Measurement Study," *ACM Transactions on Sensor Networks*, vol. 15, pp. 1-35, 2019.
- [13] A. Farhad, D.-H. Kim, and J.-Y. Pyun, "Scalability of LoRaWAN in an Urban Environment: A Simulation Study," *2019 Eleventh International Conference on Ubiquitous and Future Networks (ICUFN)*, pp. 677-681, 2019.
- [14] E. Harinda, S. Hosseinzadeh, H. Larijani, and R. M. Gibson, "Comparative Performance Analysis of Empirical Propagation Models for LoRaWAN 868MHz in an Urban Scenario," *2019 IEEE 5th World Forum on Internet of Things (WF-IoT)*, pp. 154-159, 2019.

- [15] R. Apriantoro, A. Suharjono, K. Kurnianingsih, and I. K. A. Enriko, "Investigation of Coverage and Signal Quality of LoRaWAN Network in Urban Area," *2020 International Conference on Computer Engineering, Network, and Intelligent Multimedia (CENIM)*, pp. 326-331, 2020.
- [16] K. A. Ahmad, J. D. Segaran, F. R. Hashim, and M.T. Jusoh, "LoRa Propagation at 433 MHz in Tropical Climate Environment," *Journal of Fundamental and Applied Sciences*, vol. 9, pp. 384-394, 2018.
- [17] J. Petajajarvi, K. Mikhaylov, A. Roivainen, T. Hanninen, and M. Pettissalo, "On the Coverage of LPWANs: Range Evaluation and Channel Attenuation Model for LoRa Technology," *2015 14th International Conference on ITS Telecommunications (ITST)*, pp. 55-59, 2015.
- [18] D. Dobrilovic, M. Malic, D. Malic, and S. Sladojevic, "Analyses and Optimization of Lee Propagation Model for LoRa 868 MHz Network Deployments in Urban Areas," *Journal of Engineering Management and Competitiveness*, vol. 7, pp. 55-62, 2017.
- [19] P. Jörke, S. Böcker, F. Liedmann, and C. Wietfeld, "Urban Channel Models for Smart City IoT-Networks Based on Empirical Measurements of LoRa-Links at 433 and 868 MHz," *2017 IEEE 28th Annual International Symposium on Personal, Indoor, and Mobile Radio Communications (PIMRC)*, pp. 1-6, 2017.
- [20] S. Bertoldo, L. Carosso, E. Marchetta, M. Paredes, and M. Allegretti, "Feasibility Analysis of a LoRa-Based WSN Using Public Transport," *Applied System Innovation*, vol. 1, no.4, 2018.
- [21] R. Sanchez-Iborra, J. Sanchez-Gomez, J. Ballesta-Viñas, M.-D. Cano, and A. F. Skarmeta, "Performance Evaluation of LoRa Considering Scenario Conditions," *Sensors*, vol. 18, p. 772, 2018.
- [22] F. C. de Oliveira, and J. M. C. Brito, "A Comparative Study of Performance Analysis of Empirical Propagation," *ICN 2021: 20th International Conference on Networks*, pp. 20 - 26, 2021.
- [23] N. A. B. Masadan, M. H. Habaebi, and S. H. Yusoff, "LoRa LPWAN Propagation Channel Modelling in IIUM Campus," *2018 7th International Conference on Computer and Communication Engineering (ICCCCE)*, pp. 14-19, 2018.
- [24] N. A. B. Masadan, M. H. Habaebi, and S. H. Yusoff, "Long Range Channel Characteristics through Foliage," *Bulletin of Electrical Engineering and Informatics*, vol. 8, 2019.
- [25] M. R. Ansah, R. A. Sowah, J. Melià-Seguí, F. A. Katsriku, X. Vilajosana, and W. O. Banahene, "Characterizing Foliage Influence on LoRaWAN Pathloss in a Tropical Vegetative Environment," *IET Wireless Sensor Systems*, vol. 10, 2020.
- [26] R. Anzum, M. H. Habaebi, M. R. Islam, G. P. N. Hakim, M. U. Khandaker, H. Osman, S. Alamri, and E. AbdElrahim, "Multiwall Path-Loss Prediction Model Using 433 MHz LoRa-WAN Frequency to Characterize Foliage's Influence in a Malaysian Palm Oil Plantation Environment," *Sensors*, vol. 22, 2022.
- [27] M. H. Habaebi, A. S. M. Rofi, M. R. Islam, and A. Basahel, "ANN-based LoRaWAN Channel Propagation Model," *International Journal of Interactive Mobile Technologies*, vol. 16, no. 11, pp. 91–106, 2022.
- [28] S. Hosseinzadeh, M. Almoathen, H. Larijani, and K. Curtis, "A Neural Network Propagation Model for LoRaWAN and Critical Analysis with Real-World Measurements," *Big Data and Cognitive Computing*, vol. 1, pp. 7, 2017.
- [29] P. Fraga-Lamas, M. Celaya-Echarri, P. L. Iturri, T. Fernández-Caramés, L. Azpilicueta, E. Aguirre, M. Suárez-Albela, F. Falcone, and L. Castedo, "Analysis, Design and Empirical Validation

of a Smart Campus Based on LoRaWAN," In *Proceedings of 5th International Electronic Conference on Sensors and Applications*, pp. 15–30, 2018.

[30] N. Naik, "LPWAN Technologies for IoT Systems: Choice Between Ultra Narrow Band and Spread Spectrum," *2018 IEEE International Systems Engineering Symposium (ISSE)*, pp. 1-8, 2018.

[31] U. Raza, P. Kulkarni, and M. Sooriyabandara, "Low Power Wide Area Networks: An Overview," *IEEE Communications Surveys and Tutorials*, vol. 19, pp. 855-873, 2016.

[32] L. Li, J. Ren, and Q. Zhu, "On the application of LoRa LPWAN Technology in Sailing Monitoring System," *2017 13th Annual Conference on Wireless On-demand Network Systems and Services (WONS)*, pp. 77-80, 2017.

[33] W. Ayoub, A. E. Samhat, F. Nouvel, M. Mroue, and J.-C. Prévotet, "Internet of Mobile Things: Overview of LoRaWAN, DASH7, and NB-IoT in LPWANs Standards and Supported Mobility," *2018 25th International Conference on Telecommunications (ICT)*, 2018.

[34] I. Cheikh, R. Aouami, E. Sabir, M. Sadik, and S. Roy, "Multi-Layered Energy Efficiency in LoRa-WAN Networks: A Tutorial," *IEEE Access*, vol. 10, pp. 9198-9231, 2022.

[35] N. Sornin, and O. B. Seller, "US9252834B2 - Low Power Long Range Transmitter", Google Patents, 2016. [Online]. Available: <https://patents.google.com/patent/US9252834B2/en> (accessed Dec. 11, 2022).

[36] P. Gkotsiopoulos, D. Zorbas, and C. Douligeris, "Performance Determinants in LoRa Networks: A Literature Review," *IEEE Communications Surveys and Tutorials*, vol. 23, no. 3, pp. 1721-1758, 2021.

[37] J. Haxhibeqiri, E. D. Poorter, I. Moerman, and J. Hoebeke, "A Survey of LoRaWAN for IoT: From Technology to Application," *Sensors*, vol. 18, no. 11, 2018.

[38] M. H. M. Ghazali, K. Teoh, and W. Rahiman, "A Systematic Review of Real-Time Deployments of UAV-Based LoRa Communication Network," *IEEE Access*, vol. 9, pp. 124817-124830, 2021.

[39] M. Bor, J. Vidler, and U. Roedig, "LoRa for the Internet of Things," *European Conference/Workshop on Wireless Sensor Networks*, 2016.

[40] M. Cattani, C. A. Boano, and K. Römer, "An Experimental Evaluation of the Reliability of LoRa Long-Range Low-Power Wireless Communication," *Journal of Sensor and Actuator Networks*, vol. 6, no. 2, pp. 7-26, 2017.

[41] E. Pietrosevoli, *LoRa Details*, 2017. [Online]. Available: <https://dokumen.tips/documents/loro-details-lora-details-ermanno-pietrosevoli-lora-and-lorawan-lora-is-strictly.html?page=1> (accessed Dec. 15, 2022).

[42] U. Raza, P. Kulkarni, and M. Sooriyabandara, "Low Power Wide Area Networks: An Overview." *IEEE Communications Surveys and Tutorials*, vol.19, no.2, pp. 855-873, 2017.

[43] T. T. Nguyen, H. H. Nguyen, R. Barton, and P. Grossetete, "Efficient Design of Chirp Spread Spectrum Modulation for Low-Power Wide-Area Networks," in *IEEE Internet of Things Journal*, vol. 6, no. 6, pp. 9503-9515, 2019.

[44] Semtech Corporation, "Semtech SX1276 Datasheet", 2020. [Online]. Available: <https://www.semtech.com/products/wireless-rf/loro-transceivers/sx1276> (accessed Dec. 15, 2023).

- [45] K. Q. Abdelfadeel, V. Cionca and D. Pesch, "Fair Adaptive Data Rate Allocation and Power Control in LoRaWAN," *2018 IEEE 19th International Symposium on "A World of Wireless, Mobile and Multimedia Networks" (WoWMoM)*, pp. 14-15, 2018.
- [46] K.-Y. Liang, and S. L. Zeger, "Regression Analysis for Correlated Data," *Annual Review of Public Health*, vol. 14, pp. 43-68, 1993.
- [47] A. C. Rencher, and G. B. Schaalje, "Linear Models in Statistics", John Wiley and Sons, 2008.
- [48] S. P. Gordon, and F. S. Gordon, "Deriving the Regression Equation without Using Calculus," *Mathematics and Computer Education*, vol. 38, no.1, pp. 64-68, 2004.
- [49] S. H. Brown, "Multiple Linear Regression Analysis: A Matrix Approach with MATLAB," *Alabama Journal of Mathematics*, vol. 34, pp. 1-3, 2009.
- [50] A. Zyoud, "3D Femtocell Path Loss Model in Wireless Network," Ph.D. Dissertation, International Islamic University Malaysia, Kuala Lumpur, Malaysia, 2017.
- [51] G. R. MacCartney, T. S. Rappaport, S. Sun, and S. Deng, "Indoor Office Wideband Millimeter-Wave Propagation Measurements and Channel Models at 28 and 73 GHz for Ultra-Dense 5G Wireless Networks", IEEE access, vol.3, pp. 2388-2424, 2015.
- [52] M. Habaebi, and A. Zyoud, "Femtocell Path Loss and Interference Modelling in 4G Wireless Networks", IIUM Press, International Islamic University Malaysia, 2017.
- [53] G. George, and J. Idogho, "Path Loss Prediction Based on Machine Learning Techniques: Support Vector Machine, Artificial Neural Network, and Multi Linear Regression Model," *Open Journal of Physical Science (OJPS)*, vol. 3, pp. 1- 22, 2022.
- [54] J. J. Moré, "The Levenberg-Marquardt Algorithm: Implementation and Theory," *Numerical Analysis*, vol. 630, pp. 105-116, 1978.
- [55] A. R. Conn, N. I. Gould, and P. L. Toint, "Trust Region Methods Trust Region Methods (MOS-SIAM Series on Optimization)", Society for Industrial and Applied Mathematics, 2000.
- [56] G. R. MacCartney, J. Zhang, S. Nie, and T. S. Rappaport, "Path loss Models for 5G Millimeter Wave Propagation Channels in Urban Microcells", In *2013 IEEE Global Communications Conference (GLOBECOM)*, pp. 3948-3953, 2013.
- [57] T. S. Rappaport, F. Gutierrez, E. Ben-Dor, J. N. Murdock, Y. Qiao, and J. I. Tamir, "Broadband Millimeter-Wave Propagation Measurements and Models Using Adaptive-Beam Antennas for Outdoor Urban Cellular Communications", *IEEE Transactions on Antennas and Propagation*, vol. 61, no. 4, pp. 1850-1859, 2013.
- [58] A. Zyoud, M. H. Habaebi, and R. Islam, "Parameterized Indoor Propagation Model for Mobile Communication Links", *Microwave and Opticl Technology Letters*, vol. 58, no.4, pp. 823-826, 2016.
- [59] T. S. Rappaport, Y. Xing, G. R. MacCartney, Jr., A. F. Molisch, E. Mellios, and J. Zhang, "Overview of Millimeter Wave Communications for Fifth-Generation (5G) Wireless Networks— With a Focus on Propagation Models", *IEEE Transactions on Antennas and Propagation*, vol. 65, no. 12, pp. 6213-6230, 2017.
- [60] A. Zyoud, J. Chebil, M. H. Habaebi, R. Islam, and A. Zeki, "Comparison of Empirical Indoor Propagation Models for 4G Wireless Networks at 2.6 GHz", In *Proceedings Engineering and Technology*, pp. 7-11, 2013.

- [61] J. Kenney, and E. Keeping, "Mathematics of Statistics (Part One)", David Van Nostrand, vol. 1, 1962.
- [62] H. Frank, and S. C. Althoen, "Statistics: Concepts and Applications Workbook", Cambridge University Press, 1994.
- [63] W.J. DeCoursey, "Statistics and Probability for Engineering Applications", *Elsevier Science*, 2003
- [64] "SX1276 Development Kit User Guide," Semtech Corporation, 2014. [Online]. Available: <https://semtech.my.salesforce.com/sfc/p/#E0000000JeIG/a/2R000000HUWW/.c3ek4syCdhUJvRzKxO.54AYoGhOth.V20WdthQYU4> (accessed May 19, 2023).
- [65] "SX1276RF1JAS," Semtech Corporation, [Online]. Available: <https://www.semtech.com/products/wireless-rf/lora-connect/sx1276rf1jas#documentation> (accessed May 19, 2023).
- [66] J. Chebil, A. Lwas, Md. Islam, and A. Zyoud, "Comparison of Empirical Propagation Path Loss Models for Mobile Communications in the Suburban Area of Kuala Lumpur", In *2011 4th International Conference on Mechatronics (ICOM)*, pp. 1-5, 2011.
- [67] J. Chebil, A. Lwas, Md. Islam, and A. Zyoud, "Investigation of Path Loss Models for Mobile Communications in Malaysia", *Australian Journal of Basic and Applied Sciences*, vol. 5, no. 6, pp. 365-371, 2011.
- [68] J. Chebil, A. Lwas, Md. Islam, and A. Zyoud, "Adjustment of Lee Path Loss Model for Suburban Area in Kuala Lumpur-Malaysia", In *Proceedings of International Conference on Computer Communication and Management (ICCCM 2011)*, vol. 5, pp. 252-257, 2011.